UNIVERSITÉ LILLE1 – SCIENCES ET TECHNOLOGIES
Laboratoire Génie Civil et géo-environnement

THÈSE

Pour obtenir le grade de Docteur de
l'Université Lille1 - Sciences et Technologies

Discipline : Génie Civil

Amélioration des propriétés mécaniques du béton à partir de l'insertion des nanotubes de carbone: une étude par la dynamique moléculaire

Présentée et soutenue publiquement par

Anna LUSHNIKOVA

le **22 Mai 2017** devant le jury :

Rajeev AHULA, Professeur, University of Uppsala (Suède)	Rapporteur
Anatoly B. BELONOSHKO, Professeur, KTH – Stokholm (Suède)	Rapporteur
Daniel TUNEGA, Dr-HDR, University of Vienna (Autriche)	Examinateur
Isam SHAHROUR, Professeur, Université de Lille 1 - Sciences et Technologies (France)	Examinateur
Yuanyuan ZHENG, Maître de conférences, Université de Lille 1 - Sciences et Technologies (France)	Examinateur
Ali ZAOUI, Professeur, Université de Lille 1 - Sciences et Technologies (France)	Directeur de thèse

This thesis was prepared in:

Laboratoire Génie Civil et géo-environnement
Université Lille1 – Sciences et Technologies, Avenue Paul Langevin,
59655, Villeneuve d'Ascq, cedex, France

Acknowledgement

There are so many people to thank for helping me during a few past years.

My deep gratitude goes first to my supervisor **Professor Ali Zaoui**, who expertly guided me during of all period of my thesis work. The door to Prof. Zaoui office was always open for any question about my research. He consistently steered me in the right the direction. I want to thank him for helping me professionally as well as personally. His support was essential to my success here.

I am also very grateful to **Professor Isam Sharour** to give me the possibility to find my own level and work in excellent condition.

I would like to thank **Dr. Yuanyuan Zheng** to providing indispensible advices, information, and support in different aspects of my research project.

I would also like to thank the committee members including **Prof. Rajeev Ahuja**, **Prof. Anatoly Belonoshko**, **Dr. Daniel Tunega** for finding time in their busy schedule for serving in the committee, reviewing my thesis and offering some valuable suggestions and comments on the work.

I would like to thank the **French government** for providing me with the financial support for my thesis-work.

My appreciation also extends to my all laboratory colleagues and my friends **Wei, Jishuai, Amine, Majdouline, Faten, Ping, Ammar, Monique, Romaric, Marie-Laure, Laurent, Nicolas, Delphine, Patrick, Juliette, Dominique, Eric, Alain, Martine, Anne-Claire, … ,** who give me support in different situations of my life.

In particular, I very grateful to my French family **Anne-Marie, Philippe, Brigitte, Xavier, Christelle, Christophe, Isabelle, Henri, Sylvie, Bruno, Christelle, Stéphane, Leslie, Jacqueline, Marie-Claire, Nathalie, … ,** for their invaluable help every time. They are one of the most important peoples of my life.

Finally, I must express my very profound gratitude to the most important people of my life, **my lovely parents Olga and Andrey** for their love and belief in me, for providing me with unfailing support and continuous encouragement throughout my years of study, through the process of researching and writing this thesis and though of my life. This accomplishment would not have been possible without them; all that I have in my life would not have been possible without them.

Contents

GENERAL INTRODUCTION

Overview

In the modern construction industry, concrete is one of the main structural materials. The level of production is constantly increasing, since 6 billion tons of cement are consumed per year. However, conventional concrete has a number of disadvantageous features, such as low tensile strength. As a result, concrete materials suffer from critical shrinkage cracking. The main way of improving the quality of concrete is by improving the mechanical properties of the cement paste, which can be achieved by using high-tech equipment, modern production technologies, sound materials and modifying additives. In the past, the basic methods of improving the tensile strength of concrete were the addition of chemical agents to reduce porosity due to the lowering of the water/cement ratio in cement paste and the use of steel reinforcement. These methods have improved the tensile capacity of the concrete structure, but they have also increased the cost of construction. Furthermore, in the marine environment many concrete constructions are deteriorated faster than expected due to corrosion of steel. As corrosion occurs, there is a corresponding drop in the cross-sectional area of the steel reinforcement and the corrosion products occupy a larger volume than steel, and therefore exert substantial tensile forces on the surrounding concrete. It is important to note that even the light and fluid sealing cement for oil and gas drilling rigs after its hardening have a work strain. This is due to a variety of loads acting on the cement stone that give the shrinkage cracking of concrete. At the same time, during the oil and gas drilling rings, exploitation of the cement stone can be affected also by diverse corrosion environments. It can be the processes associated with the influence of reservoir waters of varying salinity and the processes associated with the impact of oil and gas connections. In such manner, the problem of shrinkage cracking stays important also for the concrete in the oil and gas wells.

Therefore, it is very important to find new additives for modified concrete. There is a variety of nano-systems, which can be used as additives. They can significantly improve the mechanical properties of traditional mineral binders. One of these additives is the carbon structures with nanometer dimensions, in particular, carbon nanotubes (CNTs). Actually, researchers are experimentally investigating the possibility of concrete’s modification by carbon nanotubes. But even so, there are difficulties to explain the obtained data and information about the processes taking place in the cement paste during its modification with carbon nanotubes. In any case, the nature of the influence of carbon nanotubes on the mineral binder remains insufficiently studied. Computational investigations are used to obtain information and to describe observations involved in the evaluation of mechanical properties of CNTs reinforced composites at the nanoscale. In addition, computational investigations also greatly helps because they provide some initial guidelines to the experimental works which aid to minimize the scope, cost and time involved in the experiments.

Nanotechnology

Nanotechnology can be defined as science, engineering, and technology conducted at the nanolevel on the scale from 1 to 100 nanometers [1]. Thus, nanotechnology engages imaging, measuring, modeling, and manipulating matter at this minute level. Nanoscience and nanotechnology can be used across all the other science fields, such as chemistry, biology, physics, materials science, and engineering.

The first mention of the method that was later called nanotechnology came from Nobel laureate Richard P. Feynman during his famous talking "There's Plenty of Room at the Bottom" in 1959 [2]. From then onwards there have been many revolutionary developments in many countries in the different domains that have demonstrated the idea of Feynman being able to manipulate matter at an extremely small scale.

Two basic approaches are comprised into the term of nanotechnology. These are the “Top-down” and the “Bottom-up” (Fig. 1). Regarding “Top-down” approach, the larger structure is reduced in size to the nanoscale preserving its original properties without control at the atomic level or deconstruction from a larger structure into its smaller constituent parts. As an example of this approach is the miniaturization in the electronics field. In the “Bottom-up” approach the materials are constructed from atoms or molecular components via their putting together [3]. The "Bottom-up" approach was proposed by Drexler et al. [4] and also called "molecular nanotechnology" or "molecular manufacturing". At a time when most modern technologies use the “Top-down” approach, the “Bottom-up” gives a great promise for revelation in the different fields including the domain of construction materials. Nowadays, the nanotechnology applications and advances in the construction and building materials domains are instable [5, 6]. Exploitation of nanotechnology in concrete on a commercial scale is limited to few results successfully converted into marketable products. The main progresses have been made in research on mineral binders [7]. The studies of the structure and mechanical properties of the main hydrate phases, origins of cement cohesion, cement hydration were provided in order to understanding of the fundamental processes in cement matrix at the nanoscale.

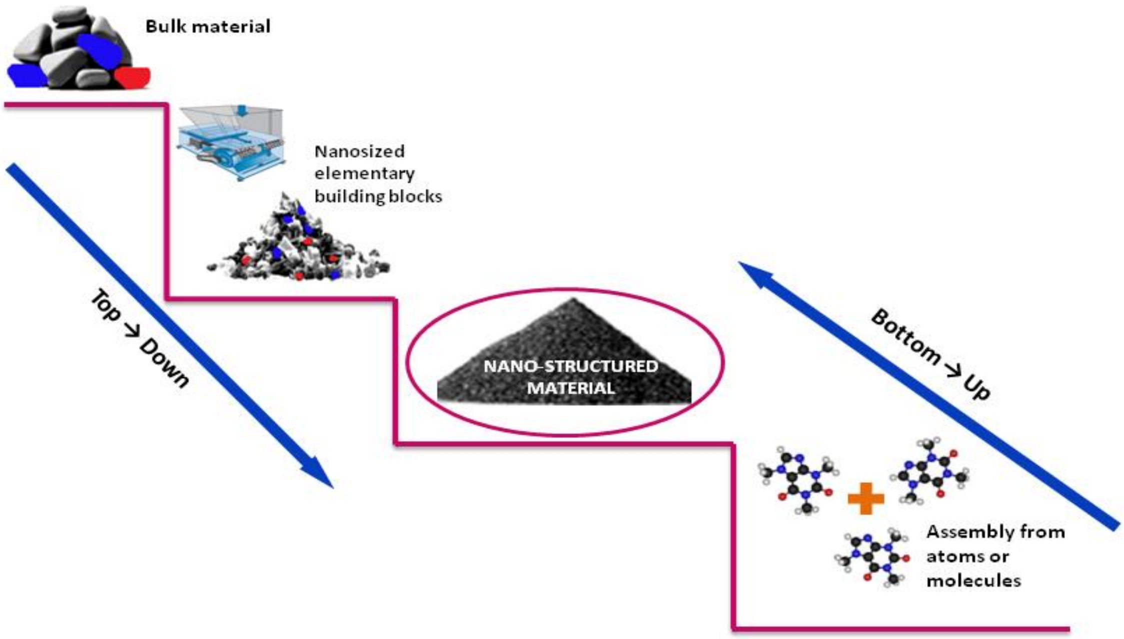

Fig. 1. Schematic representation of the "Top-down" and "Bottom-up" approaches in nanotechnology.

Nanotechnology and Concrete

Concrete is a multi-phase nanostructured composite material composed of properly proportioned mixture of water, cement, fine and coarse aggregates that age over time. The cement plays a main chemical as well as physical role to establishment the various properties of the concrete. The properties of concrete exist at the scales from nano to micro and macro [8, 9]. The key product of hydration process is the Calcium-Silicate-Hydrate (C-S-H) gel. Its importance is not only connected with the fact that it occupies 50% of the paste volume among all the reaction products, but also with the fact that it is the most accountable product for the different properties of the cement paste. C-S-H gel is the nanomaterial that keeps together the components of concrete.

In the context of the approach "Bottom-up", concrete at the nanoscale is a composite of molecular assemblage. This assemblage is accounted for the molecule's surfaces and chemical bonds that interact via various chemical reactions, intermolecular forces and intra-phase diffusion. Molecular structure, as well as bond length, energy, strength and density are the main properties at this nanoscale. The processes taking place at the nanoscale ultimately affect the properties and technical specifications of the material as a whole [7, 8, 10-13].

The nanoscience and nano-engineering (or nano-modification) are the terms that describe two main areas of nanotechnology in concrete [6]. The principal aim of nanoscience is the estimation and characterization of nano and micro cement-based materials structures. It is necessary to better understand the impact of this structure on the properties and characteristics at the macroscale using advanced technology and modeling at the atomic or molecular level. The main goal of the nano-engineering is a study of the ways to manipulate the cement-based structure at the nanoscale for the development of a new generation of multi-functional binding compositions with high mechanical, physical, chemical, electrical and other properties. Concrete may be designed at the nanoscale by implementing nanoscale blocks or objects such as different nanoparticles by way of controlling the operation of the material and adding new properties. The other way of development of concrete at nanoscale is the grafting molecules on cement particles phase, aggregates and nanosized additives. This provides the functionality of the surface, which can contribute to the improvement of boundary interactions.

Importance of Computational Material Science

The continuous development of computing power over the last years (Fig. 2) has enabled computational materials science to predict the microstructure and properties of concrete by combining physics and chemistry [14, 15]. Modeling at the atomic level by different methods such as Molecular Dynamics (MD), Monte Carlo simulation and *ab initio* has shown new opportunities in cement science and has opened the door into the processes taking place at the nanoscale that allow understanding the properties of materials at the macroscale. This allowed to develop the different strategies to improve concrete performance. In recent years, numerous studies of the C-S-H structure at the nanolevel [16-19] were provided. Several investigations about the molecular interaction between C-S-H structure with graphitic structure [20-21] also start appearing at modern science. If the experimental observations allow to describe the structure of the C-S-H, computational methods are investigating its internal behavior and providing details of the structure that cannot be obtained through experimental techniques.

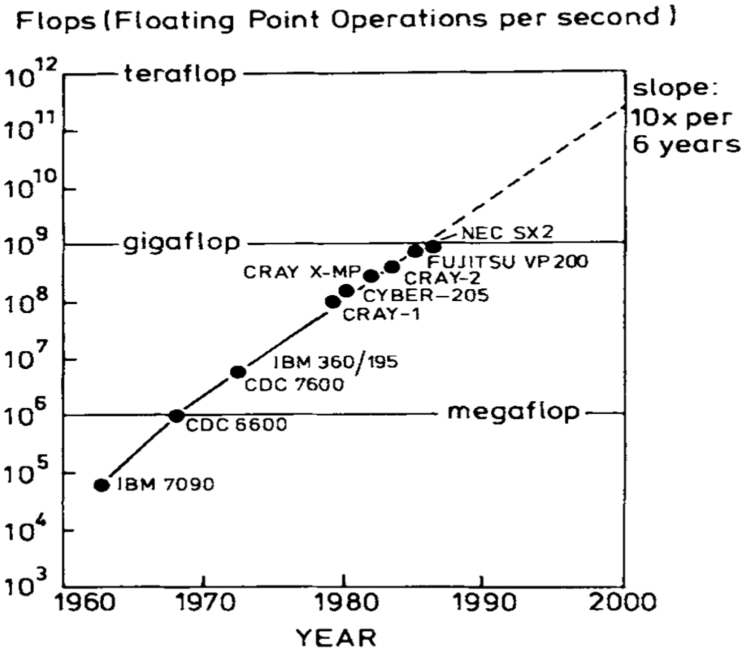

Fig. 2. Development of computing power of the most powerful computers. Adapted from Ref. [14].

However, advances will only be possible if experimental and computational results support each other. The computer simulation cannot replace the experimental measurement but it is used with good ability to complement experiments. Processes that are unapproachable to experiment can be controlled in computer simulation [14].

Addition of Nanosized and Nanostructured Material

Nanomodification of cement composites is a fast-evolving field. Synthesis of various new structures at the nanoscale enabled their using in different composites as direct additive into the matrix of the composite as well as provided the creation of the novel superplasticizers with nanoparticles for modification of the composites. Making a selection of a method for introducing the different nanoparticles into the composite matrix two fundamental possible options should be taken into account. In the first option the nanoparticles are pre-synthesized for the necessary size then introduced into the composite matrix. In the second option the necessary for modification nanoparticles are purposefully grown into the hardening system.

Regarding the nanoparticles, it has been observed, that they have a high surface area to volume ratio (Fig. 3). This fact explains the potential for tremendous chemical reactivity.

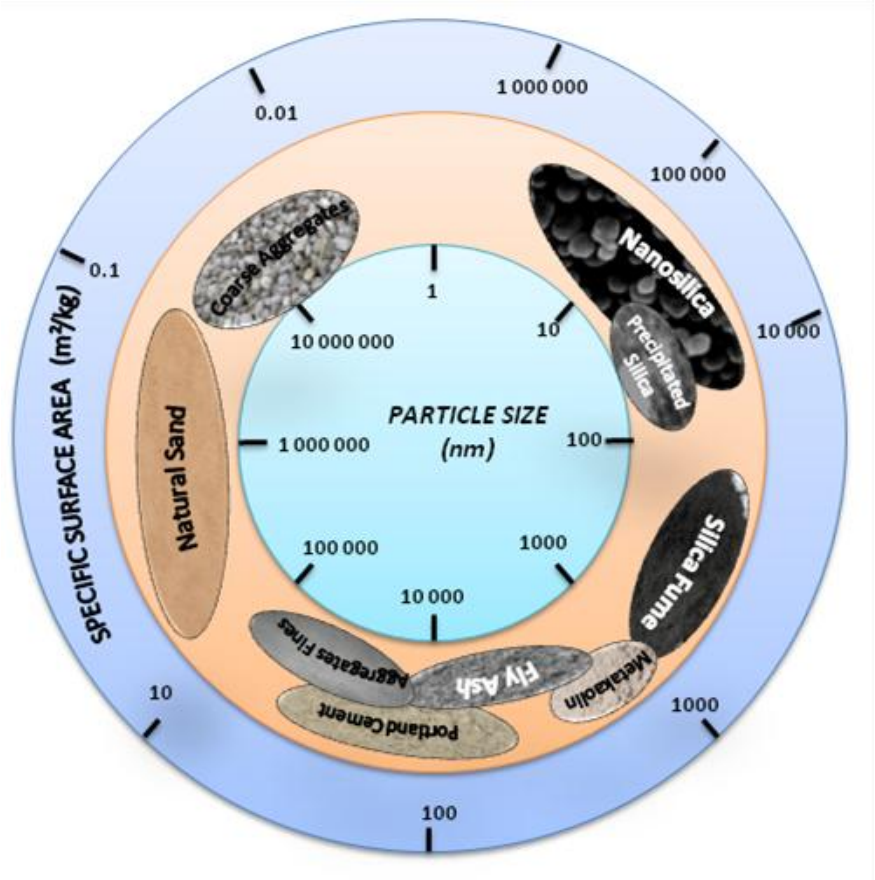

Fig. 3. Specific surface and particle size linked to concrete materials.

There are many different types of nanoparticles. The ample quantities of studies were provided with nano-silica (nano-SiO_2) [21-29] and nano-titanium oxide (nano-TiO_2) [25, 30]. It exist several investigations on the incorporating nano-iron (nano-Fe_2O_3) [23], nano-alumina (nano-Al_2O_3) [31], and nanoclay particles [32, 33]. The finite number of studies addresses the issue of nanosized cement particles and the development of nanobinders [5, 34]. Nanoparticles are able to change matrix microstructure. They can affect -as crystal seeds for cement phases- promoting cement hydration due to their high reactivity, and that the effect of this increase content of calcium hydrosilicates of high density and decrease nanoporosity. Introduction of carbon nanosystems into mineral binding matrix composition is established to result in its structuring with forming crystalline hydrate new formations of higher density and strength.

Carbon nanotubes (CNTs) are potential candidates for use as nano-reinforcements in cement-based materials. CNTs can withstand to a large elastic strainas as shown in theoretical works [35-38] and experimental measurements [39-42] concerning the tensile modulus and strength. Moreover, carbon nanotube (CNT) has a high thermal and electrical conductivity. These reasons explain the aspect of CNT's reinforcement for cement based materials.

Research Objectives and Thesis-work Breakdown Structure

The main purpose of the present thesis-work is to establish at the atomic level, an opportunity of dense concrete structure modification with CNTs as a nanodispersed additive and their influence on the modified cement matrix structure. For this objective, it is necessary to determine the atomic structure of C-S-H/CNT composite. Knowing the atomic structure, one can manipulate the system of C-S-H/CNT with the purpose of investigation the different mechanical, physical, energetic and structural properties of that system. The thesis-work is divided into three main chapters.

The first chapter contains an introduction into the principal materials used in the present study. Firstly, the description of a concrete was given. In addition the hydration process of cement was described. Afterwards, we focused our attention on the microstructure of hardened cement paste. Mineral analogs and models of C-S-H gel were delineated. In the last part of Chapter 1 carbon and carbon's allotropes which includes the carbon nanotubes will be presented.

The second chapter includes an introduction of molecular modeling. In particular, we will present the Molecular Dynamics method including its main steps and details. At the last part of Chapter 2, the determination of energetic, mechanical, physical and structural properties will be mentioned, as well as the equations used to determine these properties.

The last chapter contains five sections of the results of our study. In the first section the main mechanical properties for different types of Single Walled Carbon Nanotubes (SWCNTs) will be shown and compared with previous research works. The next three section are devoted to the influence of different type and quantity of

CNTs inserted into cement matrix. The various energetic, mechanics, physics and structural properties of concrete modified by CNTs will be detailed. We used two main model represented C-S-H gel: Tobermorite 11Å with Ca/Si ratio = 0.83 and Tobermorite 11Å with Ca/Si ratio = 1. In the last section we discuss the pressure effect on the mechanical properties of the concrete modified with carbon nanotubes.

Finally, a general conclusion will be given at the end of the manuscript.

References

[1] United States National Nanotechnology Initiative. (n.d.). Retrieved from http://www.nano.gov/nanotech-101/what/definition/

[2] R. P.Feynman, There's plenty of room at the bottom (repit from speech given at annual meeting of the American Physical Society), Engineering and Science, 23 (5) (1960) 22–36.

[3] F. Sanchez, K. Sobolev, Nanotechnology in Concrete - A Review, Constr. Build. Mat 24 (11) (2010) 2060–2071.

[4] K. E. Drexler, C. Peterson, G. Pergamit, Unbounding the future: the nanotechnology revolution, New York: William Morrow, 1991.

[5] K. Sobolev, M. Ferrada-Gutiérrez, How nanotechnology can change the concrete world: part1., Am. Ceram. Soc. Bull. 84 (10) (2005) 16–20.

[6] Z. Bittnar, P. J. M. Bartos, J. Nemecek, V. Smilauer, J. Zeman, Nanotechnology in construction: a roadmap for development, in: 3rd International Symposium on Nanotechnology in Construction (NICOM 3), Prague, Czech Republic, 2009.

[7] K. L. Scrivener, R. J. Kirkpatrick, Innovation in use and research on cementitious material, Cem. Concr. Res. 38 (2) (2008) 128–136.

[8] H. Jennings, J. W. Bullard, J. J. Thomas, J. E. Andrade, J. J. Chen, G. W. Scherer, Characterization and modeling of pores and surfaces in cement paste: correlations to processing and properties, J. Adv. Concr. Technol. 6 (1) (2008) 5–29.

[9] F. Sanchez, A. Borwankar, Multi-scale performance of carbon microfiber reinforced cement-based composites exposed to a decalcifying environment, Mater. Sci. Eng. A 527 (13-14) (2010) 3151–3158.

[10] K. P. Chong, E. J. Garboczi, Smart and designer structural material systems, Prog. Struct. Engng. Mater. 4 (4) (2002) 417–430.

[11] E. J. Garboczi, D. P. Bentz, Modeling of the microstructure and transport properties of concrete, Constr. Build. Mater. 10 (5) (1996) 293–300.

[12] E. J. Garboczi, D. P. Bentz, Multi-scale analytical/numerical theory of the diffusivity of concrete, Adv. Cem. Based Mater. 8 (12) (1998) 77–88.

[13] Y. Xi, K. Willam, D. M. Frangopol, Multiscale Modeling of Interactive Diffusion Processes in Concrete, J. Eng. Mech-ASCE 126 (3) (2000) 258–265.

[14] W. F. van Gunsteren, H.J.C. Berendsen, Computer Simulation of Molecular Dynamics: Methodology, Applications, and Perspectives in Chemistry, Angew. Chem. Int. Ed. Engl. 29 (1990) 992–1023.

[15] E. J. Garboczi, D. P. Bentz, G. J. Frohnsdorff, The Past, Present, and Future of the Computational Materials Science of Concrete, in: Material science of concrete workshop (in honor of J. Francis Young). Proceedings. Lake Shelbyville, IL, Center for Advanced-Cement-Based Materials (ACBM), 2000.

[16] P. Faucon, J. M. Delaye, J. Virlet, J. F. Jacquinot, F. Adenot, F. Adenot, Study of the structural properties of the C-S-H(I) by molecular dynamics simulation, Cem. Concr. Res. 27 (10) (1997) 1581–1590.

[17] S. V. Churakov, Structure of the interlayer in normal 11 A° tobermorite from an ab initio study, Eur. J. Mineral. 21 (1) (2009) 261–271.

[18] P. Faucon, A. Delagrave, J. C. Petit, C. Richet, J. M. Marchand, H. Zanni, Aluminum Incorporation in Calcium Silicate Hydrates (C−S−H) Depending on Their Ca/Si Ratio, J. Phys. Chem. B, 103 (1999) 7796–7802.

[19] S. Churakov, Hydrogen bond connectivity in jennite from ab initio simulations, Cem. Concr. Res. 38 (12) (2008) 1359–1364.

[20] F. Sanchez, L. Zhang, Molecular dynamics modeling of the interface between surface functionalized graphitic structures and calcium-silicate-hydrate: interaction energies, structure, and dynamics, J. Colloid Interface Sci. 323 (12) (2008) 349–358.

[21] J. Bjornstrom, A. Martinelli, A. Matic, L. Borjesson, I. Panas, Accelerating effects of colloidel nano-silica for beneficial calcuim-silicate-hydrate formation in cement, Chem. Phys. Lett. 392 (1-3) (2004) 242–248.

[22] T. Ji, Preliminary study on the water permeability and microstructure of concrete incorporating nano-SiO2, Cem. Concr. Res. 35 (10) (2005) 1943–1947.

[23] H. Li, H. G. Xiao, J. P. Ou, A study on mechanical and pressure-sensitive properties of cement mortar with nanophase materials, Cem. Concr. Res. 34 (3) (2004) 435–438.

[24] B. W. Jo, C. H. Kim, G. H. Tae, J. B. Park, Characteristics of cement mortar with nano-SiO_2 particles, Constr. Build. Mater. 21 (6) (2007) 1351–1355.

[25] H. Li, M. H. Zhang, J. P. Ou, Abrasion resistance of concrete containing nanoparticles for pavement, Wear, 260 (11-12) (2006) 1262–11266.

[26] Y. Qing, Z. Zenan, K. Deyu, C. Rongshen, Influence of nano-SiO_2 addition on properties of hardened cement paste as compared with silica fume, Constr. Build. Mater. 21 (3) (2007) 539–545.

[27] K. L. Lin, W. C. Chang, D. F. Lin, H. L. Lou, M. C. Tsai, Effects of nano-SiO_2 and different ash-particle sizes on sludge ash–cement mortar, J. Environ.Manage. 88 (14) (2008) 708–714.

[28] D. F. Lin, K. L. Lin, W. C. Chang, H. L. Luo, M. Q. Cai, Improvements of nano-SiO2 on sludge/fly ash mortar, Waste Manage. 28 (6) (2008) 1081–1087.

[29] Y. Qing, Z. Zenan, S. Li, C. Rongshen, A comparative study on the pozzolanic activity between nano-SiO_2 and silica fume, J. Wuhan. Univ. Technol. 21 (3) (2008) 153–157.

[30] H. Li, M. H. Zhang, J. P. Ou, Flexural fatigue performance of concrete containing nano-particles for pavement, Int. J. Fatigue, 29 (7) (2007) 1292–1301.

[31] Z. Li, H. Wang, S. He, Y. Lu, M. Wang, Investigations on the preparation and mechanical properties of the nano-alumina reinforced cement composite, Mater. Lett. 60 (3) (2006) 356–359.

[32] T. P. Chang, J. Y. Shih, K. M. Yang, T. C. Hsiao, Material properties of portland cement paste with nano-montmorillonite, J. Mater. Sci. 42 (17) (2007) 7478–7487.

[33] W. Y. Kuo, J. S. Huang, C. H. Lin, Effects of organo-modified montmorillonite on strengths and permeability of cement mortars, Cem. Concr. Res. 35 (6) (2006), 886–895.

[34] S. J. Lee, W. M. Kriven, Synthesis and hydration study of Portland cement components prepared by the organic steric entrapment method, Mater. Struct. 38 (1) (2005) 87–92.

[35] E. Hernandez, C. Goze, P. Bernier, A. Rubio, Elastic properties of C and BxCyNz composite nanotubes, Phys. Rev. Lett. 80 (1998) 4502–4505.

[36] J. P. Lu, Elastic properties of carbon nanotubes and nanoropes, Phys. Rev. Lett. 79 (1997) 1297–1300.

[37] M. F. Yu, B. S. Files, S. Arepalli, R. S. Ruoff, Tensile loading of ropes of single wall carbon nanotubes and their mechanical properties, Phys. Rev. Lett. 84 (2000) 5552–5555.

[38] J. P. Salvetat, G. A. Briggs, Elastic and shear moduli of single-walled carbon nanotube ropes, Phys. Rev. Lett. 5 (1999) 944–947.

[39] B. Q. Wei, R. Vajtai, P. M. Ajayan, Reliability and current carrying capacity of carbon nanotubes, Appl. Phys. Lett. 79 (2001) 1172–1174.

[40] J. Hone, M. Whittney, A. Zettle, Thermal conductivity of single-walled carbon nanotubes, Synth. Met. 103 (1999) 2498–2499.

[41] E. W. Wong, P. E. Sheehan, C. M. Liebert, Nanobeam mechanics: Elasticity, strength and toughness of nanorods and nanotubes, Science, 277 (1997) 1971–1975.

[42] M. M. Treacy, T. W. Ebbesen, J. M. Gibson, Exceptionally high Young's modulus observed for individual carbon nanotubes, Nature, 381 (1996), 680–687.

CHAPTER 1: DESCRIPTION OF THE MATERIALS STUDIED

1.1. Concrete. Hydration of Cement

Concrete is a composite material prepared by the proportioned mixture of water, cement, fine and coarse aggregates. To establishment the various properties of the concrete, it is important to emphasize that the cement plays a major role chemically as well as physically.

Cement is gray, fine powder, and chemically formed by numerous compounds. Several components constituents of cement, such as Dicalcium Silicate $2CaO \cdot SiO_2$ (C_2S), Tricalcium silicate $3CaO \cdot SiO_2$ (C_3S), Tricalcium Aluminate $3CaO \cdot Al_2O_3$ (C_3A), and Tetracalcium Alumino-ferrite $4CaO \cdot Al_2O_3 \cdot Fe_2O_3$ (C_4AF) can be distinguished [1]. The main role of these four components is the participation in the process of gaining strength at different stages during cement hydration. It is possible to describe the hydration process such as simultaneously ongoing reactions of the anhydrous components with water, regardless of the fact that the components do not hydrate at the same time. The compound C_3S is in charge of the initial set and the gain strength of concrete. These processes are fast. Nevertheless, C_3A hydrates and hardens the quickest. This is due to the fact that C_3A dispenses appreciable quantity of heat at a sweep and promotes the early strength to a certain extent. Owing to this it is necessary to add gypsum to the cement mixture during the producing process of the cement. Two other components also support liability for strength rise. Because C_2S hydrates and hardens at a slower rate, it takes one week time to strength gain. Nonetheless C_4AF hydrates apace. The sequence of cement hydration is illustrated in Fig. 1.1.

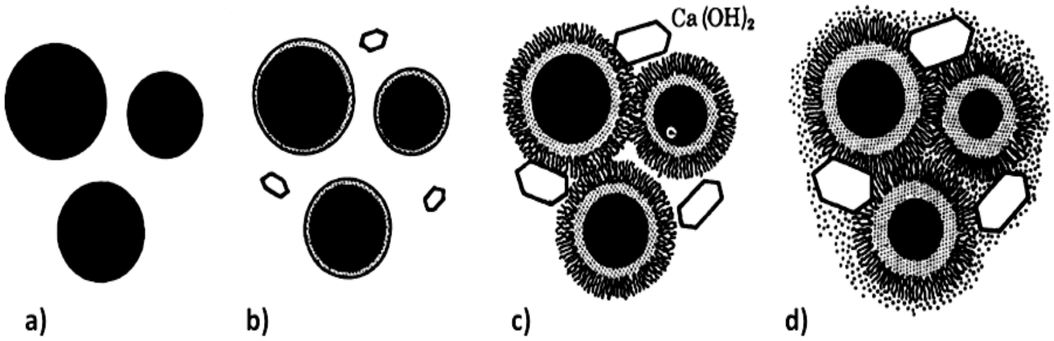

Fig. 1.1: Progression of cement hydration:
Cement particles in water (a); Formation of C-S-H (b); C-S-H growth around the cement grains (c); Fully grown C-S-H and Calcium hydroxide (d).
Adapted from Ref. [2].

1.2. Microstructure of Hardened Cement Paste

Hardened cement paste (HCP) microstructure is represented by various types of solids, and pores with different sizes and shapes. The Calcium-Silicate-Hydrate (C-S-H) gel is the principal hydration product in hardened cement paste responsible for most of the engineering properties. The key aspect of C-S-H gel is the possibility to form a continuous layer that binds together the original cement particles into a cohesive whole. At the same time it is a strong and stable phase. The other hydration products compose the discrete strong crystals, but these crystals don't have the strong connections with the solids phases and hence cannot bring in the overall strength. The possibility of C-S-H gel acting such as a binding phase can be explained from the nano-scale structure. The C-S-H gel represents the evolving porous system with two morphologies.

The C-S-H gel does not take the form of a monolithic solid phase because it gains momentum outward from the particles of cement. However, the C-S-H gel has the internal system of gel pores. These pores are much smaller than the original capillary pores. The water is contained in the gel pores of the C-S-H. This presence of the water can be explained by the effect that the liquid water contained in the gel is physically isolated and is not part of the solid C-S-H phase chemically. Consequently the water does not react with the cement minerals. The C-S-H gel with the internal porous, take a good deal of volume, much more than the original C_3S and C_2S minerals. In the model, C-S-H gel is enlarged tops out giving the continuous phase. Thus there is a first set strength in the formation of a strong solid material. It is important to note that after mixing, the total volume of the cement paste changes weakly, consequently the increasing of the solid phases provide the decreasing of the capillary pores into the system. In the case when water-cement ratio is low, the structure becomes discontinuous. This can really reduces the permeability of the cement paste, i.e. the liquid water and dissolved ions are unable to move easily through the pores of the system.

From the image taken by SEM in backscattered mode shown in Fig. 1.2, two obviously different types of C-S-H gels with the distinct morphologies can be seen. One of these, the C-S-H gel of less dense morphology mainly in the space originally filled by water and other, and the C-S-H gel of more dense morphology mainly in the space originally taken place by cement particles. Based on these characteristics, the two morphologies of C-S-H gels were named "outer" product and "inner" product. In addition, it is possible to distinguish another basic hydration product (calcium hydroxide ($CaOH_2$)), which has a crystalline structure. The other components such as ettringite and monosulfate take an inconspicuous part, and it is generally represented as crystalline with various morphology and size.

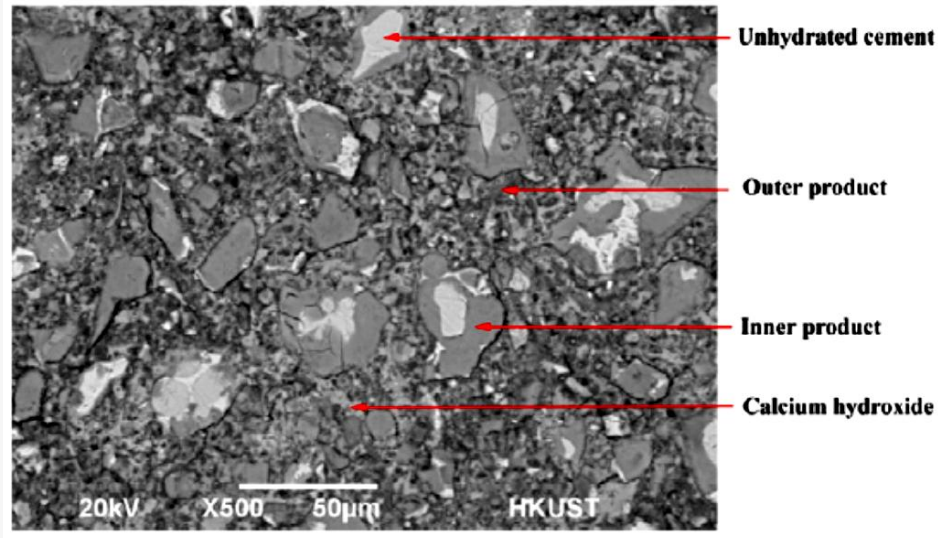

Fig. 1.2. Microstructure of Hardened Cement Paste. Adapted from Ref. [3].

To sum up, it may be noted that the various pores represent another component of the HCP. There are two main classes of the pores. The first class is the pores with diameters less than 10nm, which are meant to be the part of C-S-H gel. The second class is the pores with diameters from 10 nm to 10 µm. This is the large capillary pores. The non-consumed water in the hydration reaction stays in the capillary pores that provide the weakness of concrete. This is due to the fact that there is no strength forming C-S-H bonds. [4] Additionally, the air voids can be present that can give the empty spaces where the pastes have not been properly consolidated. The total volume of pores depends on the water-cement ratio, degree of hydration, curing condition, etc.

1.3. Mineral Analogs and Models of C-S-H Gel

It is possible to identify as a minimum thirty crystalline minerals that have the similar structure with C-S-H gel [5]. For example, afwillite at normal conditions is a thermodynamically C-S-H phase in equilibrium with water and portlantide [6]. C-S-H gel contains tobermorite and jennite structures as shown from the high resolution (transmission electron microscopy) TEM observations. The model of the tobermorite mineral is frequently used to represent the C-S-H gel [7,8].

Tobermorite (Fig. 1.3) is rare, crystalline and natural mineral with the chemical formula $Ca_5Si_6O_{16}(OH)_2{\cdot}4H_2O$. The first discovery concerning tobermorite mineral was in 1880 for in Scotland (the Isle of Mull), around the locality of Tobermory [9].

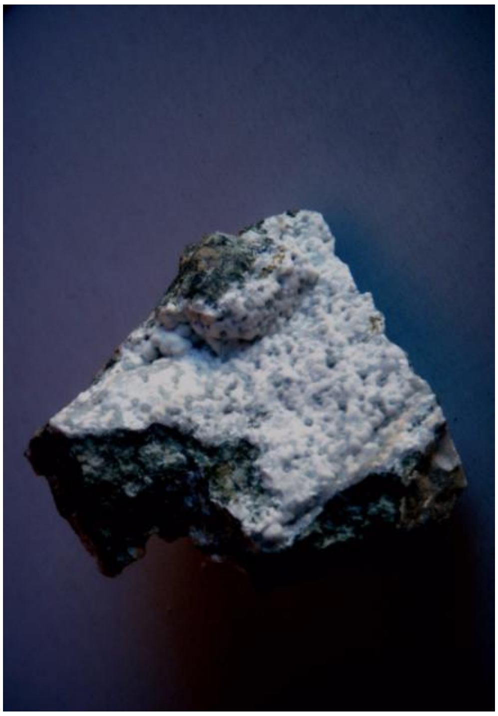

Fig. 1.3. Crystalline mass of tobermorite.
Adapted from Ref. [9].

Tobermorite has several subspecies classified by their different basal spacing as 9.3 Å, 11.3 Å and 14 Å [10], which are usually termed as 9 Å, 11 Å and 14 Å [11] and called Tobermorite 9Å, Tobermorite 11Å and Tobermorite 14Å respectively. This interlayer spacing distance (Fig. 1.4) represent the degree of hydration of tobermorite, which changed by heating. Tobermorite 14Å transforms to Tobermorite 11Å by heating from 80 to 100°C, and further heating at 300°C for few hours gives rise to Tobermorite 9Å. The different techniques such as electron diffraction, electron microscopy, X-ray diffraction and solid-state nuclear magnetic resonance (SSNMR) are used to study the thermal behavior of tobermorite and their corresponding synthetic minerals [10, 12-16].

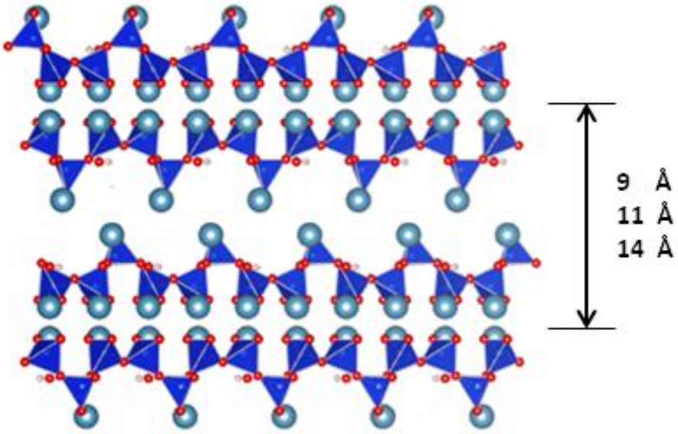

Fig. 1.4. The interlayer spacing distance corresponding to the degrees of tobermorite's hydration.

The model Tobermorite 11Å is the most used model to describe the crystalline C-S-H gel [17-19]. There are two of the most famous models at the atomic level: one model disclosed by Hamid [20] and another one by Merlino et al. [21]. The main specification that differentiates Merlino's model from the one of Hamid's model is the different methods of forming silicate chains (Fig. 1.5).

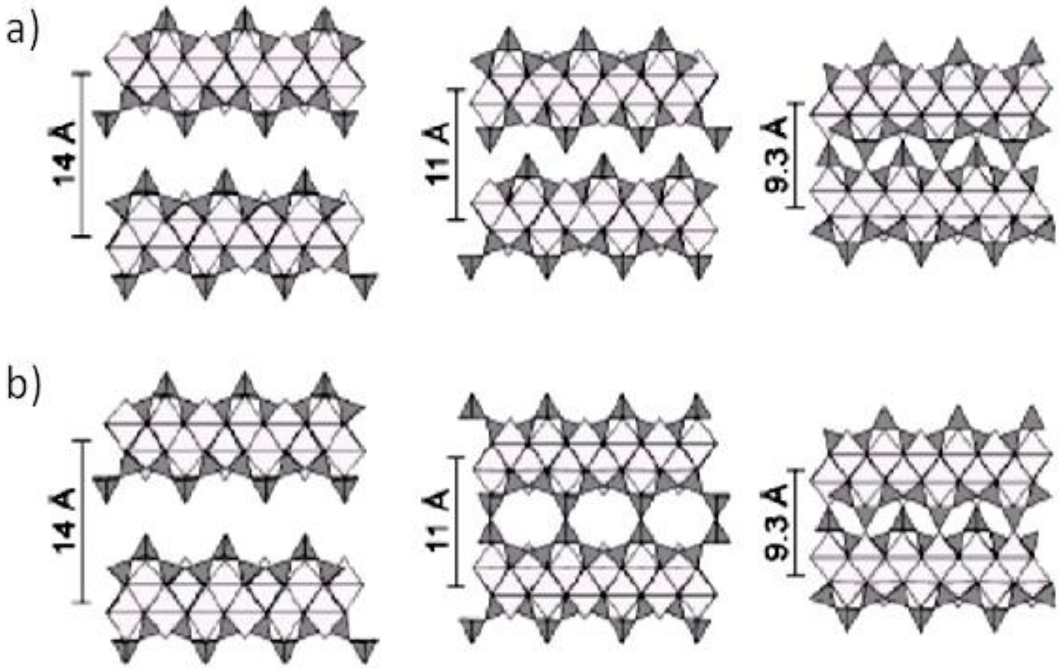

Fig. 1.5. Schematic view of the stable phases of tobermorite with decrease of basal space for: Hamid's model (a) and Merlino's model (b).
Adapted from Ref. [22].

In Hamid's model the structure of independent layers consider the silicate chains of dreieketten type where the periodicity of tetrahedrons during the chain's length is three (Fig. 1.5a). Two tetrahedrons adjacent to silica are associated with the same polyhedron of calcium oxide through their edges. The third tetrahedron is oriented in the direction opposite to the layer of calcium oxide forming a bond with the silica in the chain. In the ideal structure of tobermorite, this chain is saturated by oxygen atom. Therefore when the Ca/Si ratio increases, oxygen atoms are ionized and replaced by calcium ions. By contrast, the Merlino's model have the silicate chains of wollastonite type, i.e. the tetrahedron of silica chemically bonded to each other in manner face to face (Fig. 1.5b). These Si-O-Si chemical linkages that induce the formation of cavities are close to those seen in zeolites [23].

1.4. Carbon and Carbon's Allotropes

Carbon (C) represents a nonmetallic chemical element in Groupe 14 (IVa) of the periodic Table. This element is widespread in nature. However, the carbon is not particularly plentiful. It occupies only about 0.025 percent of Earth crust but carbon forms more compounds than all the other elements taken together [24].

When an element exists in more than one crystalline form, those forms are called allotropes. Diamond and graphite are the two most current allotropes of carbon, yet in recent decades other allotropes and forms of carbon have been discovered. This is graphene, fullerene, nanotube, etc.

Diamond (Fig 1.6a) is a mineral composed of pure carbon, which is formed deep in the mantle and after that it is brought to the surface through kimberlite pipes, lamprophyres, eclogites and other rocks that originate from deep within the mantle. The carbon atoms of diamond are arranged in a variation of the face-centered cubic crystal structure (Fig. 1.6b). It is the most naturally hard material and the most popular gemstone. On the Mohs scale of mineral hardness, the diamond achieves the maximal value of 10. This extreme hardness explains a number of important industrial applications of diamond. Industrial diamond normally has an irregularly shape, flaws, poor color and hence low value as gem. It is used principally in the modern metal working and mining industries as a cutting tool or abrasive material. Another application of the diamond is using them in the jewelry. If, aside from high hardness the diamond has the magnificent brilliance and sparkle, all these characteristics make it unrivalled as gem.

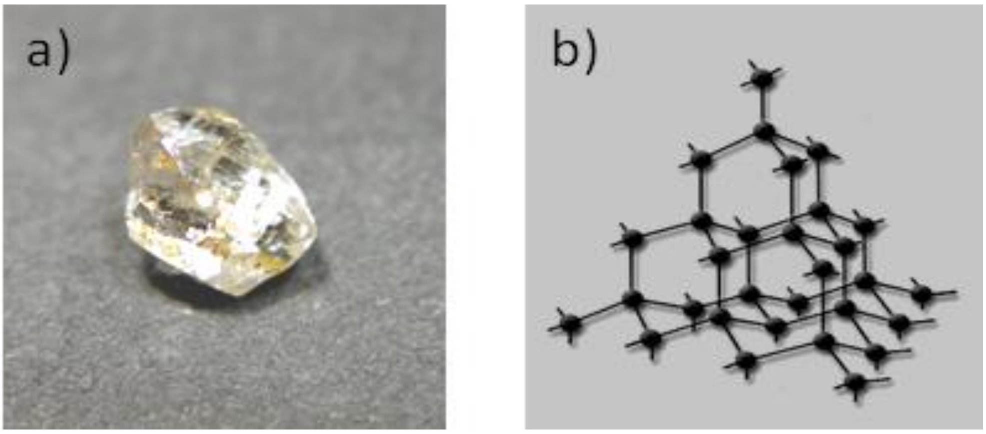

Fig. 1.6. Mineral of diamond. Adapted from Ref. [9] (a); Diamond atomic structure (b).

Another mineral consisting of carbon is **graphite** (Fig 1.7a). Usually it is possible to locate graphite in flakes in metamorphosed rocks riched in carbon. Sometimes it is also possible to find them in veins and in pegmatites. Graphite has a layered structure. This structure is represented by six carbon atoms arranged in widely spaced horizontal sheets, which is called "graphene". The distance between layers of graphite equal 0.3354 nm (Fig 1.7b). Graphite is opaque, very soft mineral having the hardness from 1 to 2 conforming to the requirements of the Mohs scale of mineral hardness. The colors of graphite vary between dark gray to black. Because of the fatness of graphite, it leaves a black mark. This explains the name "Graphite", which originate from the Greek verb "graphein" that means "write". Graphite is used in pencils, lubricants, foundry facing, crucibles, polishes, batteries, brushes for electric motors and cores of nuclear reactors.

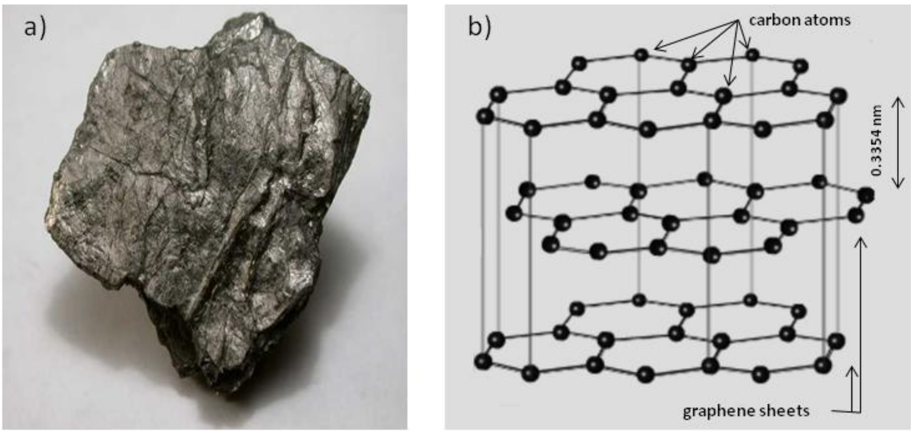

Fig. 1.7. Mineral of graphite. Adapted from Ref. [9] (a); Graphite atomic structure (b).

Graphene is represented such as a layer of carbon atoms, which forms hexagonal lattice with the distance between atoms equal 0.148 nm (Fig 1.8). Graphene is a parent form of all graphitic structures of carbon. For example, graphite is constructed of relatively weakly coupled graphene layers (Fig. 1.7b); carbon nanotube represents the cylinder obtained by the rolling up of the graphene sheet (Fig. 1.11); and fullerene is formed by a pattern of spherical molecules made from graphene with some hexagonal rings replaced by pentagonal rings.

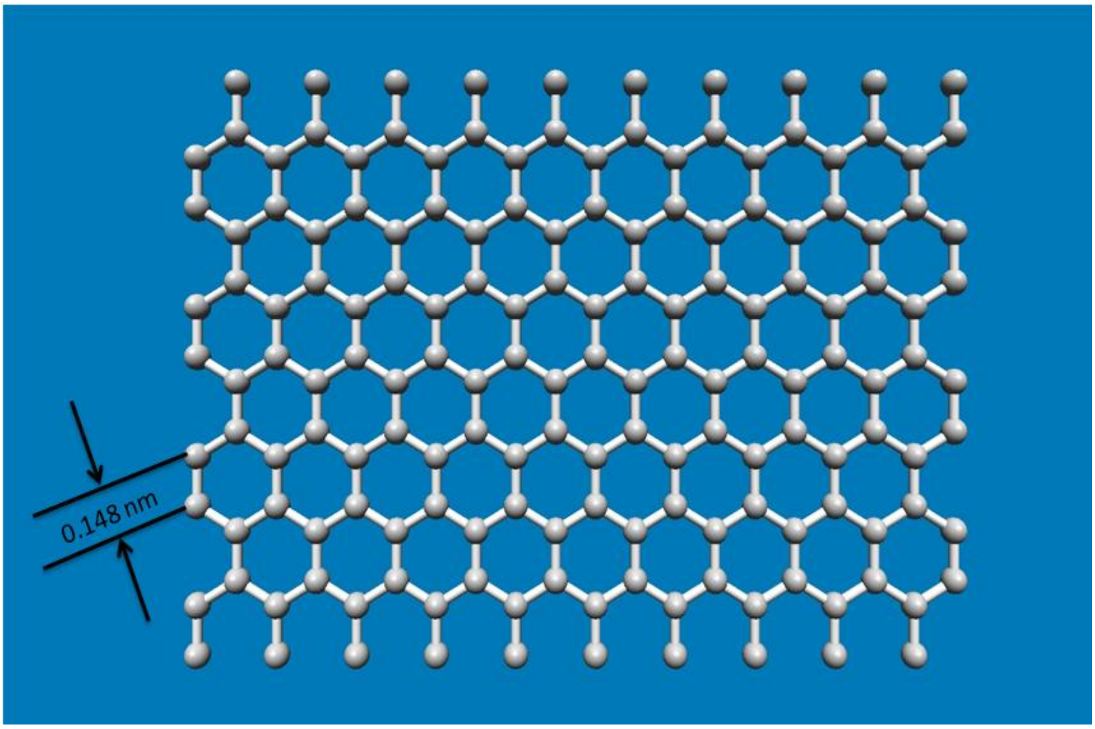

Fig. 1.8. Graphene atomic structure.

The history of the graphene's development is presented in Fig. 1.9. Graphene has many applications in different fields. Using graphene, for example, it is possible to make transistors and other electronic devices with advantage of thinning these devices relative to the devices made of traditional materials. Owing to electrical conducting, transparence, strength and flexibility of graphene, it can be used in touch screens. Possessing the very high thermal conductivity graphene could be used to remove heat from electronic circuits. Also, by virtue of high mechanical strength of graphene it is possible to use them as a scaffold for studying biological molecules and materials. It is important to note that graphene is perspective additive in the construction materials which allow improving various properties.

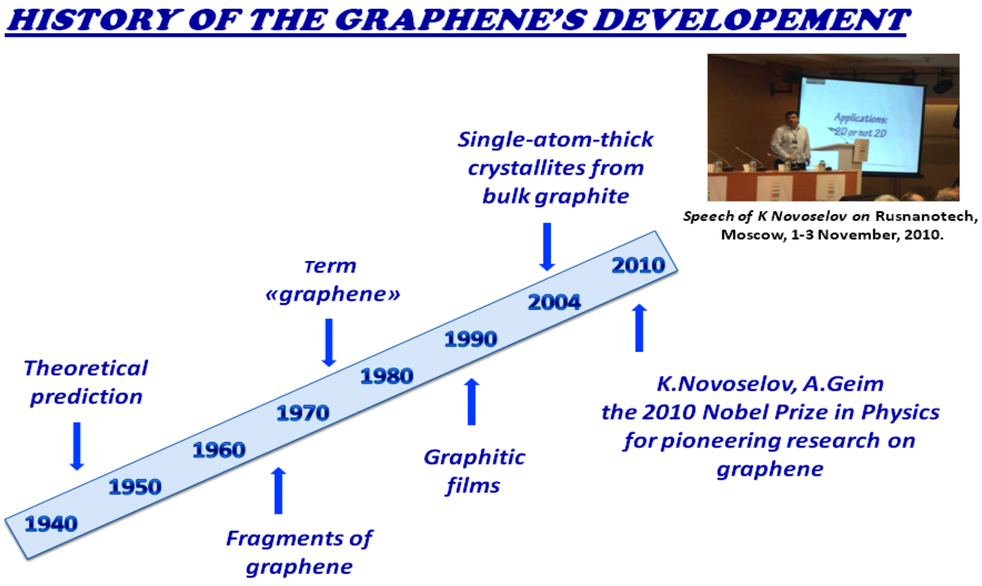

Fig. 1.9. History of the graphene's development.

Fullerene is a molecule of carbon having usually the form of a hollow sphere, ellipsoid, or other shapes. In 1985, the chemists Kroto and Smalley [25] used a laser to vaporize graphite rods in an atmosphere of helium gas. They have found intense peaks corresponding to cluster compounds of carbon into the mass spectrum of graphite vapor. The more stable of them were C_{60} and C_{70}. As a result of structural analysis it was noted that the first one had a form resembling to a football ball and the second had the form resembling to a soccer ball. Later, they were named fullerenes in honor to American architect Buckminster Fuller, who received a patent in 1954 for the type construction in the form of polyhedral spheroids for covering large areas. In process of time, it was obtained the other smaller metastable species, such as C_{28}, C_{36}, and C_{50}.

The form of hollow carbon molecules was new and as contrasted to diamond and graphite, the structure of which is a periodic lattice of atoms, a third form of crystalline carbon (fullerene) is a molecular. C_{60} fullerene (Fig 1.10a) or also named buckminsterfullerene is the molecule C_{60} composing of 60 carbon atoms joined together by single and double bonds to form a hollow sphere with 12 pentagonal and 20 hexagonal faces [25]. C_{70} fullerene (Fig 1.10b) is the fullerene molecule consisting of 70 carbon atoms also joined together by single and double bonds forming 25 hexagons and 12 pentagons faces with a carbon atom at the vertices of each polygon and a bond along each polygon edge.

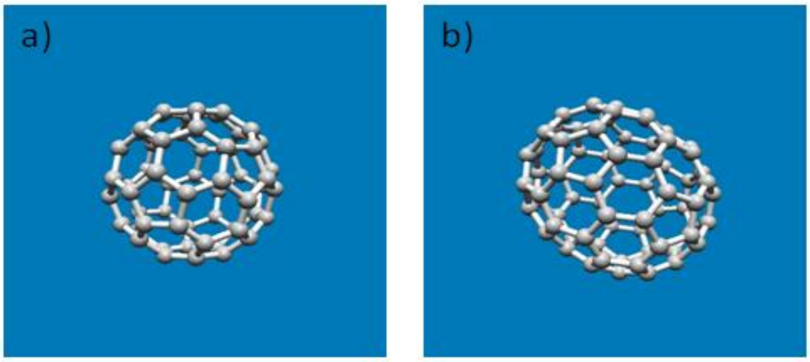

Fig. 1.10. Atomic structure of C_{60} (a) and C_{70} (b) fullerenes.

In 1990 Huffman and Wolfgang Krätschmer announced a simple method for producing macroscopic quantities of fullerenes. For this, they were using an electric arc between two graphite rods in a helium atmosphere to vaporize carbon [26]. Their technique was fairly acceptable for any laboratory that has caused multitudinous studies in this sphere. The fullerene's discovery opens the door for new chapter of nanoscience and nanotechnology.

Carbon nanotube (CNT) is also an allotrope of carbon (Fig 1.11). Since their discovery in 1991 [27], carbon nanotubes (CNTs) possess an exceptional interest from fundamental and practical point of view [28-32]. CNT are chemically stable, mechanically very strong and electrically conductive supramolecules with a diameter smaller than 100 nm, and reaching to the micron-sized length. Because of this, they open up new opportunities for practical application in electronic and photonic devices [33-36], in composites materials [37-39] to different field of the industry.

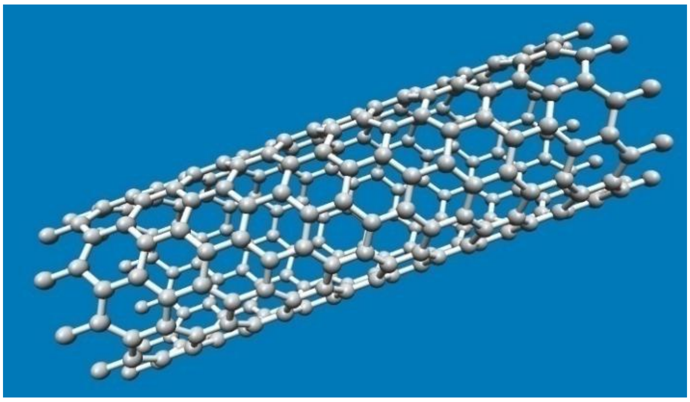

Fig. 1.11. Atomic structure of carbon nanotube.

Ideal CNT can be presented like a fragment of the monolayer of graphite or, in other words, graphene rolling up to the cylinder or tube form. Generally, carbon nanotubes can be classified by the number of tubes, length and chirality. In a number equal to the number of tube, three types of nanotubes can be identified: Single Walled Carbon Nanotubes (SWCNTs), Double Walled Carbon Nanotubes (DWCNTs) and Multi Walled Carbon Nanotubes (MWCNTs). SWNTs have only one single layer of graphene cylinder (Fig. 1.12a), correspondingly DWNTs have two layer of graphene cylinder (Fig.1.12b) and MWNTs have many layers of graphene cylinder (Fig. 1.12c).

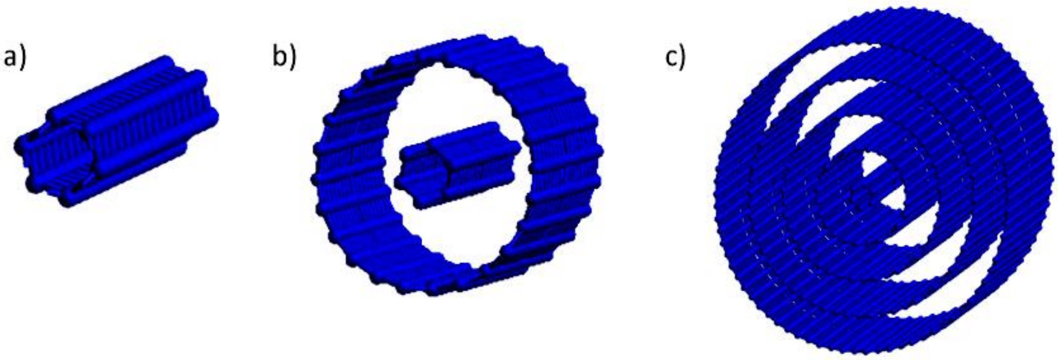

Fig. 1.12. Structure of the Single Walled Carbon Nanotube (a); Double Walled Carbon Nanotube (b); Multi Walled Carbon Nanotube (c).

Depending on the rolling up direction of 2-dimensional layer of carbon atoms, SWCNT has different conformations, which are determined by chiral angle θ and chiral vector C_h:

$$\theta = \arctan\left(-\frac{\sqrt{3}m}{2n+m}\right), \qquad (1)$$

$$C_h = n \times \overrightarrow{a_1} + m \times \overrightarrow{a_2}, \qquad (2)$$

where m, n are the integers; and $\overrightarrow{a_1}$, $\overrightarrow{a_2}$ are the unit vectors.

The rolling up of the graphene sheet (Fig. 1.13a) is performed in such a way that the two points connected by the chiral vector coincide with each other. The number of possible chiral vectors determined by a combination of the integers m and n. These integers determine the chirality of CNT, obtained by folding the graphene sheet along the appropriate vector. “Zigzag” ($m \neq 0$, $n = 0$) and “Armchair” (m = n ≠ 0) are two common types of nanotubes based on the manner the graphene sheet can be folded to form CNT, as shown in Fig 1.13b.

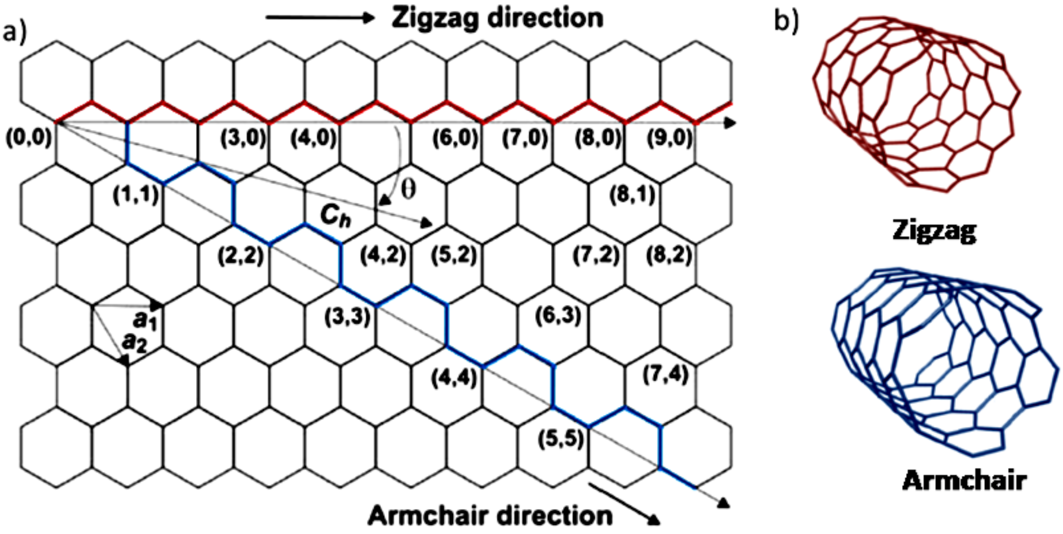

Fig. 1.13. Structure of the 2-dimensional lattice of graphene sheet and its main geometrical characteristics (a); Zigzag and armchair nanotube's forms (b).

References

[1] P. Barnes, J. Bensted, Structure and Performance of Cements, Second Edition, London: CRC Press, 2001.

[2] D. Double, P. C. Hewlett, K. S. Sing, J. F. Raffle, New developments in understanding the chemistry of cement hydration, Phil. Trans. R. Soc. A 310 (1983) 53–66.

[3] C. Hu, Y. Gao, B. Chen, Y. Zhang, Z. Li, Estimation of the poroelastic properties of calcium-silicate-hydrate (C-S-H) gel, Mater. Des. 92 (2016) 107–113.

[4] E. J. Garboczi, D. P. Bentz, Microstructure Property Relationships in Concrete: From Nanometers to Centimeters, in: 2nd Canmet/ACI. Advances in Concrete Technology. International Symposium. Supplementary Papers, Las Vegas, NV, Malhotra,1995.

[5] I. G. Richardson, The calcium silicate hydrates, Cem. Concr. Res. 38 (2008) 37–158.

[6] J. P. Long, J. C. McConell, A mineral application of X-ray absorption microspectroscopy: the hydration of larnite, Mineral Mag. 32 (10) (1958) 117–127.

[7] N. J.Coleman, C. J. Trice, J. W.Nicholson, 11Å tobermorite from cement bypass dust and waste container glass: A feasibility study, Int. J. Miner. Process. 93(1) (2009) 73-78.

[8] A. Gmira, R. J. M. Pellenq, I. Rannou, L. Duclaux, C. Clinard, T. Cacciagueura, N. Lequeux, H. Van Damme, A structural study of dehydration/rehydration of tobermorite, a model cement compound, Stud. Surf. Sci. Catal. 144 (2002) 601-608.

[9] Mindat.org and the Hudson Institute of Mineralogy 1993-2016. Retrieved from http://www.mindat.org/min-3985.html/

[10] J. D. C. McConnell, The hydrated calcium silicates riversideite, tobermorite, and plombierite, Mineral Mag. 30 (1954) 293–305.

[11] E. Bonnacorsi, S. Merlino, Modular microporous minerals: cancrinite-davyne group and C-S-H phases, Rev. Mineral. Geochem. 57 (2005) 241–290.

[12] X. Cong, R. J. Kirkpatrick, ^{29}Si and ^{17}O NMR investigation of the structure of some crystalline calcium silicate hydrates, Adv. Cem. Based Mater. 3 (1996) 133–143.

[13] S. Komarneni, D. M. Roy, C. A. Fyfe, G. J. Kennedy, Naturally occurring 1.4 nm tobermorite and synthetic jennite: characterization by ^{27}Al and ^{29}Si MASNMR spectroscopy and cation exchange properties, Cem. Concr. Res. 17 (6) (1987) 891–895.

[14] T. Maeshima, H. Noma, M. Sakiyama, T. Mitsuda, Natural 1.1 and 1.4 nm tobermorites from Fuka, Okayama, Japan: chemical analysis, cell dimensions, ^{29}Si NMR and thermal behavior, Cem. Concr. Res. 33 (10) (2003) 1515–1523.

[15] W. Wieker, A. R. Grimmer, A. Winkler, M. Mägi, M. Tarmak, E.Lippmaa, Solid-state high-resolution ^{29}Si NMR spectroscopy of synthetic 14 Å, 11 Å and 9 Å tobermorites, Cem. Concr. Res. 12 (3) (1982) 333–339.

[16] P. Yu, R. J. Kirkpatrick, Thermal dehydration of tobermorite and jennite, Concr. Sci. Eng. 1 (1999) 185–191.

[17] A. Zaoui, Insight into elastic behavior of calcium silicate hydrated oxide (C-S-H) under pressure and composition effect, Cem. Concr. Res. 42 (2) (2012) 306–312.

[18] D. Hou, Z. Li, Molecular dynamics study of water and ions transport in nano-pore of layered structure: A case study of tobermorite, Microporous Mesoporous Mater. 195 (2014) 9–20.

[19] S. Wang, X. Peng, L. Tang, L. Zeng, C. Lan, Influence of inorganic admixtures on the 11 Å-tobermorite formation prepared from steel slags: XRD and FTIR analysis, Constr. Build. Mater. 60 (2014) 42–47.

[20] S. R. Hamid, The Crystal Structure of the 11A Natural Tobermorite Ca2.25[Si3O7.5(OH)1.5].1H2O, Zeitschrift für Kristallographie, 154 (1981) 189-198.

[21] S. Merlino, E. Bonaccorsi, T. Armbruster, Tobermorites: Their real structure and order-disorder (OD) character, Am. Mineral. 84 (1999) 1613–1621.

[22] A.Gmira, M. Zabat, R. J. M. Pellenq, H. Van Damme, Microscopic physical basis of the poromechanical behavior of cement-based materials. Mater. Struct. 37 (2004) 3–14.

[23] R. J. M. Pellenq, N. Lequeux, H. Van Dammen, Engineering the bonding scheme in C-S-H: the iono-covalent framework, Cem. Concr. Res. 38 (2008) 159–174.

[24] Encyclopædia Britannica, Inc, 2016. Retrieved from https://global.britannica.com/science/carbon-chemical-element/

[25] H. W. Kroto, J. R. Heath, S. C. O'Brein, R. F. Curl, R. E. Smalley, C60:Buckminsterfullerene, Nature, 318 (6042) (1985) 162–163.

[26] W. Krätschmer, L. D. Lamb, K. Fostiropoulos, D. R. Huffman, Solid C_{60} : a new form of carbon, Nature, 347 (1990) 3535–3358.

[27] S. Iijima, Helical microtubules of graphitic carbon, Nature, 354 (1991) 56–58.

[28] C. N. R. Rao, B. C. Satishkumar, A. Govindaraj, M. Nath, Nanotubes, ChemPhysChem, 2 (2001) 78–105.

[29] T. D. Burchell, Carbon Materials for Advanced Technologies, Amsterdam: Pergamon, 1999.

[30] J. Jortner, C. N. R. Rao, Pure Appl. Chem. 74 (9) (2002) 1491–1506.

[31] M. S. Dresselhaus, G. Dresselhaus, P. Avouris, Carbon Nanotubes: Synthesis, Structure, Properties, and Applications, Berlin: Springer – Verlag, 2001.

[32] S. Reich, C. Thomsen, J. Maultzsch, Carbon Nanotubes: Basic Concepts and Physical Properties, Weinheim: Wiley-VCH Verlag, 2004.

[33] V. M. Harik, Mechanics of carbon nanotubes: applicability of the continuum-beam models, Comput. Mater. Sci. 24 (2002) 328–342.

[34] H. Lu, L. Zhang, Analysis of localized failure of single-wall carbon nanotubes, Comput. Mater. Sci. 35(4) (2006) 432–441.

[35] K. Kashiwagi, S. Yamashita, Y. Nasu, H. Yaguchi, C. S. Goh, S. Y. Set, Planar waveguide-type saturable absorber based on carbon nanotubes, Appl. Phys. Lett. 89 (2006) 081125–081127.

[36] A. Martinez, S. Uchida, Y. W. Song, T. Ishigure, S. Yamashita, Fabrication of carbon nanotube-nolymethyl-methacrylate composites for nonlinear photonic devices, Opt. Express 16 (2008) 11337–11343.

[37] D. Micheli, R. Pastore, A. Vricella, R. B. Morles, M. Marchetti, A. Delfini, F. Moglie, V. M. Primiani, Electromagnetic characterization and shielding effectiveness of concrete composite reinforced with carbon nanotubes in the mobile phones frequency band, Mater. Sci. Eng. B 188 (2014) 119–129.

[38] Z. Terzopoulou, D. N. Bikiaris, K. S. Triantafyllidis, G. Potsi, D. Gournis, G. Z. Papageorgiou, P. Rudolf, Mechanical, thermal and decomposition behavior of poly(ε-caprolactone) nanocomposites with clay-supported carbon nanotube hybrids, Thermochim. Acta 642 (2016) 67–80.

[39] T. Ji, Y. Feng, M. Qin, W. Feng, Thermal conducting properties of aligned carbon nanotubes and their polymer composites, Composites Part A 91 (1) (2016) 351–369.

CHAPTER 2: THEORETICAL BACKGROUND

2.1. Molecular Modeling Status in Modern Science

Since the mid-1990s, molecular modeling, as one of the most powerful approaches and methods of computer analysis, has acquired exceptional importance in physics, biochemistry and nanotechnology research. Accuracy, efficiency, a direct comparison with experiment and increasing with each passing year computation capacity make the methods of molecular modeling an indispensable tool in science and technology. The key to determine the nature of the majority of macroscopic natural phenomena lies precisely in the knowledge of the laws of the processes taking place in the atomic and molecular level. Today, the use of methods of molecular modeling has reached the point at which it is possible to provide a real view of the processes and mechanisms that occur in physical, chemical and biological systems. Moreover, molecular modeling is one of the fastest growing fields in science. It can be described as the employment of computational techniques to construct molecules and perform a variety of calculations on these molecules in order to predict their chemical and physical characteristics. Summing it up, molecular modeling allows to determine the information about the molecule or a system of molecules, such as chemical structure, number and type of atoms, bonds, bond lengths, angles and dihedral angles; properties, i.e. molecular energy, bulk, shear, Young's, stress moduli, Poisson ratio, elastic constants et etc; and its activity, i.e. chemical reaction with other molecules such as bond break, bond formation. All this, can help to understand the experimental observation or predict experimental results.

2.2. Introduction to Molecular Dynamics

As mentioned above, Molecular Dynamics (MD) is one of the most powerful computational methods, effectively used for the simulation of physical and biological systems [1]. It allows computing trajectories of individual atoms and the polymer chains, investigates the dynamics of the interaction of particles in condensed systems at the molecular level [2, 3]. MD has a high time-space resolution and provides information about the processes occurring in atomic and molecular level, and at times of the order of a few nanoseconds [4, 5]. This method is particularly useful for the study of physical systems and biochemical macromolecules on a scale where quantum effects are less significant than the electrostatic interactions [6-8]. The first mention of the Molecular Dynamics method is given in Ref. [9]. Modern development of computer technology allows to model the dynamics of molecular systems consisting of a large number of particles from tens to thousands up to millions, with a large set of parameters, and a variety of conditions that simulate the physical experiment. For all those reasons and advantages of this method, we have used it along this thesis.

Firstly, to perform MD simulation it is necessary to prepare the specimen containing N particles (atoms). In order to describe the motion of atoms or particles we solve Newton's equation of motion for this system. Molecular dynamic methods normally generate atomic trajectories such as atomic positions, velocities. If the atomic positions and velocities of the individual atoms are known, then the properties of system can be determined. To compute the atomic trajectories, the interaction model should be involved. Giving the special condition such as boundary conditions and necessary ensemble we equilibrate the system until the properties do not change with time.

Equations of motion and force field potentials

Molecular Dynamics, in its simplified understanding, is based on the well-known equation of classical mechanics, i.e. the second equation of Newton's law:

$$m_i a_i = F_i \qquad \text{or} \qquad m_i \frac{d^2 r_i(t)}{dt^2} = F_i(r),\ i = 1,2,\dots,n \tag{1}$$

which determine the relationship of the three quantities $\{r_i, m_i, F_i\}$ – spatial position or the radius vector of the atom, mass and force with time. Spatial position $r = \{r_1, r_2, \dots, r_n\}$ determines the topology of the potential molecular field $U(r)$, upon which the force can be estimated:

$$F_i(r) = -\frac{\partial U(r)}{\partial r_i} \tag{2}$$

Fig. 2.1 illustrates the topology of the potential field. This chart shows the mutual alignment or the chemical bonds of a system of four atoms.

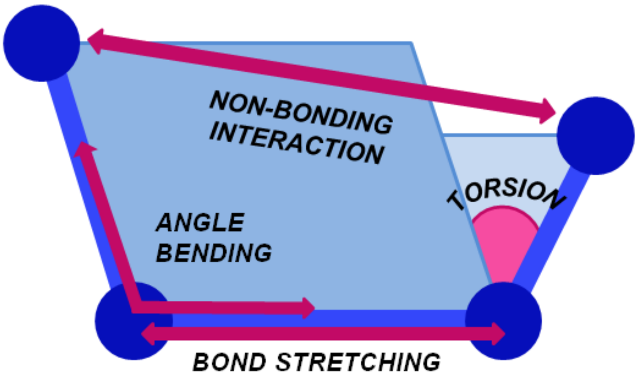

Fig. 2.1. Schematic view of chemical bonding of atoms.

Chemical molecule is marked by the presence of the bond stretching of two atoms, the angle bending of three atoms and the torsion of four atoms. There is also the participation of non-bonding interactions of Van der Waals, and if atoms have the charge there are the Coulomb interactions. Thus, through Molecular Dynamics method, it is possible to effectively simulate a variety of systems, from the simple atomic and molecular fragments to the most complex integrated systems. From this perspective the total potential of the system is determinate by summing up the potential energy associated with all types of interactions. The total potential energy of a chemical molecule U is composed as follows:

$$U = U^{bonded} + U^{nonbonded} , \tag{3}$$

$$U^{bonded} = U^{bond-stretch} + U^{bond-angle} + U^{\ torsion} , \tag{4}$$

$$U^{nonbonded} = U^{VanderWaals} + U^{Coulomb} , \tag{5}$$

where U^{bonded} represents the potential of bonding interaction. More specifically $U^{bond-stretch}$ (U_b) is the potential of the bond stretching of two atoms; $U^{bond-angle}$ (U_θ) is the potential of the angle bending of three atoms; $U^{\ torsion}(U_\varphi)$ is the potential of the torsion of four atoms. $U^{nonbonded}$ introduces potential of bonding interaction, $U^{VanderWaals}$ is the potential of Van der Waals interactions; $U^{Coulomb}(U_{el})$ is the Coulomb interactions.

In the above example of system of four atoms one can summarize in mathematical form of these potentials. The valence link is described by the spring form as:

$$U_b = \frac{1}{2}\sum_{b} K_b\,(r - b_0)^2 \tag{6}$$

where r is the distance between two atoms, b_0 is the equilibrium length of bond, and K_b is the coefficient of bonding stretch.

The valence angles are given by following potential:

$$U_\theta = \frac{1}{2}\sum_{\theta} K_\theta\,(\theta - \theta_0)^2\,, \tag{7}$$

where K_θ is effective elasticity of the valence angle, θ is the value of valence angle, and θ_0 is the equilibrium value of valence angle.

The potential of torsion interactions (harmonic bonding) is presented by the formula:

$$U_\varphi = \frac{1}{2}\sum_{\varphi} K_\phi\,[\cos(n\varphi - \delta) + 1] \tag{8}$$

where K_ϕ is a constant, $n\varphi$ is the multiplicity factor, and δ is the harmonic contribution in the potential of torsion angle.

There are several pair potentials representing the Van der Waals interaction. One of the most usual formulas is Lennard-Jones potential:

$$U_{LJ} = 4\epsilon\left[\left(\frac{\sigma}{r_{ij}}\right)^{12} - \left(\frac{\sigma}{r_{ij}}\right)^{6}\right], \tag{9}$$

where σ is the effective atom’s diameter, ϵ is depth parameter, and r_{ij} is the distance between atoms.

Buckingham potential can also characterize the Van der Waals interactions:

$$U_{BUCK} = Aexp\left(-\frac{r_{ij}}{\rho}\right) - \frac{C}{r_{ij}^6}, \tag{10}$$

where A is the amplitude, and ρ is the effective range.

Another example of potential, which describes the Van der Waals interaction is Born–Mayer–Huggins potential:

$$U_{BMH} = Aexp\,[B(\sigma - r)] - \frac{C}{r_{ij}^6} - \frac{D}{r_{ij}^8}\ , \tag{11}$$

where A, B, C, D, σ are constant parameters determined empirically or on the basis of simulative calculations.

Electrostatic interactions are given by Coulomb potential:

$$U_{el} = \sum_{LJ} \frac{q_i q_j}{\varepsilon r_{ij}} \tag{12}$$

where $q_i q_j$ are partial charges on atoms, and ε is dielectric constant of a medium . Some of the potential interactions of atoms are illustrated in Fig. 2.2.

The calculation of coordinates and velocities of the atoms is performed using the integration algorithm of equations of motion with preset conditions. Thus, the numerical solution of equations (1) can be found if the positions and velocities of all particles in the initial moment are known. For that it is enough to present the Taylor expansion of the coordinates and velocities and use the equation (1):

$$r_i(t+\Delta t) = r_i(t) + v_i(t)\Delta t + \frac{1}{2}a_i(t)\Delta t^2 \tag{13}$$
$$v_i(t+\Delta t) = v_i(t) + a_i(t)\Delta t\ ,$$

where $a_i = \frac{F_i}{m}$ is acceleration of particle i.

There are various algorithms for solving the equations (1). The Algorithm of Verlet is the most widely used and simple algorithm [10]:

$$r_i(t+\Delta t) = r_i(t) + v_i(t)\Delta t + \frac{1}{2}a_i(t)\Delta t^2 \tag{14}$$
$$v_i(t+\Delta t) = v_i(t) + \frac{1}{2}[a_i\,(t) + a_i(t+\Delta t)]\Delta t\ ,$$

Knowing the coordinates, velocities and accelerations of the particle at time t, we determine -first- the coordinates at the time $(t + \Delta t)$ (fist equation (14)), after that, through the equation (2), we calculate the acceleration at $(t + \Delta t)$ via the already obtained coordinates. Finally, using the second part of the equation (14), we calculate the velocities at $(t + \Delta t)$.

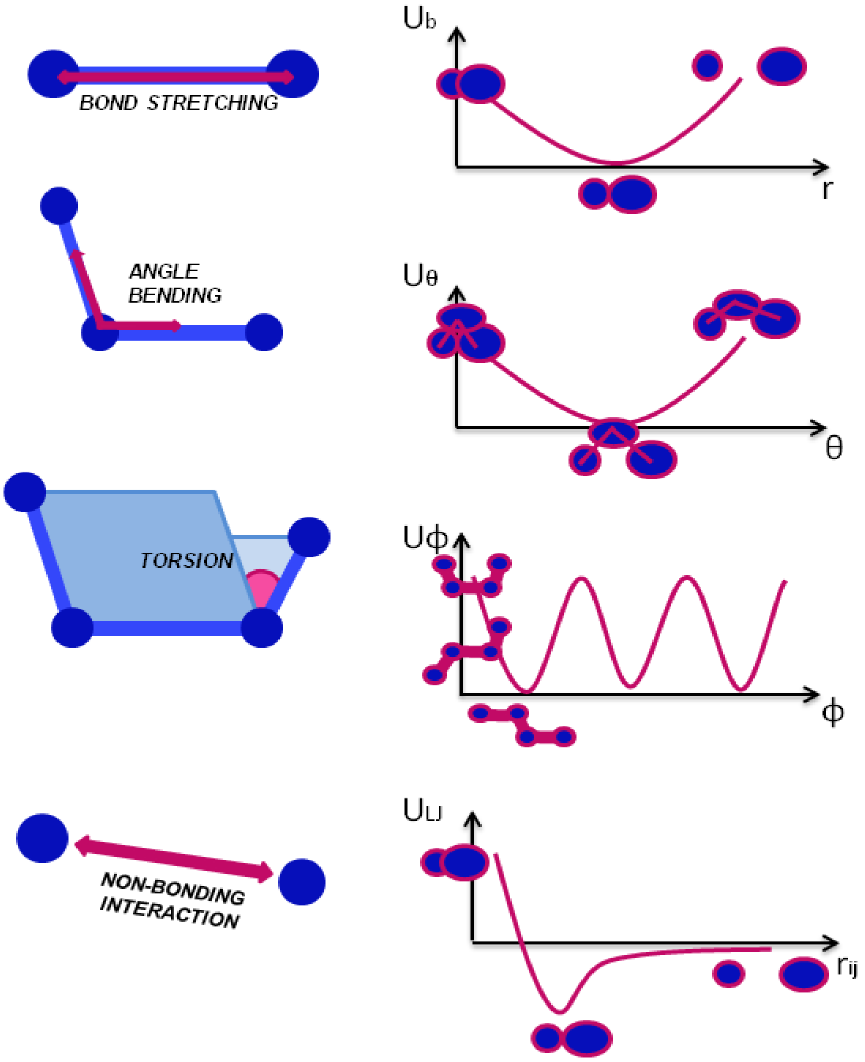

Fig. 2.2. Schematic views and graphs of the various potential interactions of atoms.

After the modeling step, it is possible to handle the next steps of Molecular Dynamics simulation, i.e.:

1. Specification of the initial positions and velocities of the particles.
2. Calculation of the local minimum on the global potential energy of the system.

3. Definition the new positions and velocities using one of the algorithms, as described above.

4. Repetition of the procedures from step 2 until convergence.

Several other examples of the genetic algorithm used to find the minimum energy structure for the present material are shown below.

The most computationally expensive step utilized to perform the energy minimization is a Newton-Raphson Method. The potential energy of a system can be expressed by a Taylor series at the current geometry and the equation for updating the geometry such as:

$$X_{new} = X_{old} - \frac{E^{'}(X_{old})}{E^{"}(X_{old})} \tag{15}$$

where X_{new} is the value of the geometry at the next step, and X_{old} is the value of the geometry at the current step, E is the potential energy.

It is important to note that the correction term depends on the first derivate of the potential energy surface at the current geometry and also on the second derivate of the surface potential energy. It is necessary to calculate these derivatives at each step, what makes the Newton-Raphson Method very expensive. Moreover, it is needed the fewest steps to achieve the minimum in this method.

In the Newton-Raphson Method much of the time is spent in inverting the Hessian matrix and by virtue of the fact that the changes in the Hessian matrix are very small for every step and thus it is waste of time. However, in the Broyden-Flether-Golgfarb-Shanno (BFGS) Method this problem can be avoided. In BFGS Method the inversion of Hessian matrix is modified suitably at every time step instead of recalculating the inversion of Hessian matrix. The BFGS algorithm is rated as one of the most efficient method used in the optimization studies. This method is very efficient when it is used for smaller system and less number of variables.

The Steepest Descent Method is quite effective when the initial configuration is far away from the minimum energy configuration. This method depends on the approximation, and second derivative is assumed to be constant. The equation to update the geometry becomes as:

$$X_{new} = X_{old} - \gamma\, E'(X_{old}) \tag{16}$$

where γ is a constant.

This method is faster than the Newton-Raphson one, because the gradients at each point should be calculated without requiring calculation of the second derivatives. This is called the Steepest Descent Method because the direction in which the geometry is first minimized is the direction where the gradient is largest at the initial point. Once the minimum in the first direction is achieved, a second minimization starts from that point and moves in the steepest remaining direction. This process continues for so long until a minimum is achieved in all directions to within a sufficient tolerance.

The *Conjugate Gradient Method* is based on the aspect that the first portion of the search takes place in the direction of the largest gradient, like in the Steepest Descent method. Nevertheless, Conjugate Gradient Method also uses the previous direction in the next search to present some fluctuation that often upset the Steepest Descend Method as it moves toward the minimum. The residuals calculated in the Conjugate Gradient Method are orthogonal to preceding directional search vectors. This aspect assures of the fresh and independent directional search vector throughout the iteration process until such time as the residue becomes zero. This allows the method to move rapidly to the minimum [11].

After the modeling of the system is prepared, we can proceed to the stage of the MD simulation. Sometimes, while the integration of the equations of motion allows exploring the constant-energy surface of a system, it is interesting to keep the temperature and pressure of the system constant during the molecular simulation, to mimic experimental conditions. In order to accomplish this there are several ensembles used in MD simulation.

Ensembles

There are various ensembles used for the MD simulation. Let us describe some of them thereafter.

The NVE ensemble, also named as a microcanonical ensemble, is an ensemble where the number of particles (N), the energy (E) and the volume (V) of the system are constants. The NVE ensemble got by resolving Newton's equation without any temperature and pressure control with conservation of the energy when this ensemble is generated. The simulation where the energy is maintained constant is not preferable for equilibration. This is due to the fact that without the energy flow facilitated by the temperature control methods, the desired temperature cannot be attained. At the same time, for example, if the goal is a study of the constant-energy surface of the conformational space or for other reasons where we don't want the perturbation introduced by temperature and pressure bath coupling, this ensemble can be useful.

The NVT ensemble, also known as a canonical ensemble, is an ensemble where the number of particles (N), the volume (V) and the temperature (T) of the system are constants. The ensemble is obtained by controlling the temperature via direct scaling during the initialization stage and by temperature-bath coupling during the data collection phase. The volume is kept constant during the simulation. It can be useful to exploit this ensemble in the cases when conformational searches of molecules are carried out in vacuum without periodic boundary conditions. The volume, pressure, and density are not defined without periodic boundary conditions. Dynamics constant-pressure cannot be performed. Even if periodic boundary conditions are presented but the pressure is not a significant factor, the NVT ensemble provides the advantage of less perturbation of the trajectory, via to the absence of coupling to a pressure bath.

The NPT ensemble also refers to an isothermal-isobaric ensemble. It is an ensemble where the number of particles (N), the pressure (V) and the temperature (T) of the system are constants. It stands to reason that, this ensemble allows control over both the temperature and pressure. The unit cell vectors are allowed to change and the pressure is arranged by adjusting the volume. This ensemble is used when the correct pressure, volume, and densities are important during the simulation. It can be also performed during equilibration to achieve the needful temperature and pressure before changing to the NVE or NVT ensemble when data collection starts.

Thermostats and Barostats

In the context of a physical or chemical experiment, the samples are often exposed to some heat treatment or to external pressure. Therefore, modeling should also be carried out in conditions as close as possible to the realities of experiment. In the molecular modeling, this role is played by variety algorithms of implementation of the barostat or thermostat. Thereafter, we present few of them, which are described in details in Refs. [12, 13].

For the purpose of relaxation (equilibration) of a system in the conditions of the predetermined external temperature, the molecular system is placed into contact with the thermal reservoir (thermostat). Usually, the interaction with the thermostat is modeled by addition the force of friction:

$$Q_\alpha = m_\alpha \mu(t) v_\alpha \tag{17}$$

where m_α is mass of particle, v_α is velocity of particle, and $\mu(t)$ is a coefficient chosen in such a way that the force provides the change of the system energy according to:

$$\frac{\partial E}{\partial t} = \frac{1}{t_E} K - E_K(t) \tag{18}$$

where E is the energy of isolated system (if there is no interaction with the reservoir it is preserving), t_E is time of interaction with the reservoir (the time of relaxation of the system until the temperature of off-site tankage; under normal conditions it is taken in the range values [0.5, 2] ps), E_K is the kinetic energy of the system setting the temperature T, and K is a constant equal to the average kinetic energy corresponding to the temperature of the reservoir T_0. The values of E_K and K are calculated by following equations:

$$E_K = \sum_{\alpha=1}^{N} m_\alpha \, (v_\alpha)^2 \tag{19}$$

$$K = \frac{3}{2} N k_B T_0 \tag{20}$$

where N is the number of atoms, and k_B is Boltzmann constant.

From equations of motion we will have the following form ($\alpha = 1, 2, \dots, n$):

$$\frac{\partial}{\partial t} p_\alpha = -\frac{\partial U}{\partial x_\alpha} + \mu(t) m_\alpha v_\alpha \tag{21}$$

$$m_\alpha \frac{\partial}{\partial t} x_\alpha = \ p_\alpha \tag{22}$$

$$\mu = \frac{1}{2t_E}\left(\frac{K}{E_K(t)} - 1\right) \tag{23}$$

where p_α is a kinetic momentum of particle, x_α is the atom's coordinate.

The calculation of trajectories in Molecular Dynamics, through these equations, is called "weak coupling to an external bath". This simulation method of thermal reservoir is also known as Berendsen thermostat method. Berendsen algorithm is widely used for MD simulation of molecules with a large number of degrees of freedom, for systems with small number of atoms it does not work. Nose-Hoover thermostat is another algorithm, which is also widely used in molecular dynamic simulations. The Nose-Hoover thermostat keeps the energy of the system, but does not preserve the total momentum, and the Berendsen termostat keep the total momentum of the system or the total amount of motion but not the energy.

The comparison of the Nose-Hoover thermostat and Berendsen thermostat clearly shows the similarities, at the same time, a slight difference related to unequal role of the coefficient of friction. The coefficient of friction in the Nose-Hoover thermostat contributes as an additional term; while in the Berendsen thermostat, the coefficient of friction is a speed factor. This small difference in mathematical notation generates a deep difference in the physical interpretation showing that the Nose-Hoover thermostat and Berendsen thermostat differently conserve the energy and total momentum of the system. However, it should be emphasized that in the case of an isolated system, the total momentum and angular momentum are maintained. In addition, the total energy is preserved, and the temperature is obtained by averaging the temperature values T(t) over some interval of time.

Periodic boundary conditions

The main goal of computer molecular modeling is to bring step by step the system, consisting usually of a large ensemble of particles to thermodynamic equilibrium (relaxed) state. The calculation of an equilibrium state of the system is the essence, and at the same time, a huge difficulty faced by computer methods of molecular analysis. Computer simulations are usually carried out on a moderately small number of particles, 10≤N≤10000 [13]. The following diagram (Fig.2.3) shows a triangle, which represents a dependence of the number of particles N on the relaxation time t. From this triangle we can see that with an increase of atom's number the time interval decreases, i.e. it is harder to achieve a relaxation time with the increasing of the number of particles in the system. However, from year to year, the necessity to cover a growing size of molecular system is increased. It's self-evident that such simulations cannot be performed by any computer. This problem of limit of simulation box can be solved by using periodic boundary conditions.

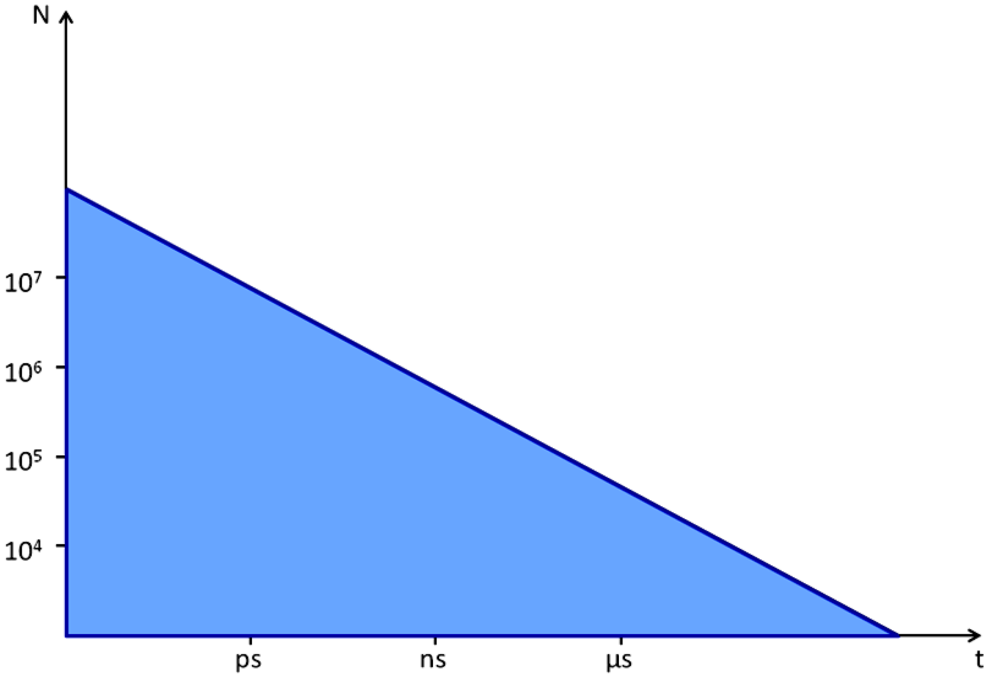

Fig. 2.3. Triangle of dependence of the number of particles N on the relaxation time t.

Fig. 2.4 demonstrates the principle of periodic boundary conditions. If for the selected atom 1 the distance to the interacting atom 2 would be more than half of the length of the MD box, then the atom 2 is eliminated, and instead its periodic image 2* is taken.

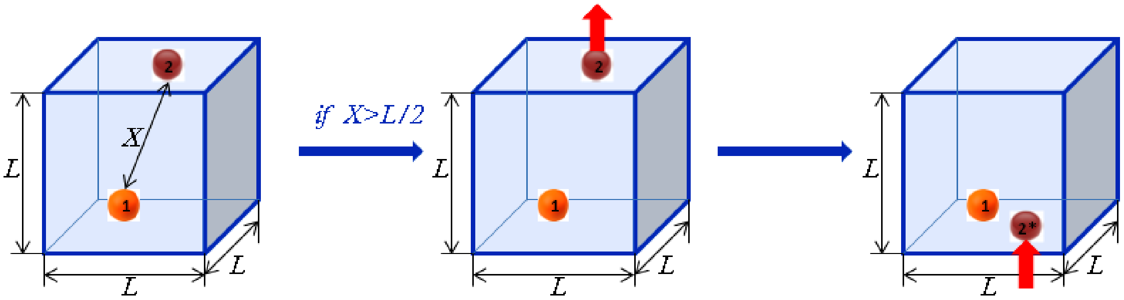

Fig. 2.4. Principle of the simulation of periodic boundary conditions.

By analogy with Fig. 2.4 given above, Fig. 2.5 shows the periodicity into the system. If the selected atom leaves the MD simulation box (left or right), it is again thrown in the opposite direction inside the cell. Thus, the motion of the atoms is always carried out in a periodic medium, simulated by multiple repetition of the original cell.

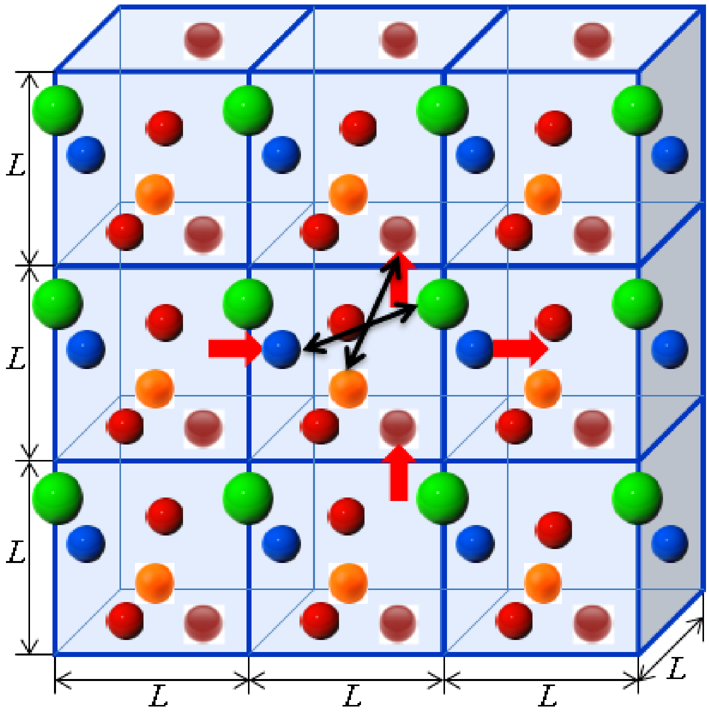

Fig. 2.5. Periodic boundary conditions in MD simulation.

The second main problem during the simulation is the calculation of long-range potentials of electrical nature, in particular, when we work with the systems containing a vast number of atoms. The correct accounting of electrostatic effect of number of particles equal to N^2 = NxN, is the central problem in the MD simulation. Evaluation of the entire spectrum of NxN-interaction for systems containing a large set of particles can take years, even for a single structure. Therefore, in some cases, the Coulomb potentials can be calculated, simplifying the task via introducing “cuttof” radius (Fig. 2.6).

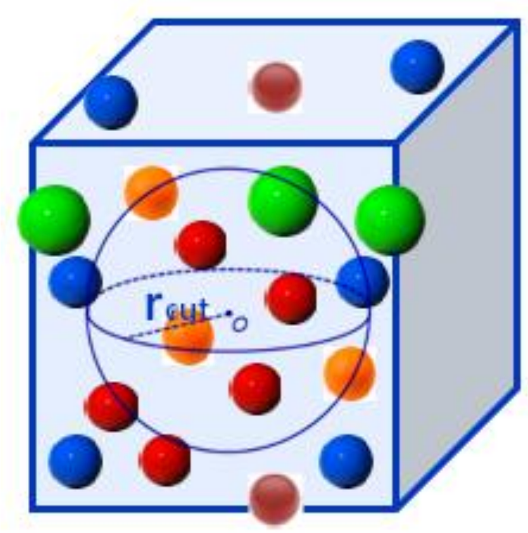

Fig. 2.6. Introduction of the "cuttof" radius in MD simulation.

This means that only the potential pair for $r \leq r_{cut}$ is considered, where r_{cut} is the "cut-off" radius represented as blue circle in the Fig. 2.6. The "cut-off" radius should be sufficiently large to perform the reliability of the potential calculation. Normally the "cut-off" radius is taken small or equal to half of the length of the MD cell.

2.3. Determination of Energetic, Mechanical, Physical and Structural Properties

Having obtained the optimized molecular structure, it is then possible to calculate a wide range of various properties. This includes the energetic, mechanical, physical and structural properties. The expressions used for the calculation of the individual properties and their descriptions are briefly described below.

Energetic Properties

Generally, the interfacial bonding energy is the energy difference (ΔE) between the total energy of system and the sum of energies of each individual composite in this system. In our case:

$$\Delta E = E_{total} - (E_{com.1} + E_{com.2}) , \qquad (24)$$

where E_{total} is the total energy of the system, $E_{com.1}$ is the energy of the first composite into the structure, and $E_{com.2}$ is the energy of second composite into the structure.

In order to understand the interaction between the components into the structure the work of adhesion is calculated according to the following equation:

$$W_A = \frac{\Delta E}{2A}, \tag{25}$$

where ΔE is an interfacial energy, and A is interfacial contact area (factor 2 takes into account the presence of two equivalent interfaces).

Mechanical Properties

Many mechanical properties such as Bulk modulus (B), Shear modulus (G), Young's modulus (Y) and Plane Stress modulus (M) as well as Poisson's ratio (ʋ), Pugh modulus ration, Zener anisotropy factor (A), and two types of acoustic velocities: longitudinal (V_p) and transversal (V_s) can be calculated to characterize the structure.

The Bulk and Shear moduli give the information concerning the hardness of a material during the various types of deformation. There are three different definitions proposed by Reuss, Voigt and Hill [14]:

$$\mathrm{B_{Voigt}} = \frac{1}{9}\left(\mathrm{C_{11} + C_{22} + C_{33}} + 2 * (\mathrm{C_{11} + C_{13} + C_{23}})\right), \tag{26}$$

$$\mathrm{B_{Reuss}} = \left(\mathrm{S_{11} + S_{22} + S_{33}} + 2 * (\mathrm{S_{12} + S_{13} + S_{23}})\right)^{-1}, \tag{27}$$

$$\mathrm{G_{Voigt}} = \frac{1}{15}(\mathrm{C_{11} + C_{22} + C_{33}} + 3 * (\mathrm{C_{44} + C_{55} + C_{66}}) - \mathrm{C_{12} - C_{13} - C_{23}}), \tag{28}$$

$$\mathrm{B_{Reuss}} = \frac{15}{4(\mathrm{S_{11} + S_{22} + S_{33} - S_{12} - S_{13} - S_{23}}) + 3(\mathrm{S_{44} + S_{55} + S_{66}})}, \tag{29}$$

where $\mathrm{C_{ij}}$ is a elastic tensor, and $\mathrm{S_{ij}}$ is a compliance tensor.

The arithmetic mean value of Reuss and Voight averages give the Hill average for Bulk and Shear moduli correspondingly:

$$B_{Hill} = \frac{B_{Voigt} + B_{Reuss}}{2}, \quad (30)$$

$$G_{Hill} = \frac{G_{Voigt} + G_{Reuss}}{2}, \quad (31)$$

Further, the Young's modulus and Plane Stress modulus [15] for isotropic case can be calculated relating the Bulk and Shear moduli such as:

$$Y = \frac{9GB}{G+3B}, \quad (32)$$

$$M = 4G\,\frac{3B+G}{3B+4G}, \quad (33)$$

The values of Bulk, Shear, and Young's moduli give the important information about the composite. The Bulk modulus specifies the behavior of the material, its strain under the hydrostatic stress, the change of volume with constant shape. From the Shear modulus value, one can obtain the information about the strain under shear or torsional stress, the change of shape with constant volume. Young's modulus reflects the strain under the uniaxial or bending stress, that cause the change as to volume and shape.

Complementary to Young's modulus, Poisson's ratio refers to constants characterizing the elastic properties of the material. Poisson's coefficient is the ratio of the absolute value of the transverse contraction strain to longitudinal extension strain. Furthermore, it provides more information about the characteristics of the bonding forces. The value of Poisson's coefficient for a stable, isotropic, linear, and elastic material goes between −1.0 and 0.5. For the central force of solids, the lower limit of Poisson's ratio value is 0.25 and the upper limit of Poisson's ratio value 0.5 [16]. In the isotropic case, Bulk and Shear moduli can be related to obtain the Poisson's ratio via this equation:

$$\upsilon = \frac{3B-2G}{2(3B+G)}, \quad (34)$$

The ductility of the structures also plays an important role. The material is considered to be brittle if its Pugh's ration B/G > 1.75, and it is considered to be ductile with the Pugh's ration B/G < 1.75, following the Pugh's criterion [17].

For the anisotropic cases, it is important to evaluate the anisotropy of the system from the anisotropy Zener factor A, according to the following equation:

$$\mathrm{A} = \frac{2\,\mathrm{C}_{44}}{\mathrm{C}_{11}-\mathrm{C}_{12}}, \tag{35}$$

The Zener anisotropy factor shows the degree of anisotropy in solid materials. The value A equal to 1 for a fully isotropic materials. Otherwise, in the case of smaller factor A (or greater than 1) Zener factor shows the degree of elastic anisotropy.

The elastic wave velocities will also be investigated here. In the propagation of oscillations, the particles don't move with the wave, they fluctuate around their equilibrium positions. Depending on the direction of oscillations of the particles there are two types of the elastic wave velocities: longitudinal (V_p) and transversal (V_s) wave velocities. Both of types can propagate in solids and have a great importance for the evaluation the seismic data. The elastic wave velocities can be calculated relating Bulk, Shear moduli and the density (ρ) of the system:

$$V_s = \sqrt{\frac{G}{\rho}}, \tag{36}$$

$$V_p = \sqrt{\frac{4G+3B}{3\rho}}, \tag{37}$$

Physical Properties

External mechanical forces acting on certain areas of a piezoelectric crystal, can cause, not only the mechanical stresses and strains, but also electric polarization, and hence the appearance of surfaces with electrical charges of opposite signs. When the direction of mechanical forces is in the opposite direction then the direction of polarization and the sign of charges become opposites. This phenomenon is called the direct piezoelectric effect. Piezoelectric effect is reversible. When the electric field exposed to the piezoelectric, mechanical stresses and strains appear. If the direction of the electric field is reversed accordingly, the direction of the stress and strain change as well. This phenomenon is called the inverse piezoelectric effect. The piezoelectric constants d_{ij} are very important. The first subscript i of d, showing the direction of polarization, appear in the material when the electric field equal to zero or else, in the direction of the applied field strength. The direction of the applied stress or the induced strain is respectively shown by the second subscript j of d. The value of d is an important indicator of material validity for strain-dependent exploitation.

Structural Properties

Radial Distribution Function (RDF) is one of the main quantities used in the study of the various phases of gases, solids and liquids. The mathematical formulation of the RDF is expressed as follows:

$$\rho g(r) = \frac{1}{N} < \sum_{i}^{N} \sum_{j \neq i}^{N} \delta[r - r_{ij}] > \tag{38}$$

where N is the number of atoms, ρ is the atomic density equal to N/ρ, r_{ij} is the radius-vector between two atom's centers i and j, $\delta(r)$ is delta function of Dirac, and <…> means average ensemble.

For the distances less than one atomic diameter we have $g(r) = 0$. For the long distances in the liquids, the chosen atom doesn't affect the other atomic locations, i.e. $g(r) = 1$.

Basing on the above formulation of RDF, the main properties and behavior of the above RDF are known as follows:

- The RDF measures how atoms arrange themselves around other atoms. The RDF is proportional to the location of two atoms separated by the distance.
- The RDF plays a central role in molecular modeling. It can be obtained from experiments to determine the structure of the material (X-ray-structural analysis and neutron diffraction analysis).
- At the small separation of the atoms (short r), the function tends to zero. This means the achievement of effective distance at which the atoms cannot approach to each other.
- On the RDF graph it is possible to have the appearance of strongly pronounced peaks, which indicates how the atoms are grouped around a given atom.

- The appearance of peaks on the long distance indicates a high degree of order.
- Typically, at high temperatures the peaks on the RDF graph are wide that indicate the thermal motion. At the same time, the peaks at low temperatures are acicular, especially, for the crystal structure materials, where the atoms are strongly confined at their positions.
- At very large distances any RDF tends to value equal to 1. It means that at such distances the RDF describes the average density.

References

[1] M.P. Allen, D.J. Tildesley, Computer simulation of liquids, Oxford: Clarendon Press, 1989.

[2] F. H. Stillinger, T. A. Weber, Computer simulation of local order in condensed phases of silicon, Phys. Rev. B 31 (8) (1985) 5262–5271.

[3] S. Ihara, S. Itoh, J. Kitakami, Mechanisms of cluster implantation in silicon: A molecular dynamics study, Phys. Rev. B 58 (16) (1998) 10736–10744.

[4] H. P. Cheng, Cluster-surface collisions : Characteristics of Xe_{55}- and C_{20}-Si [111] surface bombardment, J. Chem. Phys. 111 (16) (1999) 7583–7592.

[5] L. Qi, W. L. Young, S. B. Sinnot, Effect of surface reactivity on the nucleation of hydrocarbon thin film through molecular-cluster beam deposition, Surf. Sci. 426 (1999) 83–91.

[6] T. Narumi, R. Susukita, T. Ebisuzaki, G. McNiven, B. Elmegreen, Molecular dynamics machine: Special-purpose computer for molecular dynamics simulations, Molec. Simul. 21 (1999) 401–415.

[7] Z. Pan, Molecular dynamics simulation of slow gold clusters impacting on gold, Nucl. Instr. Meth. Phys. Res. B 66 (3) (1992) 325–332.

[8] l. Qi, S. B. Sinnott, Effect of cluster size on the reactivity of organic molecular clusters: Atomic simulations, Nucl. Instr. Meth. Phys. Res. B 140 (1-2) (1998) 39–46.

[9] B. J. Alder, T. E. Wainwright, Molecular dynamics by electronic computers, in: Transport processes in statistical mechanics, Ed. I. Prigogine, New York: Interscience, 1958.

[10] L. Verlet, Computer "experiments" on classical fluids. I. Thermodynamic properties of Lennard-Jones molecules, Phys. Rev. 159 (1967) 98–103.

[11] J.M. Standard, Energy Minimization Methods, in: Chemistry 380.37, Illinois State University, 2015.

[12] J. M. Haile, Molecular dynamics simulation.Elementary Methods., United States: Wiley-Interscience, 1997

[13] M. P. Allen, D. J. Tildesley, Computer Simulation of Liquids, Oxford: Clarendon press, 1987.

[14] J. F. Nye, Physical properties of crystals, Oxford: Oxford University Press, 1957.

[15] E. Masoero, E. Del Gado, R.J.M Pellenq, S. Yip, F.J. Ulm, Nanoscale mechanics of colloidal C-S-H gels. Soft Matter, 10 (3) (2014) 491–499.

[16] H. Fu, D. Li, F. Peng, T. Gao, X. Cheng, Ab initio calculations of elastic constants and thermodynamic properties of NiAl under high pressures, Comput. Mater. Sci. 44 (2) (2008) 774–778.

[17] S.F. Pugh, Relations between the elastic moduli and the plastic properties of polycrystalline pure metals, Lond.Edinb.Dubl.Phil.Mag, 45 (1954) 823–843.

CHAPTER 3: RESULTS AND DISCUSSIONS

Because of the remarkable characteristics of carbon nanotubes (CNTs) such as mechanical, electrical and thermal properties[1-4], it is possible to used them in different fields of civil engineering materials. CNT nanotubes are widely used composite materials that are founded on divers matrices [5-10]. A lot of scientists put to the test to create stronger material, in more detail, polymer-based materials [11-13] after the Iijima's discovery of CNTs in 1991 [14]. Then again, many experimental studies on the cement composite material modified by CNT have been provided too. As the authors note in their works [15,16] the addition of nanotubes in the concrete on the cement binder base can raise the mechanical properties to 15-20 %.

Li et al. [16] analyzed the mechanical properties of the cementitious matrice modified with the chemically functionalized CNTs and remarked that the utilization of nanotubes give a 19% gain in compressive strength a 25% gain in flexural strength in the CNT's amount of 0.5% by weight of cement. Furthermore Makar et al. also note in their rapports [17,18] that the CNT in concentration 2% by weight of cement can strengthen cement matrix composites. In agreement with the results that were summed up, the CNT can influence to the hydration process in the early stages. According to Konsta-Gdoutous et al. [19] the addition of CNT in amount of 0.08% per weight of cement affect increasingly to Young's modulus and the flexural strength of the cement paste matrix. Saez de Ibarra et al. using the AFM nano-indentation technique [20] given notice the mild augmentation in Young's modulus for the concrete specimens including Single Wall Carbon Nanotubes (SWCNTs) and Multi Wall Carbon Nanotubes (MWCNTs). The mechanical properties of cement matrix with different amount of MWCNTs were studied by Cwirzen et al. [21]. However, incorporation of carbon nanotubes in a cement matrix was not revealed significant effect on the flexural strength or the compressive strength. Nevertheless, not so long ago, other scientists showed that the nanotubes may have a reinforcing effect on the cement matrix with w/c=0.5. Metaxa et al. show the increase of flexural strength and Young's modulus of plain cement paste by 25% [22] and at the same time Shah et al. by 50% [23]. Musso et al. [24] estimated that addition of MWCNTs in 0.5% by cement mass significant reduce the compressive strength and flexural strength.

Summing it up, it appears that different authors have the different results on the mechanical performance of cement materials. It can be explain by the various choices of type and quantity of CNTs and the different types of cement. Besides, for getting comparable results, it is necessary to produce the huge number of experiments that can be a prerequisite the taking a good deal of time and may be very expensive. For those reasons, modeling and simulation are meant to be the great help for the understanding and analyze the performance the cement concretes with CNTs.

Carbon nanotubes affect the nanoscale processes into C-S-H structure on the molecular level to keep cementitious matrix together [17, 25]. Nonetheless, the modern experimental characterization techniques are not favorable to investigate afore cited molecular-scale effects. However, modeling is certainly the helpful tool to understand profoundly the molecular-scale energetic and structural properties of the carbon-cement interaction and open the new door in the cement research. In addition, the simulation method has already been used to investigate C-S-H structure [26,27], the origin of the cohesion of cement pastes [28], and the interaction of water and solutes with cement phases [29] what allow us to use this method to study the composite cement material with carbon nanotubes.

The object of present work is the study at the nanoscale level the interaction between one of the main calcium silicate hydrate mineral of concrete Tobermorite 11Å and carbon nanotube. We focused particularly on the understanding of the influence different types of CNT on the mechanical and structural properties of the new composite material.

3.1. Mechanical Properties of Different Types of the Single Walled Carbon Nanotube

We started our research by the preparation of five different types of Single Walled Carbon Nanotubes. There are "Zigzag" carbon nanotubes: CNT (3,0) with d = 2.351 Å, CNT (4,0) with d = 3.135 Å, and CNT (5,0) with d = 3.919 Å; and "Armchair" carbon nanotubes: CNT (2,2) with d = 2.715 Å, and CNT (3,3) with d = 4.073 Å. All these nanotubes have the same length equals ~68 Å. Tersoff potential [30] presented in Table 3.1 was adapted for describing the atomic interaction in CNT structures. The corresponding atomic structures of CNTs are presented in Fig 3.1.

Table 3.1: Tersoff potential parameters

Tersoff bond order potentials								
Botwobody								
Atom1	Atom2		A (eV)	B (eV)	Λ_1 (Å^{-1})	μ (Å^{-1})	R (Å)	S (Å)
C core	C core		1393.6	346.74	3.4879	2.2119	1.8	2.1
Borepulsive								
Atom1	Atom2				Λ_3 (Å^{-1})	Λ_2 (Å^{-1})	N	μ (Å^{-1})
C core	C core				0	3	0.72751	2.2119
Boattractive theta								
Atom1	Atom2	β	Λ_2 (Å^{-1})	n	μ (Å^{-1})	c	D	h
C core	C core	1.57E-07	3	0.72751	2.2119	38049	4.3484	-0.57058

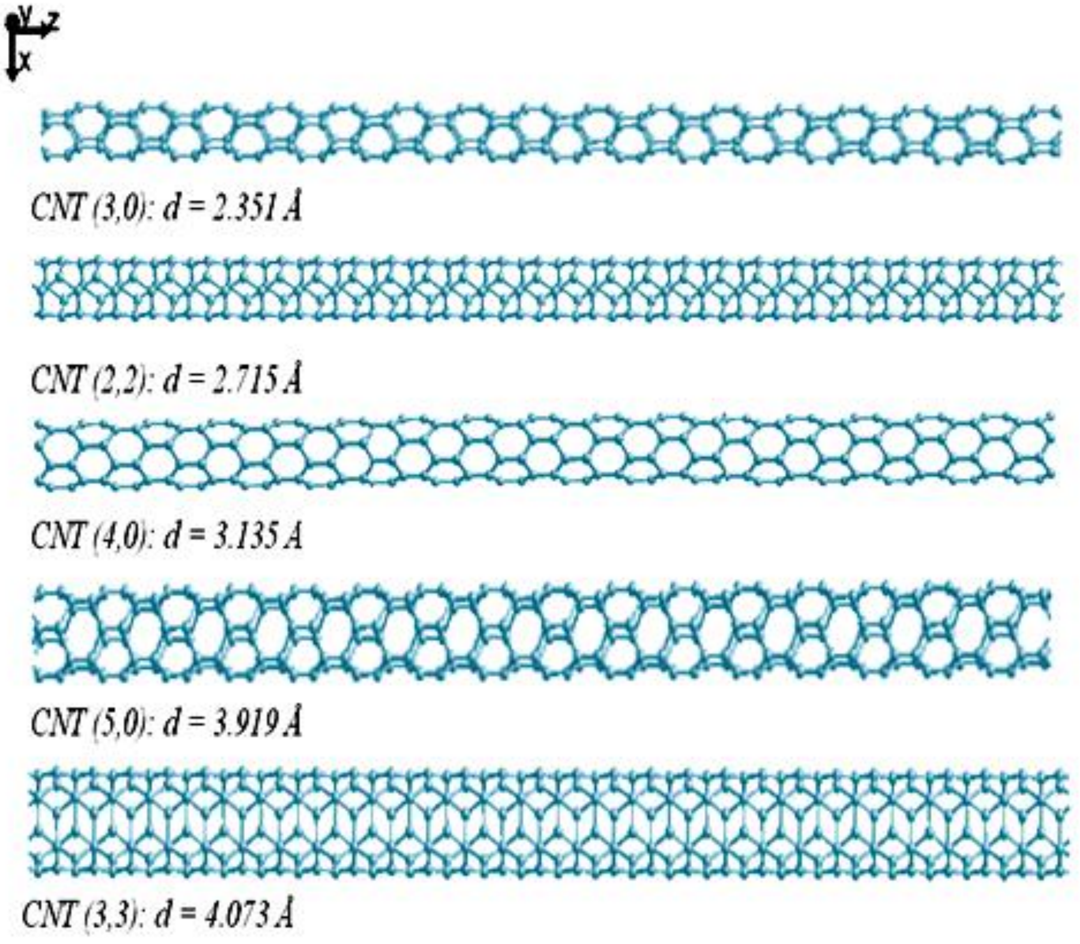

Fig. 3.1. Atomic structures of different CNT types.

We have performed optimization calculation with constant volume during the Molecular Dynamic (MD) procedure. Calculated mechanical properties of different types of carbon nanotube are presented in Table 3.2.

Table 3.2: Mechanical properties of different CNT types.

	CNT (3,0)	*CNT (2,2)*	*CNT (5,0)*	*CNT (4,0)*	*CNT (3,3)*
Bulk Modulus (TPa)	0.555	0.433	0.33	0.401	0.135
Shear Modulus (TPa)	0.145	0.282	0.08	0.237	0.294
Young's Modulus (TPa)	0.401	0.695	0.222	0.594	0.51
Stress Modulus (TPa)	0.468	0.734	0.261	0.634	0.519
Poisson's ratio (TPa)	0.379	0.233	0.388	0.253	-0.131

Because nowadays there are a sufficient number of studies of the mechanical properties of SWCNTs, we give here a comparison between our results and some previous works (Table 3.3). Favorable agreement can be noticed from the Table 3.3.

Table 3.3: Mechanical quantities of CNT, compared to preceding findings.

Method	*Structure*	*Young's Modulus (TPa)*	*Shear Modulus (TPa)*	*Reference*
TEM	Single Wall Carbon Nanotube	0.4-4.15	–	[31]
TEM		1.25	–	[32]
MRS		2.8-3.6	–	[33,34]
TLT		0.32-1.47	–	[35]
AFM		≈1	–	[36]
AFM		1.2	–	[37]
FE		0.995-1.033	0.25-0.485	[38]
MD		≈0.97	≈0.5	[39]
MD		≈1	≈0.398	[40]
MD		0.222-0.695	0.08-0.294	Present study

TEM – Transmission Electron Microscopy

MRS – Micro Raman Spectroscopy

TLT – Tensile Loading Test

FE – Finite Element

AFM – Attomic Force Microscopy

MD – Molecular Dynamics

3.2. Modification of C-S-H structure from inserted carbon nanotubes: The case of Tobermorite 11Å with 0.83 ratio of Ca/Si

3.2.1. Input preparation

The Tobermorite 11Å structure is a monoclinic structure with unit cell dimensions: a =7.39 Å, b =22.779 Å, c = 6.69 Å and α = 90°, β = 123.49°, γ = 90° (the coordinate axis is rotated in the clockwise direction as noted by Hamid [41]). The space group of this structure is group P_{21}. In our case, we used thirty crystallographic unit cells of the Tobermorite 11Å to construct a 5 x 2 x 3 supercell with total atom number of 3420 and Ca/Si ratio of 0.83.

For this study two types of carbon nanotubes were chosen: "Armchair" and "Zigzag". We prepared five CNTs of the length ~17 Å with different diameters CNT (3, 0) with d = 2.351 Å; CNT (4, 0) with d = 3.135 Å; CNT (5, 0) with d = 3.919 Å; CNT (2, 2) with d = 2.715 Å; and CNT (3, 3) with d = 4.073 Å.

It is important to realize that we are considering here the composite material, where we have the interaction between the CNT and the surface of the Tobermorite 11Å, in such a way the prepared nanotubes were incorporated into the hole of C-S-H (Fig.3.2). Firstly, the vacuum in the structure of C-S-H was created for implement the insertion nanotube in the structure of Tobermorite 11Å. Secondly, we verified the charge of the system because it is meant to be neutral. To do this, we made one hole into the C-S-H in order to preserve the neutral charge.

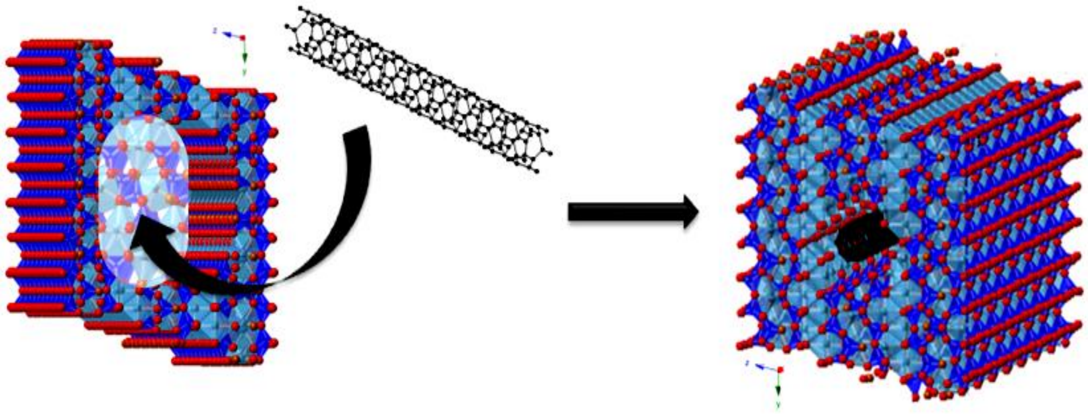

Fig. 3.2. Schematic view of the CNT's insertion into the hole of C-S-H.

The bridging silica tetrahedral (encircled in green in Fig. 4) may be absent in the Drierketten type of silicate chains observed in tobermorite like C-S-H as noticed by Plassard et al. [42]. Consequently, we can find the less stable silicon atoms in the silicon chains. The removal of this less stable silicon and interstitial calcium atoms (encircled in orange in Fig. 3.3) can let then the keep the neutral charge of system. At the same time the silica tetrahedron geometry transform to silica trigonal pyramidal geometry.

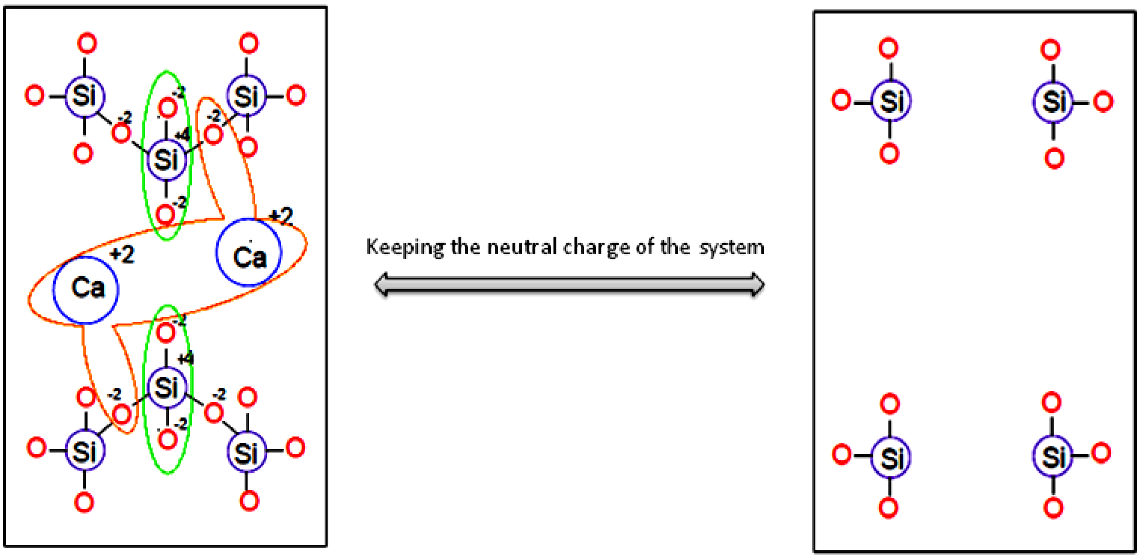

Fig. 3.3. Transformation of the silica tetrahedron geometry to the silica trigonal pyramidal geometry keeping the neutral charge of the system C-S-H.

The polarization effect is an important factor in the calculation because the system is an ionic crystal. For this reason, we used the “core-shell model” approach. In this approach the ions consider such a complex of two point charge “core” and “shell”. The “core” represent the positively charge nucleus and the “shell” represent the polarizable valence electrons. In our model all the anions such as lattice oxygen (O1), oxygen of hydroxyl (O2), and oxygen of water molecule (O3) partition into “core” and “shell”. The cations in the structure such as Ca, Si, H were considered only as cores. The potentials of the long range Coulombic interactions are used on core and shell. All the potentials of short range interactions such as Buckingham potential, Morse potential, three body potential are applied only on the shell of the polarizable anions (O1, O2, O3). The interatomic potential energy presents the interactions between atoms. For obtaining the potential energy of a system we summed up all different types of interaction that forgather in this system. In our study, we selected the parameters of Buckingham, Morse, three body, and spring potentials [43] to describe the interactions between the atoms in the structure of Tobermorite 11Å. Tersoff potential was adapted for describing the atomic interaction in CNT's structure (Table 3.1). Interaction between atoms of the Tobermorite 11Å and the CNTs were calculated as a result of the potential's parameters [43-45] by applying Lorentz-Berthelot mixing rules [44]. All potential parameters are given in Table 3.4.

Table 3.4: Potential parameters for the system Tobermorite/CNTs

Buckingham potential								
Atom1	Type	Atom2	Type	A (ev)	Rho (Å)	C6 in eV* Å 6	R_{min} (Å)	R_{max} (Å)
Ca1	Core	O1	Shell	1090.4	0.3437	0	0	12
Ca1	Core	O2	Shell	777.27	0.3437	0	0	12
Si	Core	O1	Shell	1283.9	0.32052	10.66158	0	12
Si	Core	O2	Shell	983.5	0.32052	10.66158	0	12
O1	Shell	O1	Shell	22764	0.149	27.879	0	12
O1	Shell	O2	Shell	22764	0.149	13.94	0	12
O2	Shell	O2	Shell	22764	0.149	6.97	0	12
H1	Core	O1	Shell	311.97	0.25	0	0	12
H2	Core	O3	Shell	396.27	0.25	0	0	12
Ca2	Core	O3	Shell	777.27	0.3437	0	0	12
Ca2	Core	O1	Shell	1090.4	0.3437	0	0	12
Ca2	Core	O2	Shell	1090.4	0.3437	0	0	12
Ca1	Core	O3	Shell	777.27	0.3437	0	0	12
Si	Core	O3	Shell	983.556	0.32052	10.66158	0	12
H1	Core	O3	Shell	311.97	0.25	0	1.2	12
O1	Shell	O3	Shell	22764	0.149	13.94	0	12
O2	Shell	O3	Shell	22764	149	6.97	0	12
O1	Shell	H2	Core	311.97	0.25	0	0	12
O2	Shell	H2	Core	311.97	0.25	0	0	12
Morse potential								
Atom1	Type	Atom2	Type	d (eV)	α ($Å^{-1}$)	Rho (Å)	R_{min} (Å)	R_{max} (Å)
H1	Core	O2	Shell	7.0525	3.1749	0.9428	1	1.4
H2	Core	O3	Shell	6.203713	2.22003	0.92376	1	1.4
Three body potential								
Atom1	Atom2	Atom3		β (eV rad^{-1})	$θ_0$ (^{0})	R_{max} (1-2) (Å)	R_{max} (1-2) (Å)	R_{max} (1-2) (Å)
Si core	O1 Shell	O1 Shell		2.0972	109.47	1.8	1.8	3.2
Si core	O1 Shell	O2 Shell		2.0972	109.47	1.8	1.8	3.2
O3 Shell	H2 Core	H2 Core		4.19978	108.69	1.2	1.2	1.8
Lennard Jones potential								
Atom1	Type	Atom2	Type		A ($eVÅ^{12}$)	B ($eVÅ^{12}$)	R_{min} (Å)	R_{max} (Å)
O3	Shell	O3	Shell		39344.98	42.15	0	12
C	Core	Ca1	Core		106132.3	47.32	0	12
C	Core	Ca2	Core		106132.3	47.32	0	12
C	Core	Si	Core		65306.42	48.24	0	12
C	Core	O3	Shell		142340	69.62	0	12
C	Core	O2	Shell		142340	69.62	0	12
C	Core	O1	Shell		7346.2	10.05	0	12
Core-shell spring potential								
Atom								eV $Å^2$
O1								74.92
O2								74.92
O3								209.45

3.2.2. Effect of the vacuum

There is only few published papers using the molecular dynamics simulation to study the atomic interaction between the tobermorite mineral and carbon nanotube. Sanchez at al. [46] studied the interaction between atoms of graphitic structures and the surface of the C-S-H. The distances of ~4 Å were used to model this interaction. However, this work covers only graphite planes and not the carbon nanotubes. Eftekhari et al. [47] have found that the interlayer space between the CNT and C-S-H is ~2.7 Å after system's equilibration. However, their method to design the system based on the generation a zero-diameter hole and pushing atoms backwards that is different from the method used by us. Taking all the aforesaid into consideration, for the first time is important to choose the best distance between CNT and C-S-H.

Therefore, we calculated the total interaction energy of system C-S-H/CNT using the various distances of the vacuum between CNT and C-S-H in order to determine the effect of the vacuum on the molecular mobility of the C-S-H surface's atoms in the C-S-H/CNT. We made a choice of the nanotube with the smallest diameter to have the possibility to test a lot of vacuum's distances without going beyond the box size, since the simulation box size of our system is fixed. Thereafter, the selected distance can be applied to other types of nanotubes such as reported in Ref. [47], where for different types of nanotubes were found at the same distance between C-S-H and CNT after equilibration of the system.

Fig. 3.4 shows the position of CNT into C-S-H. Six different distances (1.19Å; 2.01 Å; 2.87 Å; 3.32 Å; 3.97 Å and 4.59 Å) were tested.

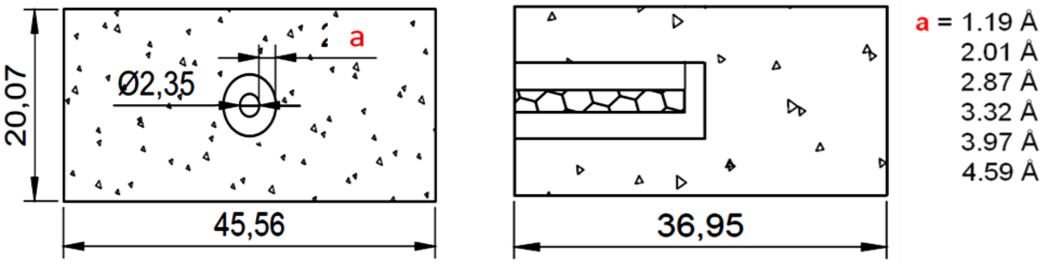

Fig. 3.4. Schematic view of the CNT's insertion into the hole of C-S-H with different distances of the vacuum between CNT and the surface of the tobermorite.

The total interaction energy (ΔE) between C-S-H and CNT (d = 2.351 Å) was obtained by calculating the energy of the equilibrated system C-S-H/CNT with different distances of the vacuum between CNT and the surface of C-S-H. As we may see from Fig. 3.5, the system is more stable for a width of the vacuum of 2Å.

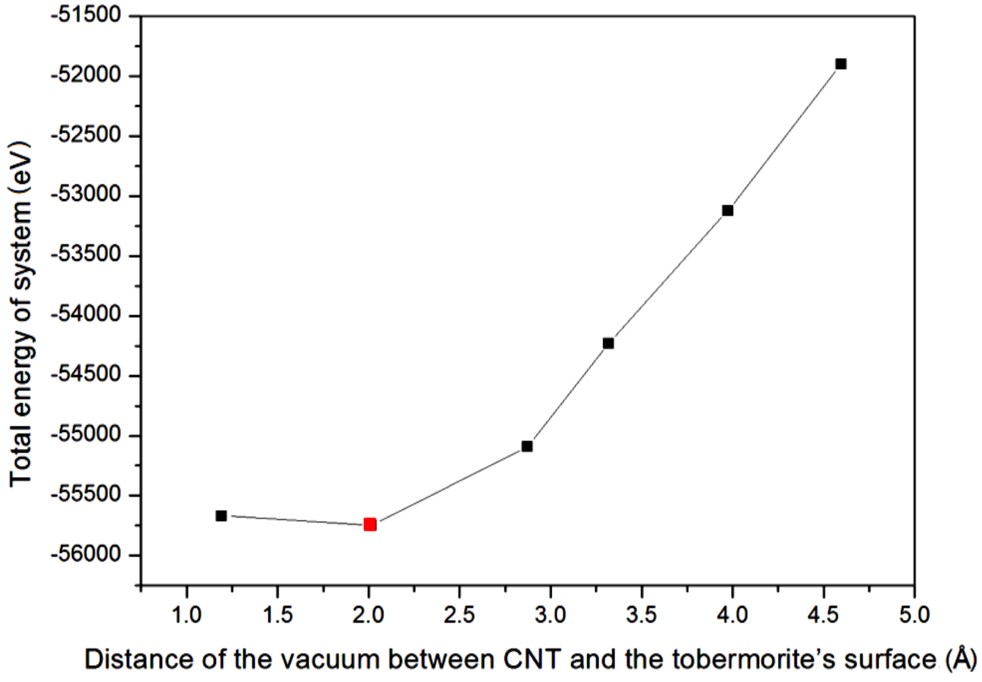

Fig. 3.5. Total interaction energy of the system C-S-H/CNT with different distance of the vacuum between CNT and the surface of the Tobermorite 11Å.

Snapshots representative of the computational cell before and after optimization of the system C-S-H/CNT are shown in Fig. 3.6. Before optimization, CNT was positioned into C-S-H at a distance of 2 Å away from each other (Fig. 3.6a). When the system was optimized we can see that these two structures have moved closer to each other and the atoms of oxygen were attracted to the structure of CNT with the formation of new morphology nearby the surface of CNT (Fig. 3.6b).

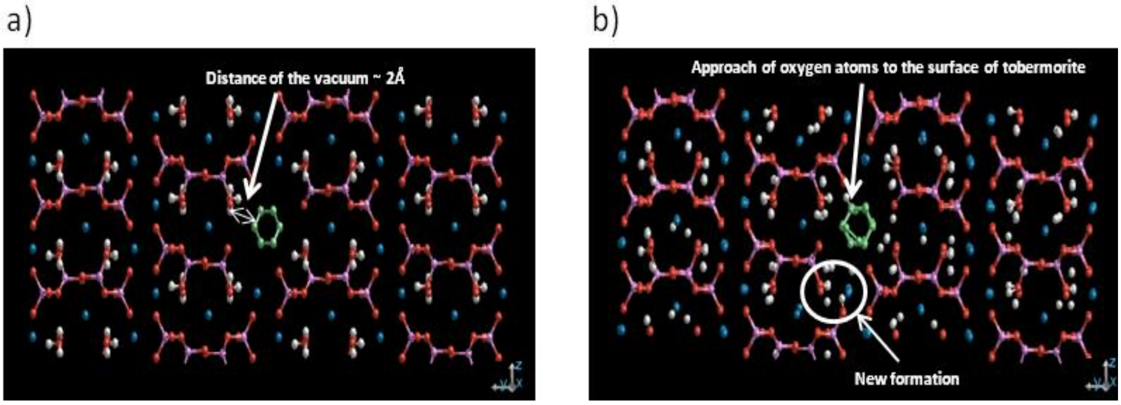

Fig. 3.6. Snapshots of the system C-S-H/CNT: before optimization (a) and after optimization (b).

3.2.3. Interaction energies

The energy calculating of the equilibrated system C-S-H/CNTs (different diameters) allows to get the total interaction energy (ΔE) between C-S-H and CNTs with different diameters. After the calculations we can note a favorable interaction between C-S-H and CNTs. This is due to the fact that the values of the total energy are negatives. The total interaction energy depends on CNT's diameter: the system is more stable for a CNT diameter of 2.351 Å (Fig. 3.7).

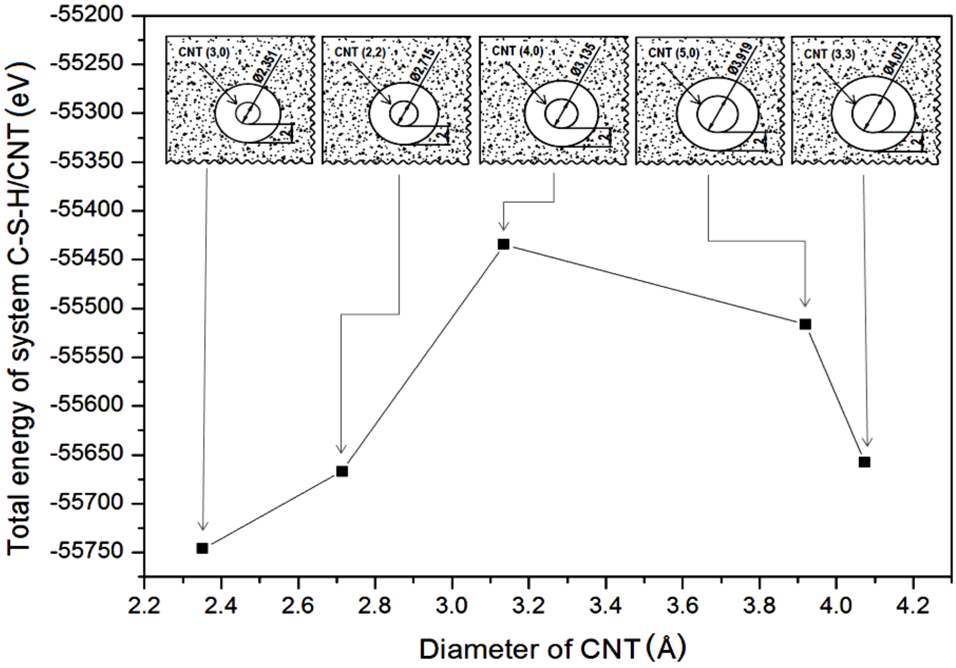

Fig. 3.7. Total interaction energy (ΔE) between C-S-H and CNTs with different diameters.

3.2.4. Work of adhesion

In order to understand which type of carbon nanotube has the better adhesion with the C-S-H, we calculate the work of adhesion. To do this, it is important to understand the contact area between the structures.

The contact area has a cylinder form, as reflected by Fig. 3.8, for this reason we can consider A as a surface area of the cylinder. However, in the case of nanotube we have the contact only along the area of the side, and due to this we have calculated the contact area as a surface area of the cylinder excluding the areas of the top and the bottom.

We display in Fig. 3.9 our results of the adhesion's work, where we see that the adhesion energy between the CNT and the Tobermorite 11Å strongly depends on the diameter of CNT. We conclude that the nanotube with the smaller diameter has the best adhesion with the tobermorite. In our case it corresponds to 2.351 Å.

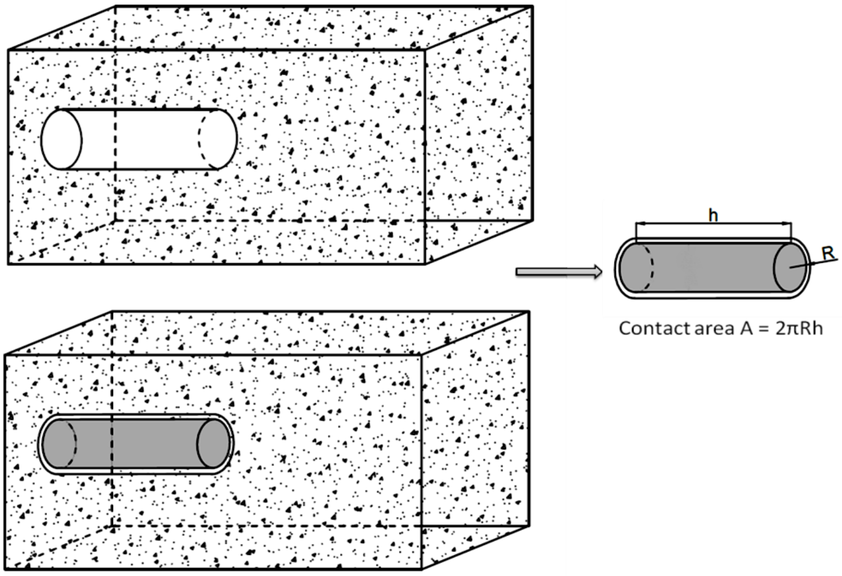

Fig. 3.8. Schematic view of contact area between CNT and C-S-H.

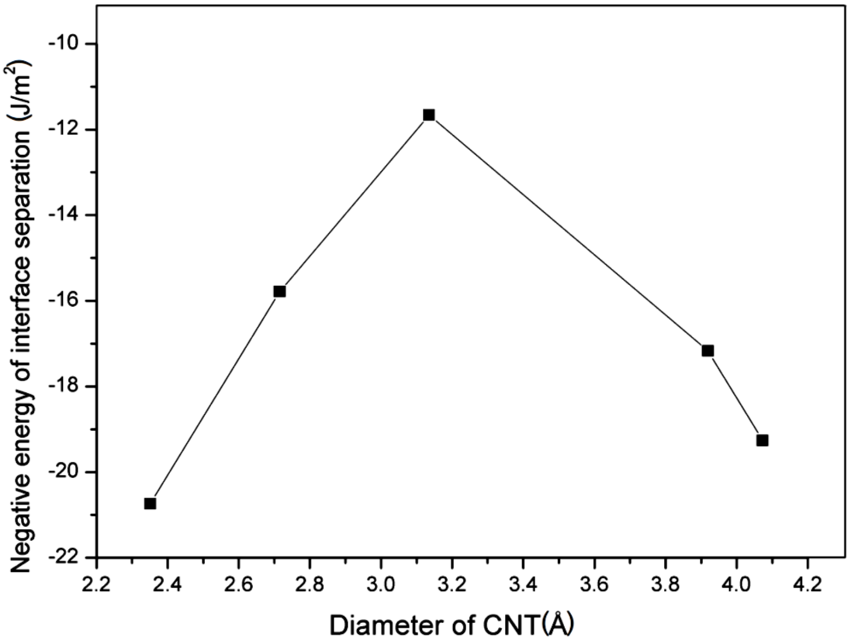

Fig. 3.9. Adhesion energy between Tobermorite 11Å and carbon nanotubes with different diameters.

3.2.5. Mechanical properties

Since this is the first work regarding the interaction between different types of CNT and Tobermorite 11Å, we compare-first- our results for Tobermorite11Å to previous *ab initio* data of Shahsavari et al. [48], the molecular dynamics results of Zaoui [43] and experimental data of Refs. [49-52], which are in favorable agreement (Table 3.5).

Table 3.5: Mechanical properties of Tobermorite 11Å compared to previous MD, *ab initio* and experimental calculations.

Method	***Material***	***Bulk Modulus (GPa)***	***Shear Modulus (GPa)***	***Young's Modulus (GPa)***	***Poisson's ratio***	***Reference***
MD (this work)	Tobermorite 11Å	65.5	30.14	78.39	0.3	
MD	Tobermorite 11Å	58	33	111.52	–	[43]
ab initio	Tobermorite 11Å	58	32.56	82.29	–	[48]
Experimental study	Tobermorite 14Å	47	–	–	–	[49]
	Concrete	27.91	18.45	45.35	0.229	[50]
		–	–	32.5	–	[51]
		–	14.01	33.1	0.182	[52]

The obtained values of the bulk, shear, Young's and plane stress moduli for Tobermorite 11Å with addition of different CNT's types are presented in Fig. 3.10. Results show that the diameter of CNT exerts an influence on the values of K, G, Y and M. From Fig. 3.9 we can see an increase of the bulk modulus according to the diameter of CNT. The shaded area shows the value of K for the Tobermorite11Å without CNTs, therefore we can conclude which system with CNT gives increase of the value of K. Bulk modulus reached 79.08 GPa (for C-S-H without CNT, it corresponds to 65.49 GPa) what gives an increase of 20.751 %. Optimal diameter of CNT used during this determination of bulk modulus was 2.351 Å.

Fig. 3.10 shows that we have several cases of increase of G value. The sample of Tobermorite 11Å without CNT gives a value of G equal to30.14 GPa. Shear modulus reached 42.29 GPa for C-S-H/CNT with CNT's diameter of 2.351 Å; 31.38 GPa (CNT's diameter 2.715 Å); 71.52 GPa (CNT's diameter 3.919 Å); 114.25 GPa

(CNT's diameter 4.073Å) that gives 40.312%, 4.114%, 137.293%, 279.064% of increase of the value of G respectively.

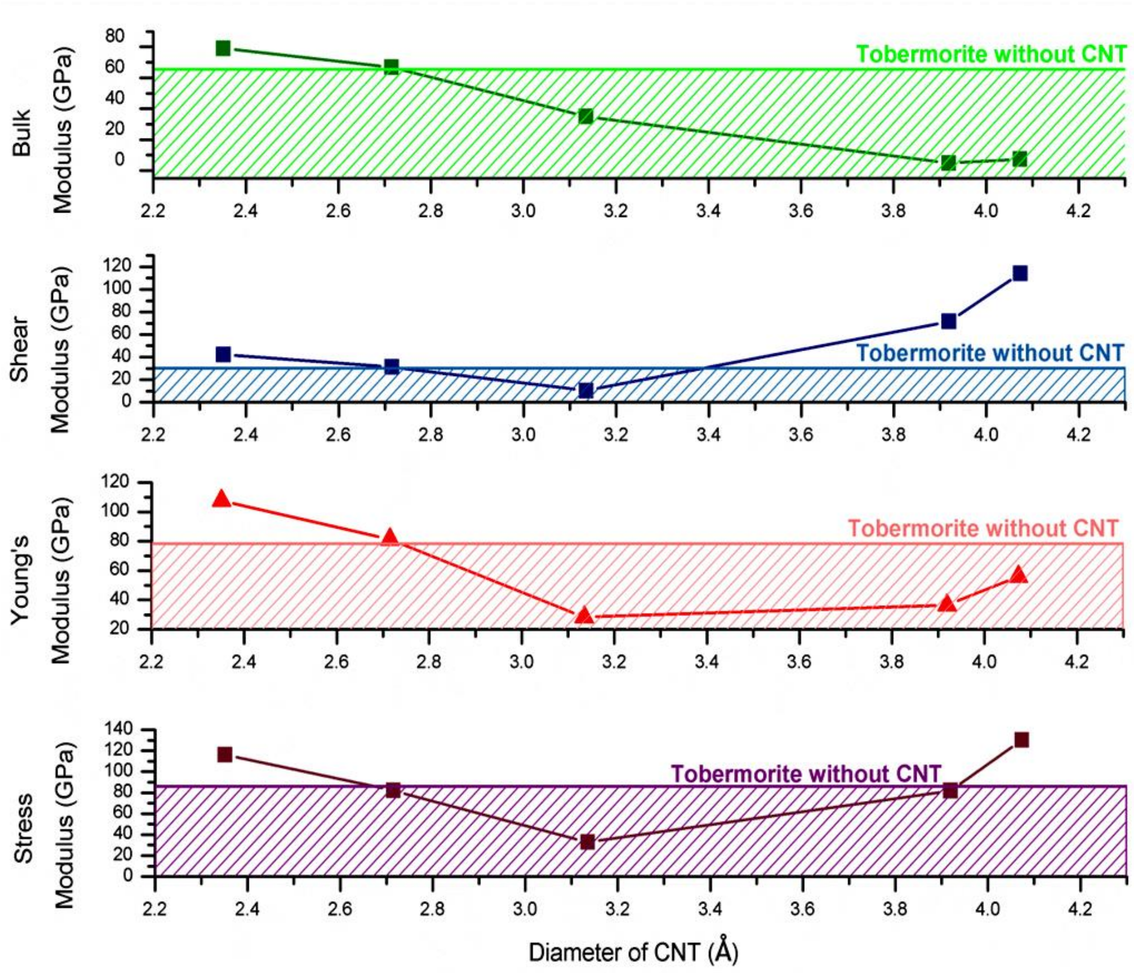

Fig. 3.10. Effect of the CNT's diameter on the Bulk, Shear, Young's and Plane Stress moduli of the system C-S-H/CNT.

For the value of Young's modulus we have also found several cases of increase compared with the value of Young's modulus for Tobermorite 11Å without CNT, which is –78.39 GPa. As Fig. 3.9 shows the value of Y achieved 107.68 GPa (CNT's diameter 2.351 Å); 81.38 GPa (CNT's diameter 2.715 Å); that gives 37.364% and 3.815% of increase the value of the Y respectively.

For the plane stress modulus we observe the increase only for two cases, for Tobermorite 11Å and CNT with diameter of 2.351Å (35.037 % of increase in reference to Tobermorite 11Å without CNT) and for Tobermorite 11Å with diameter of 4.073 Å (51.093 % of increase in reference to Tobermorite 11Å without CNT).

There are some experimental data for Young's modulus of cement paste modified by different type of carbon nanotubes. Konsta-Gdoutos et al. in their work [19] show 28.82 % raise of the Young's for the cement paste modified with 0.08 % MWCNT by weight of cement at the age of 28 days [19]. Danoglidis et al. [53] also studied the change of Young's of cement mortar after 28 days of hydration and noticed the significant increase of Young's modulus. The improvement of Young's modulus was between 42.55 % and 94.326 % versus on concentration of multi-walled carbon nanotubes (MWCNT). The behavior of the Young's modulus of ordinary portland cement pastes modified with different concentrations of MWCNT was studied by Zou et al. [54]. They also remarked an increase of the Young's modulus value. Konsta-Gdoutos et al. [15] studied the Young's modulus of cement paste modified by MWCNT, but in their case the carbon nanotubes were having different lengths. The latter confirms also the possibility of rise of the Young's modulus. The comparison between the values of Young's modulus from experimental data with the values of the current study (Table 3.6) can be complicated because of different type of carbon nanotubes involved in each case, as well as different based material (we use only one of the component of concrete's structure, i.e. tobermorite). Besides, there are different methods of preparation of the system C-S-H/CNT. However, despite these differences, there is noticeably general trend regarding the increase of the Young's modulus of concrete samples with carbon nanotubes.

It is important to note that if we have the possibility to increase those parameters, the door for many industrial applications will be open. As regard to our work, in all cases we can observe increasing values of K, G, Y and M. The most important point is that in one case we have an increase of all parameters in the same time. This is the case of C-S-H /CNT with a CNT's diameter of 2.351Å.

Table 3.6: Young's modulus for the C-S-H/CNT system compared to experimental data.

Reference	*Method*	*Matrix*	*Type of CNT*	*Young's Modulus (GPa)*
Present work	MD	Tobermorite 11Å	SWCNT (3,0)	107.68
			SWCNT (2,2)	81.38
			SWCNT (4,0)	28.45
			SWCNT (5,0)	36.57
			SWCNT (3,3)	55.98
[19]	Experimental study	Cement paste	MWCNT (0.08 wt.%)	21.9
[15]			MWCNT (0.08 wt.%)	13
[52]		Mortar	MWCNT (0.08 wt.%)	25
			MWCNT (0.1 wt.%)	27.5
			MWCNT (0.3 wt.%)	21.3
			MWCNT (0.5 wt.%)	20.1
[53]		OPC paste	MWCNT (0.038wt.%)	18.28
			MWCNT (0.075wt.%)	20.84

In the following step, the components of elasticity tensors for all models were calculated and presented in Table 3.7. It is clear that when CNT is embedded in the Tobermorite 11Å, the monoclinic structure (binary axis ∥ Y) will be changed by a triclinic structure. In all cases, CNT is inserted in the tobermorite in parallel to X axis, hence the elasticity components can be strengthened in this direction and can be weakened in other direction. C_{11} of tobermorite without CNT (Table 3.7) is 153.99; while the values of tobermorite modified by CNT have higher values, except in the case of tobermorite with CNT (2,2), where the value is less than that of the specimen without CNT. Normally, for the other directions C_{22} and C_{33}, we can see the enfeeblement of the values compared to the specimen of tobermorite without CNT, but there are also the samples which exceed the value of the sample without nanotubes. This can be explained by the different deformation behaviors of nanotube within the tobermorite.

Table 3.7: Elastic constants for Tobermorite 11Å and Tobermorite 11Å modified by CNT.

Elastic constants	Tobermorite (Ca/Si =0.83)	Tobermorite + CNT (3,0)	Tobermorite + CNT (2,2)	Tobermorite + CNT (4,0)	Tobermorite + CNT (5,0)	Tobermorite + CNT (3,3)
C_{11}	153.99	168.1	90.85	167.78	181.99	224.13
C_{12}	46.15	10.12	1.2	28.37	-145.83	14.86
C_{13}	45.13	56.29	-62.69	-39.53	52.45	-191.5
C_{14}	0	-9.88	70.03	13.98	4.17	214.18
C_{15}	2.29	-20.1	7.41	-13.25	64.06	-102.13
C_{16}	0	9.74	-4.17	17.35	214.07	-103.19
C_{22}	93.29	-10.67	34.39	45.54	284.08	32.28
C_{23}	28.85	21.54	5.48	-36.32	-33.92	-219.52
C_{24}	0	-13.15	41.89	32.1	27.32	163.42
C_{25}	0.47	-20.28	-1.96	-10.73	-88.08	-110.17
C_{26}	0	-5.05	-10.32	18.73	-398	-103.19
C_{33}	121.46	107.19	-12.17	228.36	132.07	863.88
C_{34}	0	-2.78	76.39	-63.23	5.68	-498.59
C_{35}	3.77	-20.11	19.4	-13.61	31.13	287.84
C_{36}	0	14.35	8.58	-41.52	98.97	416.93
C_{44}	12.62	-8.13	-0.4	12.78	33.79	387.2
C_{45}	0	-9.16	-4.58	13.04	12.16	-199.94
C_{46}	0.48	10.98	0.68	2.69	-14	-315.82
C_{55}	39.82	29.03	32.36	42.08	64.09	139.78
C_{56}	0	7.23	-2.73	3.95	166.44	171.71
C_{66}	32	-6.8	-19.59	-7.69	601.38	236.55

Thereafter, we have evaluated the ductility of the present structures. The material is considered to be brittle if its Pugh's ration B/G > 1.75, and the material is considered to be ductile with the Pugh's ration B/G < 1.75, following the Pugh's criterion. The Pugh's modulus ratio k=B/G for all specimens is reported in Table 3.8. For Tobermorite 11Å without CNT the value of k is greater than the critical value 1.75 that shows the brittle behavior of material. In comparing other samples of Tobermorite 11Å/CNT with Tobermorite 11Å, we see that only specimen with CNT (4.0) have the value greater than tobermorite (3.361 > 2.173). We may conclude here that this system can be break without significant deformation. At the same time we may conclude that, if the tobermorite modified with the nanotube which has the larger diameter such as 3.919 and 4.073 Å, the composite acquires a ductile behavior.

Calculated Poisson's ratio values (Table 3.8) are between −0.74 and 0.47. Typical Poisson's ratio for concrete is ~0.2.Noting, that there are the values bigger than 0.2, it may be deduced that the interatomic forces in the system tobermorite/CNT are preferential the central forces. Our study shows that it is reliable for the samples with small diameters of CNT (from 2.351Å to 3.135Å).

Table 3.8: Pugh modulus, Poisson's ratio and Zener anisotropy factor for Tobermorite 11Å and Tobermorite 11Å modified by CNT.

			Pugh modulus ratio, k = B/G	*Poisson's ratio, υ*	*Zener anisotropy factor, A*
Tobermorite without CNT			2.173	0.3	0.234
C-S-H + CNT	***Diameter of CNT (Å)***	***2.351***	1.87	0.273	-0.103
		2.715	2.128	0.47	-0.009
		3.135	3.361	0.297	0.183
		3.919	0.068	-0.744	0.206
		4.073	0.065	-0.755	3.7

To calculate the mechanical quantities and to have easy comparison with experimental data at the micro level, we considered that our system is isotropic, but at the nano level CNT can change the system for the anisotropic behavior. Thus, we have evaluated the anisotropy of the systems from the anisotropy Zener factor A. The calculated Zener anisotropy factors shown in Table 3.8 are lower than 1 (except tobermorite with CNT (3,3)), which indicates that these systems are anisotropic materials.

Thereafter, we study the type of CNTs dependence on the elastic wave velocities such as longitudinal (V_p) and transversal (V_s) wave velocities. We plot the obtained acoustic velocities values in Fig. 3.11. Insertion of CNT (3.0) increases weakly the values of V_p and V_s. However, CNT (2,2) and CNT (4,0) promote the decrease of both acoustic velocities values; while CNT (5,0) and CNT (3,3) linearly increase the values, and for tobermorite with CNT (5,0) the two curves became ample closer.

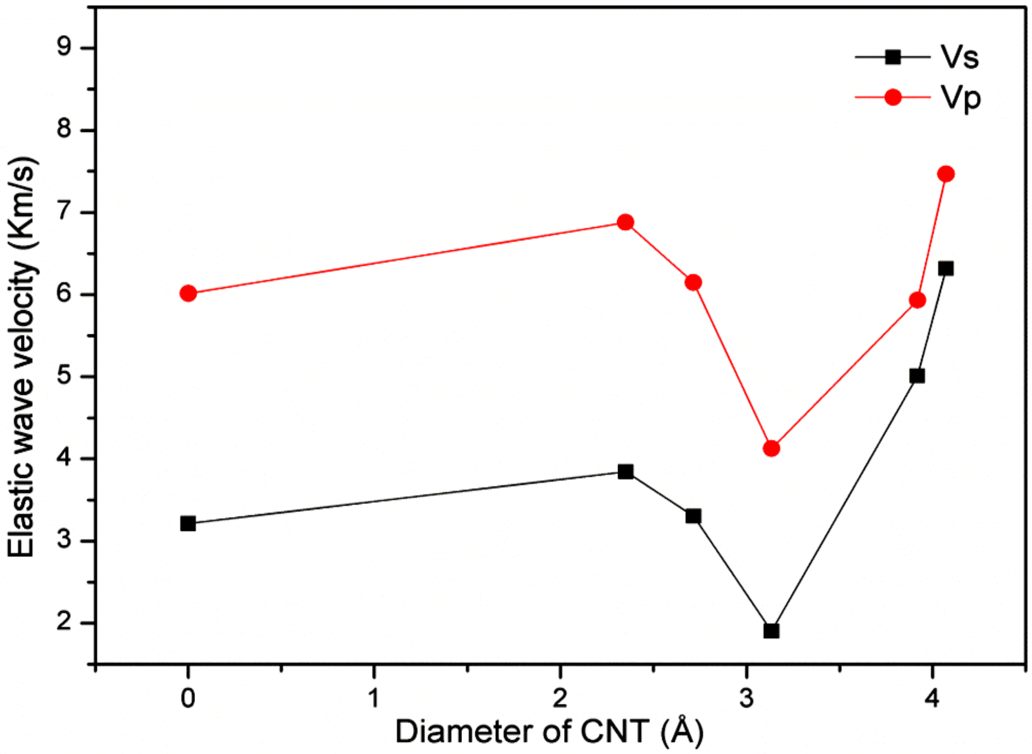

Fig. 3.11. Variation of transversal V_s and longitudinal V_p wave velocities with diameters of CNT.

3.2.6. Piezoelectric effect

The piezoelectric constants of different systems C-S-H/CNT are shown in Table 3.9. The most important values are d_{33}, d_{13} and d_{15}. The value of d_{33} induced polarization in direction 3 per unit stress applied in direction 3; d_{13} induced polarization in direction 3 per unit shear stress applied along direction 1; d_{15} induced polarization in direction 1 per unit shear stress applied in that direction.

Comparing those values for different systems, we may remark that the system without nanotube have the value 0. The inserting of carbon nanotube changes the piezoelectric constants. In addition to the diameter of the nanotubes, the nanotube's type plays a significant role. In our case, the absolute values of d_{33}, d_{13} and d_{15} for the CNTs having biggest diameters were greatly increased; whereas for the CNTs having the smallest diameters the change of the absolute values is not as high.

Table 3.9: Piezoelectric constants for Tobermorite 11Å and Tobermorite 11Å modified by CNT.

Piezoelectric constants (C/m^2)	*Tobermorite (Ca/Si =0.83)*	*Tobermorite + CNT (3,0)*	*Tobermorite + CNT (2,2)*	*Tobermorite + CNT (4,0)*	*Tobermorite + CNT (5,0)*	*Tobermorite + CNT (3,3)*
d_{11}	0	6.41	0.11	-9.86	28.02	-14.97
d_{12}	0	4.14	1.85	-8.86	-63.01	-7.36
d_{13}	0	3.17	-0.49	26.29	12.65	17.75
d_{14}	0.1	2.79	-3.33	-1.53	0.08	-15.36
d_{15}	0	-0.41	0.89	-1.72	24.95	5.58
d_{16}	0.41	-0.12	3.59	-5.39	86.11	14.94
d_{21}	-1.12	9.94	-21.31	11.11	4.66	-12.62
d_{22}	2.67	1.65	-5.78	3.27	-19.97	-30.72
d_{23}	2.52	8.08	-26.39	-18	1.74	44.29
d_{24}	0	2.91	16.79	5.94	1.95	-29.9
d_{25}	1.67	-3.39	9.78	-1.2	15.77	20
d_{26}	0	-1.58	1.77	3.95	19.75	27.36
d_{31}	0	-5.84	-6.06	1.52	-38.97	-9.99
d_{32}	0	-1.94	0.01	0.56	95.13	-13.89
d_{33}	0	-5.21	-2.22	-18.6	-14.91	-1.83
d_{34}	-0.11	2.37	1.87	7.34	2.35	2.32
d_{35}	0	0.96	2.42	0.42	-35.48	-0.39
d_{36}	1.11	-1.05	-0.38	6.2	-134.75	3.11

3.2.7. Conclusion

In this part, the concept of different types of CNTs and their possibility of incorporating into the Tobermorite 11Å structure has been studied. We have shown the necessary distance of vacuum between the Tobermorite 11Å and CNT, which equals to ~2 Å. This distance let change morphology of the structure of C-S-H in response to the creating the new formation around the nanotube, which gives the perspective to have new performance of concrete from the incorporation of CNT.

Additionally, some promising results of the mechanical properties of C-S-H reinforced with this type of CNT have been investigated. Modification of the Tobermorite 11Å by the CNT (3,0) with a diameter of 2.351Å increases all the mechanical parameters such as bulk modulus, shear modulus, plane stress and modulus Young's modulus at the same time and also gives the best adhesion between the structure of C-S-H and CNT's structure.

Besides, it is note that some nanotubes can change the behavior of composite from brittle to ductile, and more precisely, the CNTs with the bigger diameters such as 3.319 Å and 4.073 Å.

Despite the fact that at macro level the cement composite with CNTs may be considered as an isotropic material, it is in fact anisotropic at nanoscale level. Our study provided the exact values of the anisotropy for the concrete modified with carbon nanotubes.

In summary, it can be noted that the nanotubes are an excellent example of improving the mechanical properties of cement concrete. Present work allows selecting a specific type of nanotubes, depending on parameter which we want improving.

3.3. Density effect of Carbon Nanotubes in the Cementitious Composites. Case of Tobermorite 11Å with Ca/Si ratio of 0.83

3.3.1. Input preparation

In present work six different models, shown in Figure 3.12, have been applied to calculate the effect of the CNT's density into the concrete. We have used the Tobermorite 11Å developed by Hamid [43] to represent the compounding ingredient of the concrete. Classified under the space group P21, the Tobermorite 11Å structure is a monoclinic structure with unit cell dimensions: a =7.39 Å, b = 22.779 Å, c = 6.69 Å and α = 90°, β = 123.49°, γ = 90°. In our case, 105 crystallographic unit cells of the Tobermorite 11Å repeats to construct a 5 x 3 x 7 supercell (a =36.95 Å, b = 68.34 Å, c = 46.83 Å) with a total atom number of 7770.

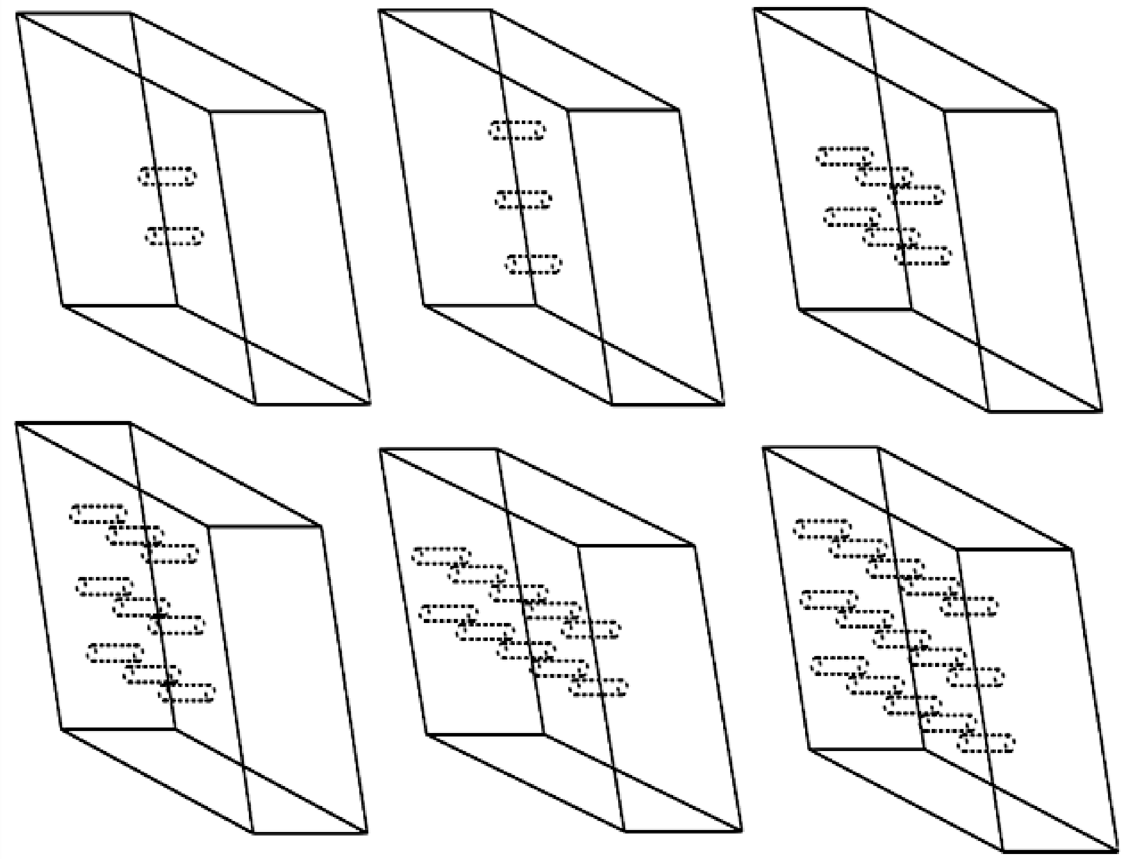

Fig. 3.12. Schematic view of the different types of CNT's inserted into the Tobermorite 11Å.

The same method to create the hole allowing the inserting CNTs into the tobermorite structure, and the same force field used in the abovementioned paragraph, were adapted for the present part.

3.3.2. Structural optimization

The checking procedure of the system stability is the task of prime importance. Thus, having determined the internal energy of the system it is possible estimate the total energy of the system. The negative value of the total energy can signify about favorable interaction between the components of the system.

The total energy variation versus the number of CNT in the system CNTs/tobermorite is shown in Fig. 3.13. Since each model has different number of atoms, we have also considered the total energy per atom. We may see that we have the same tendency in both cases. Some way or other, calculations show a favorable interaction between Tobermorite 11Å and CNTs as indicated by the negative values of the total energies.

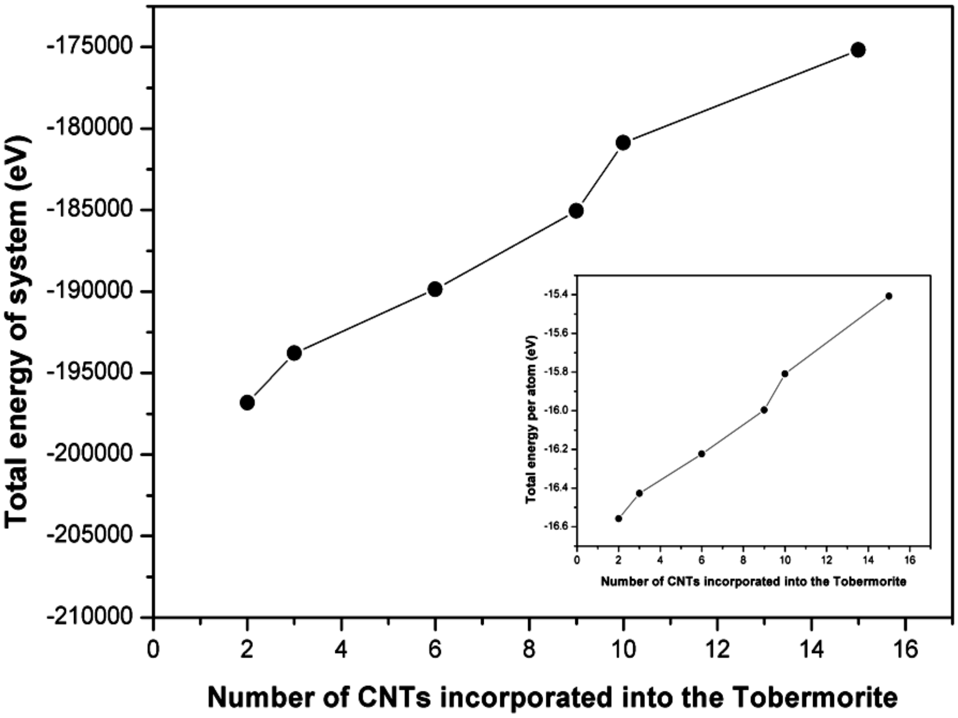

Fig. 3.13. Total interaction energy and total energy per atom of the system C-S-H/CNT with different number CNT inserted into the Tobermorite 11Å.

3.3.3. Calculation of mechanical properties

Having determined the optimized structure for each model of the system tobermorite/CNT, it is possible to calculate the various physical properties. In our study we evaluate the mechanical properties such as the bulk modulus (B), shear modulus (G), Young's modulus (Y) and the Poisson's ratio. In order to investigate the mechanical properties of Tobermorite 11Å with different number of CNTs we undertake different simulations with constant volume optimization.

Figure 3.14 shows the obtained mechanical properties of the system C-H-S/CNT. Results show that the CNT's number inserted into the Tobermorite 11Å affect the values of K, G, Y. Shear modulus and Young's Modulus reached the best values of 59 GPa and 133.79 GPa respectively when we insert 6 CNTs. The shear, Young's and bulk Modulus seem to increase rapidly with quantity of CNTs between 2 and 6, relatively stable between 6 and 9, and decrease slightly from 9.

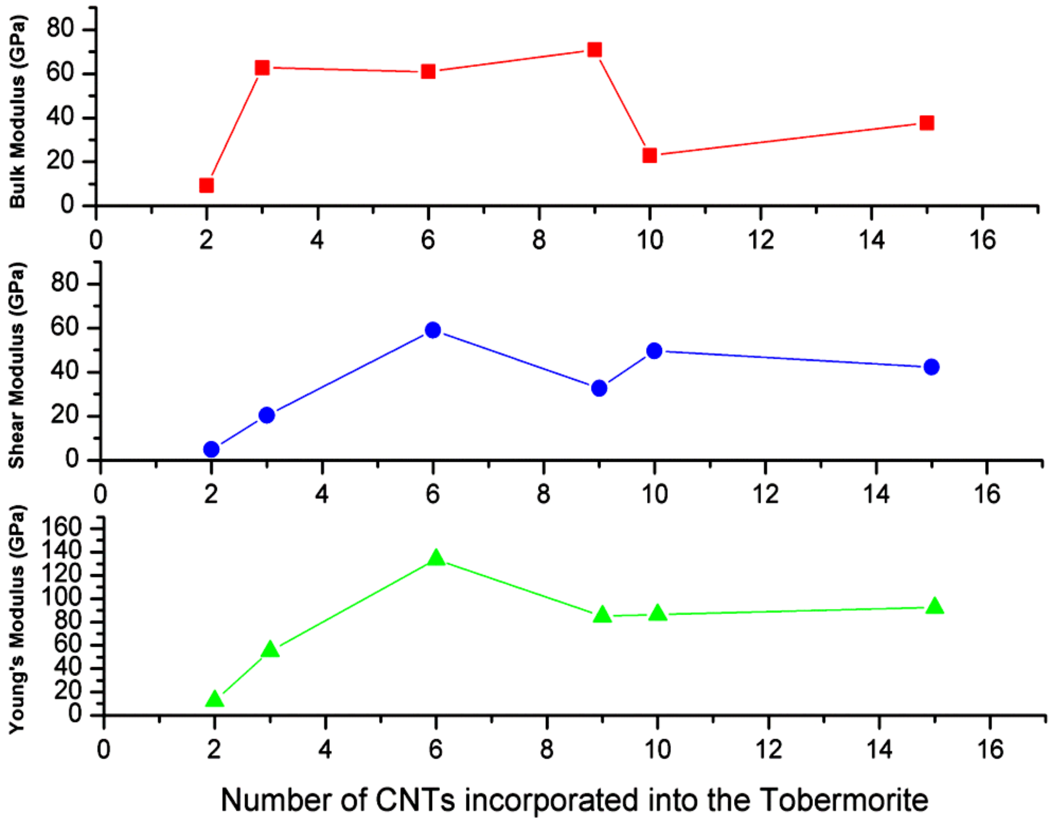

Fig. 3.14. Effect of the CNT's number on the Bulk, Shear and Young's modulus of the system C-H-S/CNT.

The obtained Poisson's ratio υ is presented in Table 3.10. Calculated Poisson's ratio values are between -0.13 and 0.3. Typical Poisson's ratio for concrete is 0.2. These results show that the concentration of nanotubes affects on the behavior of the composite. For example, when Tobermorite 11Å is modified by the nanotubes with a quantity between 2 to 9, we have the elastic behavior of the composite; when the quantity of the nanotubes is from 10 to 15 the material becomes more brittle.

Table 3.10: Poisson's ratio values of the systems tobermorite/CNTs.

	Number of CNTs incorporated into the tobermorite					
	2	***3***	***6***	***9***	***10***	***15***
Poisson's ratio	0.27	0.5	0.13	0.3	-0.13	0.09

From the previous works, we can note that the concentration of nanotubes in the cement matrix was varying from 0.5 to 2% by weigh of cement [16, 18, 20, 21, 55]. Regarding the experimental works, it is important to keep in mind that the cement is formed by different components. In such a manner, scientists in their experimental investigations have calculated the percentage of CNT by weight of cement (summation of all components of cement). It is important to note that in our simulation work we have only one component, i.e. Tobermorite 11Å, to represent the cement.

At atomic level it is possible to calculate the mass of structures. It is well known that one atomic mass unit equals to 1/12 x mass of one ^{12}C atom. Thus, atomic mass is the relative atomic mass of an atom with respect to 1/12th of the mass of carbon^{-12} atom. It is found that, the actual atomic mass of a carbon^{-12} atom is equal to 1.9926 X 10^{-26} kg. Therefore, atomic mass unit is given as:

$$1 \text{ amu} = 1.9926 \times 10^{-26}/12 = 1.6605 \times 10^{-27} \text{ kg} \quad (1)$$

The absolute mass of atom can be calculate from the following equation:

$$m_{absolute} = m_{relative} * 1\text{amu} \quad (2)$$

There are five different type of atoms in our system: tobermorite/CNT and knowing those relative mass from the Periodic Table we may calculate the absolute mass of each other:

$m(Ca)= 40.08*1.661 \times 10^{-27}$ kg $= 66.57288 \times 10^{-27}$ kg
$m(Si)= 28.086*1.661 \times 10^{-27}$ kg $= 46.650846 \times 10^{-27}$ kg
$m(H)= 1.00797*1.661 \times 10^{-27}$ kg $= 1.67423817 \times 10^{-27}$ kg
$m(O)= 15.9994*1.661 \times 10^{-27}$ kg $= 26.5750034 \times 10^{-27}$ kg
$m(C)= 12.001115*1.661 \times 10^{-27}$ kg $= 19.95052015 \times 10^{-27}$ kg

The total number of each atom is presented in Table 3.11 and the results of mass calculation and percentage of CNT by weight of Tobermorite 11Å are presented in Table 3.12.

Table 3.11: Number of atoms in the systems tobermorite/CNTs.

	Number of CNTs incorporated into the tobermorite					
	2	***3***	***6***	***9***	***10***	***15***
Total atoms number of CNT/tobermorite system	11886	11796	11702	11568	11441	11370
Total atoms number of tobermorite	11790	11652	11414	11136	10961	10650
Number of Ca atoms	1030	1014	978	942	927	900
Number of Si atoms	1236	1218	1192	1158	1132	1086
Number of H atoms	1260	1260	1260	1260	1260	1260
Number of O atoms	8264	8160	7984	7776	7642	7404
Total atoms number of CNT (number of C atoms)	96	144	288	432	480	720

Table 3.12: Absolute atomic mass of the structures and percentage of CNT by weight of Tobermorite 11Å.

	Number of CNTs incorporated into the tobermorite					
	2	***3***	***6***	***9***	***10***	***15***
Absolute atomic mass of tobermorite (kg)	347955.9*E-27	343287.2*E-27	335000.4*E-27	325490.1*E-27	319717.5*E-27	309449.3*E-27
Absolute atomic mass of CNT (kg)	1915.2*10-27	2872.9*E-27	5745.8*E-27	8618.6*E-27	9576.2*E-27	14364.4*E-27
Percentage of CNT by weight of tobermorite (%)	0.5504	0.83687	1.7151	2.648	2.995	4.642

To the best of our knowledge, no published report is available on molecular dynamics study of the CNT's density effect in the C-S-H. Therefore the comparison of the values of Young's modulus from experimental data with the values from the current study (Table 3.13) could be complicated because of the different type of carbon nanotubes, as well as different based material. As mentioned above, we used only one of the component of concrete's structure, i.e. tobermorite. In addition, there are different methods of preparation the system C-S-H/CNT. However, despite these differences we obtain values of Young's modulus, which compare well for instance to those extracted from RVE Methods [56].

Table 3.13: Young's modulus for the C-S-H/CNT system compared to experimental data.

Reference	*Method*	*Matrix*	*Type of CNT*	*Young's Modulus (GPa)*
Present work	MD	Tobermorite 11Å	SWCNT (0.55 wt.%)	12.49
			SWCNT (0.84 wt.%)	55.16
			SWCNT (1.71 wt.%)	133.79
			SWCNT (2.65 wt.%)	84.88
			SWCNT (2.99 wt.%)	86.42
			SWCNT (4.64 wt.%)	92.32
[56]	RVE numerical study	Cement model	SWCNT (0.09 wt.%)	20.34
			SWCNT (0.22 wt.%)	23.72
			SWCNT (0.42 wt.%)	40.73
			SWCNT (0.72 wt.%)	63.64
			SWCNT (1.2 wt.%)	92.28
[19]	Experimental study	Cement paste	MWCNT (0.08 wt.%)	21.9
[15]			MWCNT (0.08 wt.%)	13
[53]		Mortar	MWCNT (0.08 wt.%)	25
			MWCNT (0.1 wt.%)	27.5
			MWCNT (0.3 wt.%)	21.3
			MWCNT (0.5 wt.%)	20.1
[54]		OPC paste	MWCNT (0.038wt.%)	18.28
			MWCNT (0.075wt.%)	20.84

3.3.4. Conclusion

Different models representing the concrete modified by CNTs were constructed to investigate the density effect of carbon nanotubes in the cementitious composites. Molecular dynamics method based on energy minimization was used to analyze the stability of the system including the Tobermorite 11Å with CNTs. The present study focused mainly on the evaluation of the mechanical properties of the composites. Optimal concentration of CNT was fixed. For example, the best Shear modulus and Young's Modulus were achieved with the CNT's concentration 1.7 % per weight of Tobermorite 11Å, and the best Bulk modulus for 2.6 % per weight of

Tobermorite 11Å. In addition, the Poisson's ratio has also been evaluated. The values of the Poisson's ratio were confirmatory factor showing a dependence the material properties on the concentration of nanotubes introduced into this material, which showed the best concentration range where material increase its mechanical properties.

3.4. Modification of C-S-H Structure from Inserted Carbon Nanotubes: Effect the density of Nanotubes in the case of Tobermorite 11Å with Ca/Si ratio of 1

3.4.1. Input preparation

For this study two types of carbon nanotubes were chosen: "Armchair" and "Zigzag". We prepared five CNTs of the length ~17 Å with different diameters CNT (3, 0) with d = 2.351 Å; CNT (4, 0) with d = 3.135 Å; CNT (5, 0) with d = 3.919 Å; CNT (2, 2) with d = 2.715 Å; and CNT (3, 3) with d = 4.073 Å.

The C-S-H gel structure revealed the poorly crystallized regions having a resemblance to the structures such as tobermorite and jennite. The most used model to present the structure of C-S-H gel is Tobermorite 11Å. One of the most important factors in presenting a realistic molecular model of tobermorite is Ca/Si ratio. The best known Ca/Si ratios for Tobermorite 11Å are 0.66; 0.83 and 1 [57]. This variation depends on the age of cement pastes and the water/cement ratio. In the present study we used the Hamid's model of Tobermorite 11Å [41] with Ca/Si ratio of 1, which is presented in Fig. 2. In this model (Fig. 3.15) the silicate chains repeats at intervals of three tetrahedra forming a Drierketten type of structure where, on the one side, the silica tetrahedra connected to only one silica tetrahedra Q^1 and, the other side, with two other silica tetrahedral Q^2.

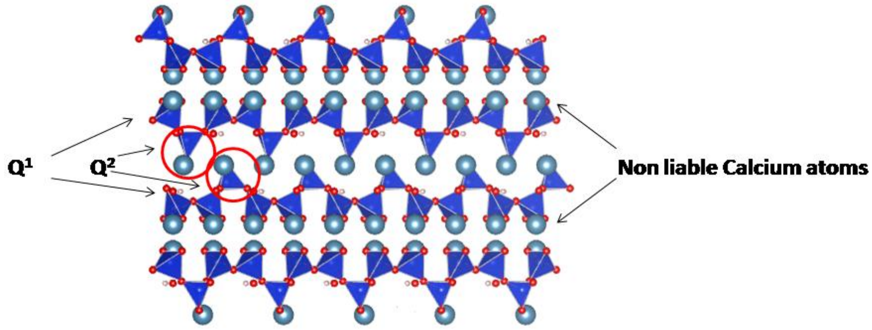

Fig.3.15. Model of Tobermorite 11Å with Ca/Si ratio of 1.

In this part of work, we used 30 and 105 crystallographic units to create a 5 x 2 x 3 and 5 x 3 x 7 supercells respectively for two main sized model of different study's purposes. In order to create the system tobermorite/CNT we inserted the carbon nanotube into the structure of the Tobermorite 11Å (Fig. 3.16). The hole in the structure of tobermorite was created keeping the neutral charge of the system. We apllied the same conditions and force field like in the previous parts.

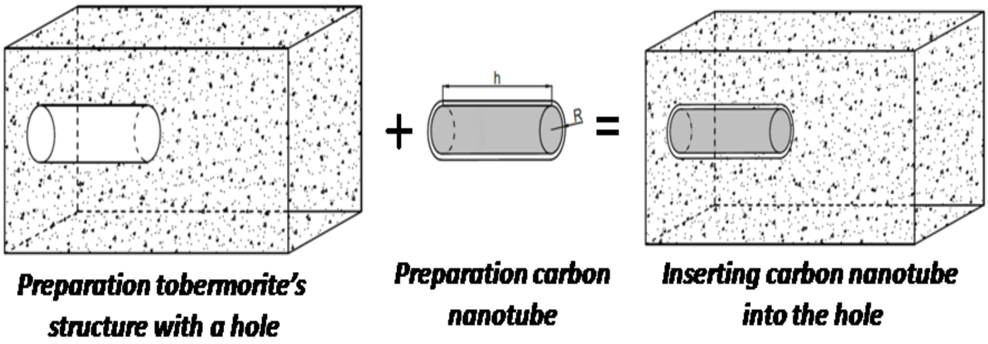

Fig. 3.16. Schematic view of the production line to system tobermorite/CNT.

3.4.2. Inter-structural interaction energy

In the first instance, it is important to know which type of CNT will be the best to modify Tobermorite 11Å with the ratio Ca/Si=1. At the same time it is necessary to understand the needful distance of vacuum between these examined structures. According to the previous study in this work, we have used the same distance between CNT and tobermorite, i.e. 2 Å.

The first task was to find the minimum energy structure for the present composite rather to find the local minimum on the global potential energy surface when the initial coordinates are in close proximity. The volume constant optimization was used during the simulation procedure. As presented in Fig. 3.17 the total interaction energy (Δ E) between the surface of Tobermorite 11Å and CNT with different diameters shows the beneficial effect on interaction between tobermorite and CNTs presented by negative values of total energy. The maximal value in absolute magnitude (encircled in red on Fig. 3.17) demonstrates the best inner structural affinity. In our case it is “Armchair” CNT (2, 2) with diameter equal to 2.715 Å.

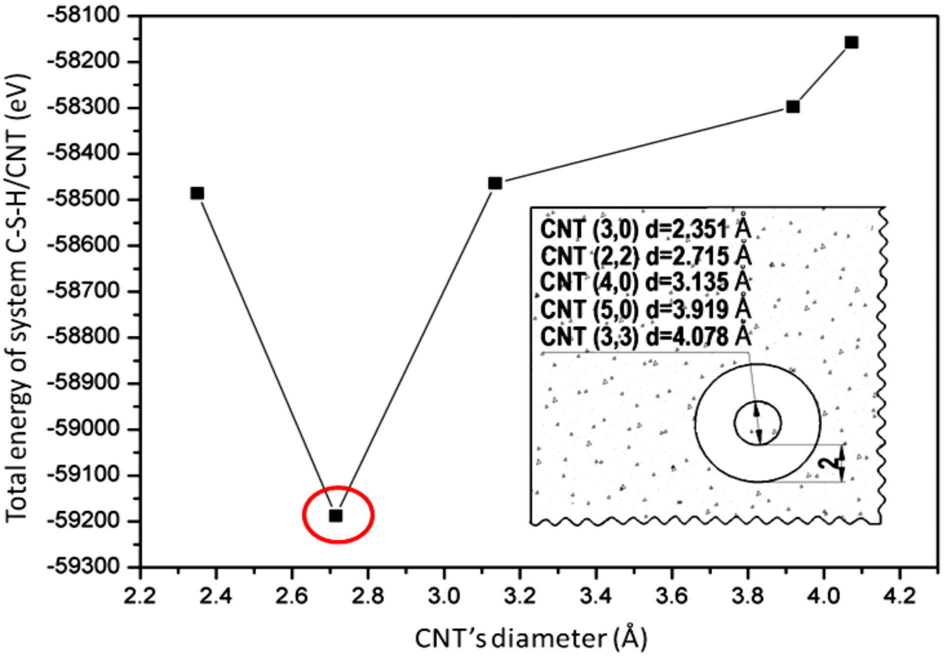

Fig. 3.17. Total interaction energy between tobermorite and CNT with different diameters.

3.4.3. Interfacial bonding energy and work of separation

Having information about the interaction between structure of CNT and structure of the tobermorite we estimated the work of separation between these two structures. The concept of interfacial bonding energy is used to describe the quantity of energy required to separate the structures hardly.

Analyzing the results plotted in Fig. 3.18 for given models on all occasions we can note the attractive forces between the present structures because of the negatives values of ΔE.

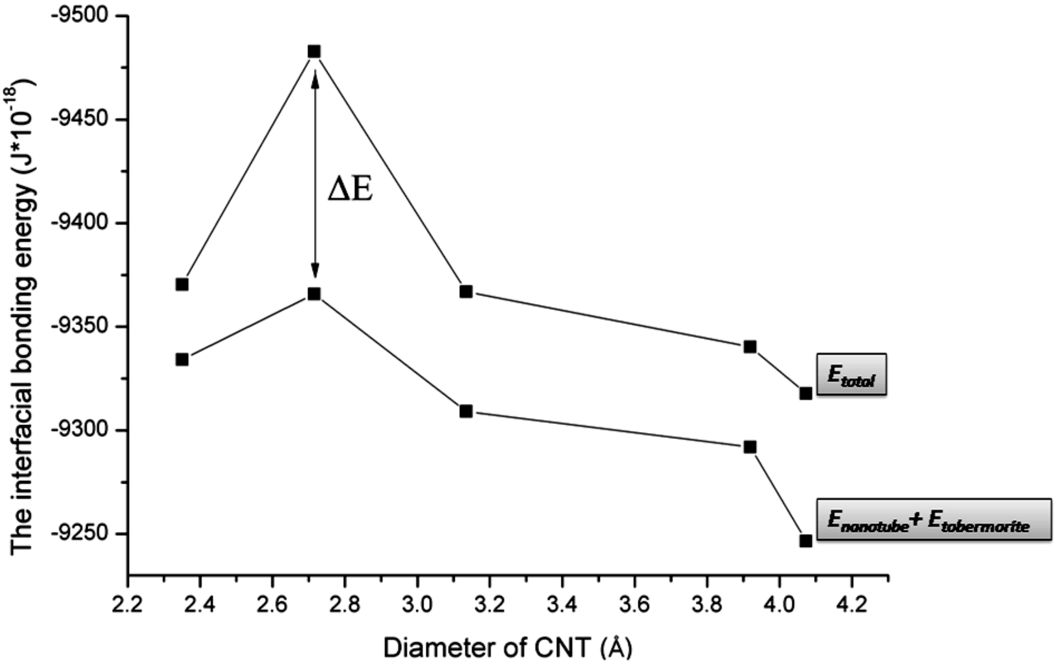

Fig. 3.18. The interfacial bonding energy of system tobermorite/CNT.

From the obtained values of ΔE and contact area *A*, we have calculated the work of separation and presented the results in Fig.3.19.

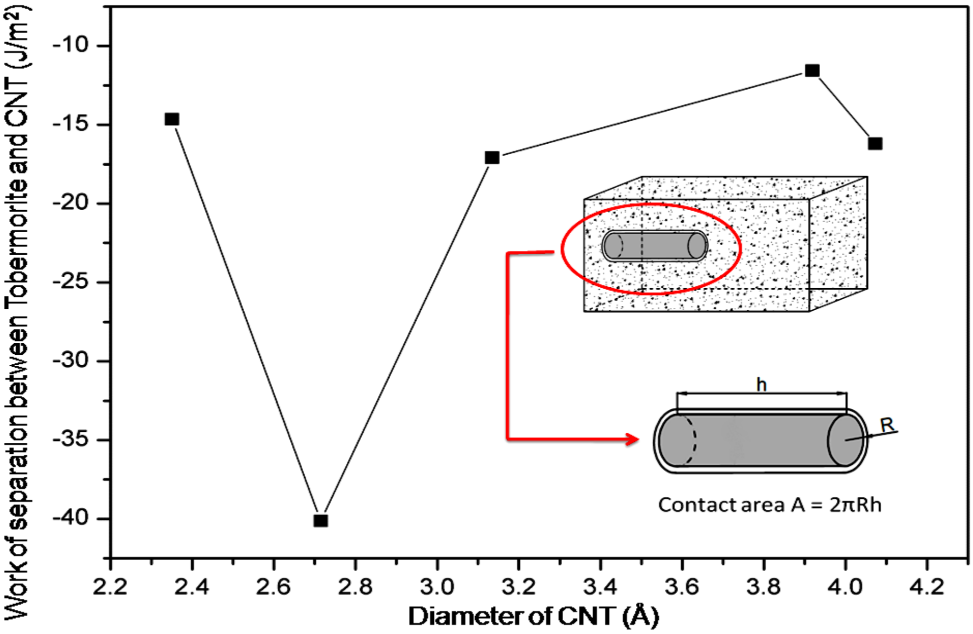

Fig.3.19. The effect of CNT's diameter on the work of separation between the structures of tobermorite and CNT.

The obtained results show that the type of carbon nanotube affects the work of separation between Tobermorite 11Å structure and nanotube's structure. Inference should be drawn that "Armchair" carbon nanotube with diameter of 2.715 Å have the best adhesion with surface of Tobermorite 11Å.

3.4.4. Mechanical properties

The various mechanical properties were estimated to describe the influence of the different carbon nanotube's types on the C-S-H gel. To give the information about the behavior of the composite under various stress conditions, the bulk, shear, Young's and plane stress moduli were calculated.

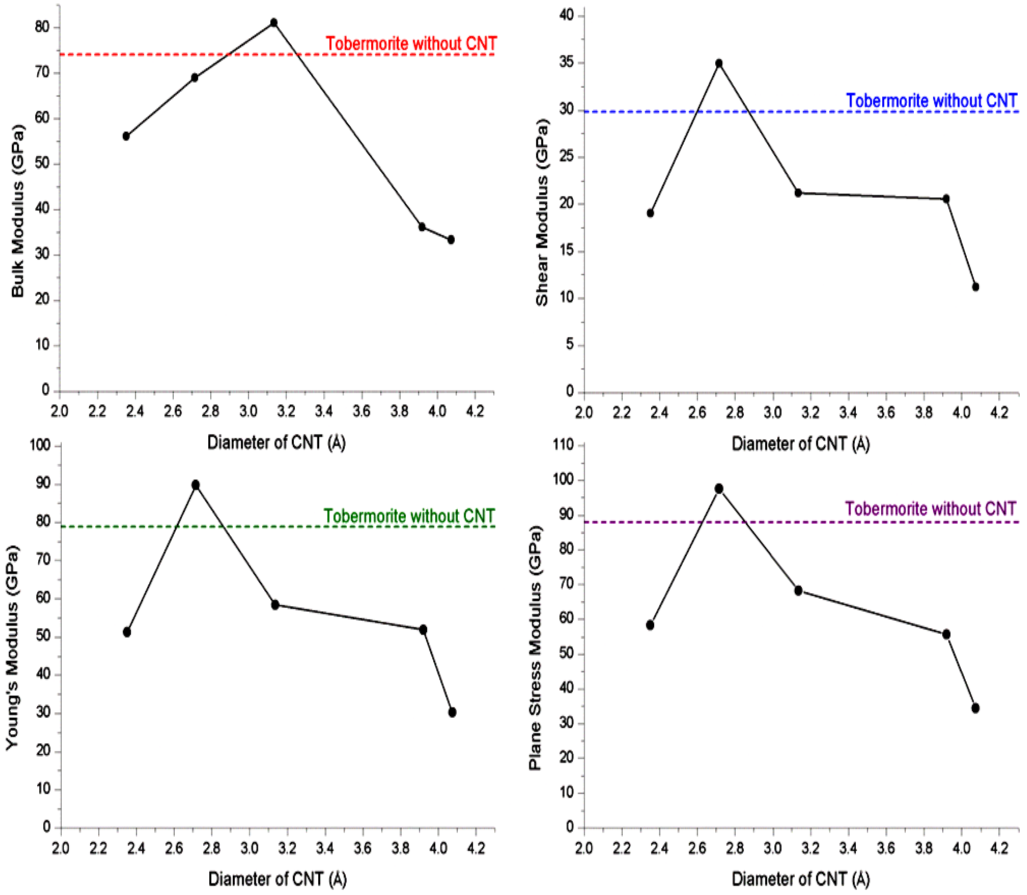

Fig. 3.20. Effect of CNT's type on the mechanical properties of the system C-S-H/CNT.

The obtained results of bulk, shear, Young's and plane stress moduli for the C-H-S modified with different types of CNT are introduced in the Fig. 3.20. On the graphs, the dash-and-dot line demonstrates the values of bulk, shear, Young's and plane stress moduli for Tobermorite 11Å without CNT. It may be noted that the different types of CNT have different effects on the values of corresponding moduli. Thus, all of the moduli, except the bulk modulus have raised their values with modification the Tobermorite 11Å by CNT (2, 2) with diameter of 2.715 Å. At this rate, the shear modulus reached 34.95 GPa that gives an increase of 17.3 %, Young's modulus reached 89.72 GPa that gives an increase of 13.8 % and the plane stress modulus reached 97.56 GPa that gives an increase of 10.8 % in comparison with the sample without CNT. However, the increasing of bulk modulus, which equals 9.4 % was obtained by modification the tobermorite by CNT (4, 0) with diameter of 3.135 Å.

Poisson's ratio characterizes the ability of a material to resist of the lateral deformation. Fig. 3.21a shows that the control simple without CNT has the Poisson's ratio of 0.32. The samples modified with CNT (3, 0), CNT (4, 0) and CNT (3, 3) amplify the Poisson's ratio value. In these circumstances we can see the rise of interaction atomic force.

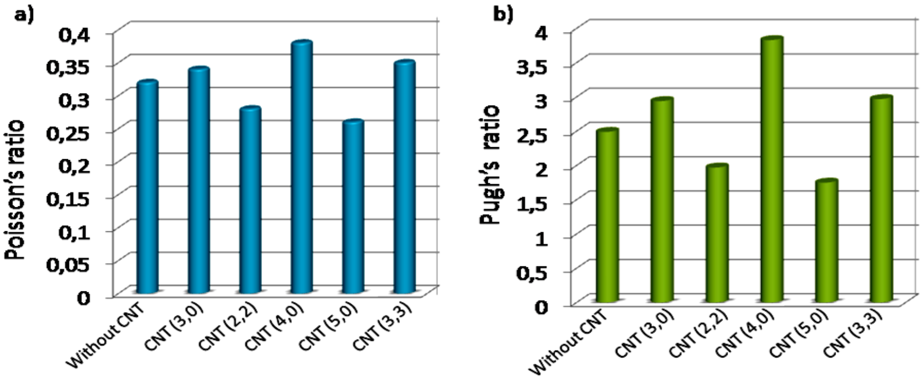

Fig. 3.21. Effect of CNT's type on Poisson's ratio (a) and Pugh's ratio (b) of the system C-S-H/CNT.

Pugh's ratio, which reflects the ductility of the structure was also calculated. From Fig. 3.21b we can see that the samples modified with CNT (2, 2) and CNT (5, 0) clearly reduce the weakness of the composite.

All the above listed properties have been calculated and compared with experimental data in consideration of isotropic behavior of the models. At the nano level, CNTs inserted into cement matrix give the anisotropic behavior for the composite. The following properties such as anisotropic Zener factor and the elastic wave velocities were calculated based on the anisotropic behavior of the system.

As a first step, the components of elasticity tensors for all present models were investigated (Table 3.14). The insertion of CNT in the structure of Tobermorite 11Å changes the monoclinic structure of tobermorite to the triclinic structure. The CNT was inserted to the structure of tobermorite in the direction parallel to X axis, consequently the elasticity components in this direction can be changes more significantly than in the other direction. From Table 3.14 we may see that C_{11} of the specimen with CNT (4,0) have the value of 183.41 GPa; while the value of tobermorite without CNT is 177.95 GPa. This suggests that in this direction the structure was strengthened. However, the modification by other types of CNT didn't give this effect. Regarding the components C_{22} and C_{33} we can note the weakening of these components in most cases of specimen with nanotubes.

Table 3.14: Components of elasticity tensors of Tobermorite 11Å and model tobermorite/CNT.

Elastic constants	*Tobermorite (Ca/Si =1)*	*Tobermorite + CNT (3,0)*	*Tobermorite + CNT (2,2)*	*Tobermorite + CNT (4,0)*	*Tobermorite + CNT (5,0)*	*Tobermorite + CNT (3,3)*
C_{11}	177.95	153.46	165.81	183.41	156.17	147.54
C_{12}	53.87	55.44	42.7	51.57	19.99	41.89
C_{13}	57.83	70.92	47.31	74.96	22.59	51.99
C_{14}	0	0.25	-1.54	-4.99	-12.32	-1.55
C_{15}	-5.2	19.88	-3.02	-2.28	21.25	6.87
C_{16}	0	22.15	-2.08	12.58	-0.55	6.30
C_{22}	121.06	131.40	97.94	86.71	56.59	88.03
C_{23}	36.37	78.02	29.25	62.28	18.86	53.45
C_{24}	0	-7.48	4.63	-7.43	-11.96	-2.39
C_{25}	-1.91	50.08	-0.52	4.35	9.08	19.31
C_{26}	0	50.19	0.59	8.62	11.31	39.06
C_{33}	149.35	137.58	141.8	168	106.23	147.79
C_{34}	0	-18.27	-0.69	-7.81	-14.10	6.97
C_{35}	-7	31.00	-4.97	-7.47	-20.55	-1.8
C_{36}	0	55.25	0.74	19.23	13.26	13.7
C_{44}	22.03	3.57	21.4	4.63	9.66	0.07
C_{45}	0	-2.61	-1.8	1.15	-7.58	5.33
C_{46}	-0.08	-9.06	-0.39	-1.89	-5.92	-2.7
C_{55}	42.57	46.97	34.51	38.99	48.03	27.76
C_{56}	0	33.66	-0.38	-3.53	-0.45	1.6
C_{66}	36.71	62.85	33.33	-10.35	12.72	19.98

After that, we were able to examine the anisotropy of the structures. Anisotropy means that the distance between the atoms and the bonding strength of atoms are different into the crystal structure. The symmetry of the crystal is lower when the anisotropy of the structure is greater. The obtained results of Zener anisotropy factors are shown in Table 3.15. In all cases the values are lower than 1, what clearly indicates the anisotropy of these systems.

Table 3.15: Zener anisotropy factor and elastic wave velocities of Tobermorite 11Å and models tobermorite/CNT

			Zener anisotropy factor A	***Longitudinal wave velocity Vs, Km/s***	***Transversal wave velocity Vp, Km/s***
Tobermorite without CNT			0.355	3.098	6.055
C-S-H + CNT	***CNT's diameter (Å)***	***2.351***	0.073	2.494	5.162
		2.715	0.073	3.377	6.143
		3.135	0.07	2.63	5.974
		3.919	0.142	2.601	4.574
		4.073	0.001	1.922	3.99

We presented the obtained acoustic velocities values in Fig. 3.15. Insertion of CNT (2.2) increases greatly the values of V_p and V_s. However, with increase of the CNT's the values of both elastic waves spiral down.

3.4.5. Piezoelectric effect

The piezoelectric constants of Tobermorite 11Å and models tobermorite/CNT are shown in Table 3.16. From the analysis of the results one can remark that the system without nanotube have the value of 0 for d_{33}, d_{13} and d_{15}. The incorporation of carbon nanotube into the tobermorite's structure changes the piezoelectric constants. The diameter of the nanotubes plays a prominent role. In our case, the speciments of Tobermorite 11Å modified by "Zigzag" CNT types have the most higher absolute values of d_{33}, d_{13} and d_{15}.

Table 3.16: Piezoelectric constants of Tobermorite 11Å and models of tobermorite/CNT.

Piezoelectric constants (C/m^2)	*Tobermorite (Ca/Si =0.83)*	*Tobermorite + CNT (3,0)*	*Tobermorite + CNT (2,2)*	*Tobermorite + CNT (4,0)*	*Tobermorite + CNT (5,0)*	*Tobermorite + CNT (3,3)*
d_{11}	0	-3.58	-1.06	-2.84	-4.29	1.3
d_{12}	0	-12.3	-0.38	-3.09	-9.81	-5.33
d_{13}	0	-16.76	2.19	-5.41	-13.84	-0.15
d_{14}	-0.21	-1.49	-0.16	-0.27	-1.81	-0.45
d_{15}	0	-15.41	-1.18	-0.19	2.56	-1.28
d_{16}	0.01	-13.72	-1.14	2.5	1.35	8.74
d_{21}	3.37	0.93	-0.14	9.79	5.58	6.09
d_{22}	0.25	-0.84	-0.96	4.04	0.79	6.05
d_{23}	-1.36	8.07	1.1	13.68	6.55	8.33
d_{24}	0	0.69	0.36	-2.33	-2.14	-1.47
d_{25}	-1.55	4.93	-0.53	1.08	5.95	0.34
d_{26}	0	1.91	-0.59	6.82	3.88	-1.64
d_{31}	0	7.06	1.74	0.46	-2.63	1.15
d_{32}	0	18.04	-0.03	0.84	-2.67	3.42
d_{33}	0	20.51	1.45	2.59	-3.37	-0.83
d_{34}	-0.38	-0.92	-0.53	-0.48	-2.12	0.88
d_{35}	0	15.31	0.31	-0.46	0.75	-1.99
d_{36}	0.73	18.34	-0.3	-2.98	-1.17	-0.15

3.4.6. Study of the Tobermorite 11Å modification by "Armchair" carbon nanotube (2,2)

The results mentioned above give the reason to investigate mechanical properties of Tobermorite 11Å structure modified by carbon nanotube (2,2) with diameter 2.715 Å.

Previously it has been shown that the distance between the structure of carbon nanotube and the tobermorite's surface is suppositional. In present work we have tested various distances of the vacuum between CNT and Tobermorite 11Å in order to the have the best mechanical properties of the composite. From there, we constructed various models of tobermorite modified by CNT with different vacuum's distance between these two structures. It was possible to create other different distances of vacuum a far cry from 2 keeping the neutral charge of the system. The distances 1.16 Å; 2.48 Å; 2.69 Å; 3.44 Å; 3.79 and 4.4 Å were tested. The influence of the spacing of vacuum between tobemorite and CNT to the total energy of system is plotted in Fig. 3.22. As seen from the figure, with the increase of the vacuum's distance between CNT and tobermorite the interaction between these structures decreases significantly. If the distance is too small, the interaction between structures is quite weak. The results confirmed once more that the best distance of vacuum is 2 Å.

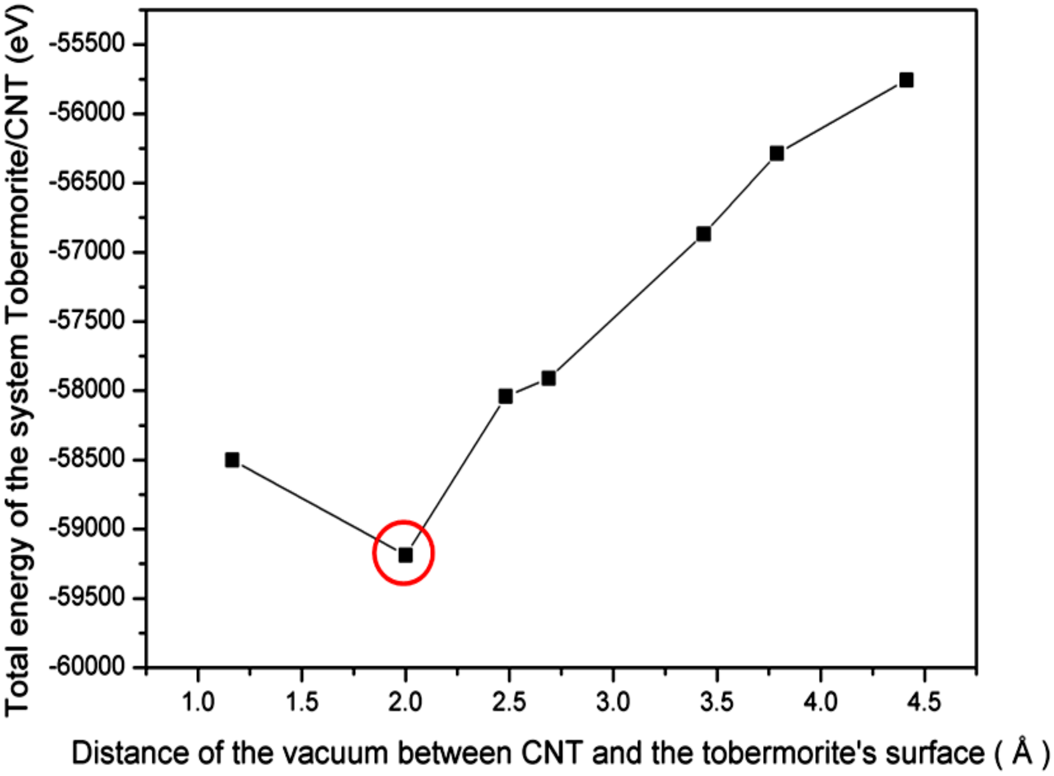

Fig. 3.22. Effect of vacuum's distance between CNT and Tobermorite 11Å surface on the total energy of the system tobermorite/CNT.

After that, the main mechanical properties such as bulk, shear and Young's moduli were investigated. Fig. 3.23 shows that the linear fit of all moduli decreases with increasing of CNT's diameters. By such manners the highest value of bulk modulus was found under 1.165 Å distance of vacuum. In the meantime the highest values of shear and Young's Moduli were found under the 2 Å of vacuum.

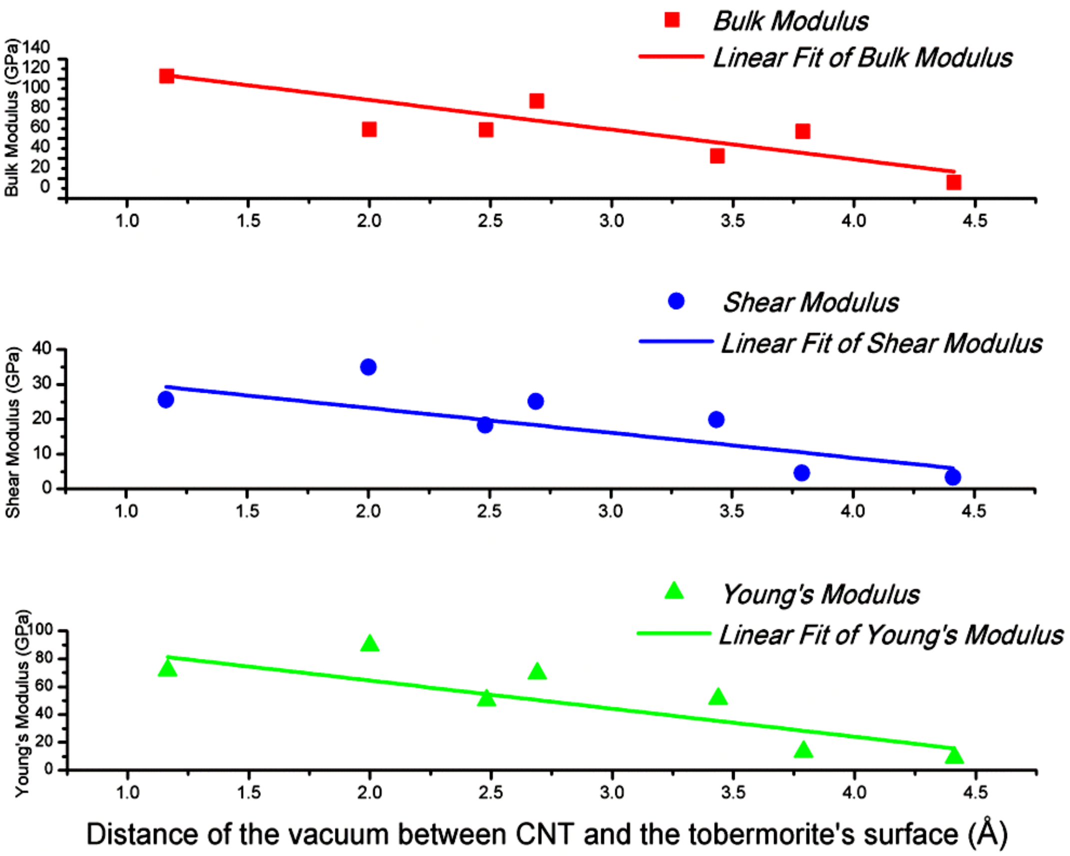

Fig. 3.23. Effect of distance of vacuum between the surfaces CNT and Tobermorite 11Å on the mechanical properties of the system C-S-H/CNT.

3.4.7. The density effect of CNTs

The preceding results were obtained for Tobermorite 11Å modified with one carbon nanotube. However, in the real conditions it is necessary to know the quantity of CNTs inserted into cement matrix. We present thereafter the investigation of the density effect of carbon nanotubes. Six diverse models displayed in the Fig. 3.12 were prepared. In all the models we used the carbon nanotube (2,2) with diameter 2.175 Å.

Firstly, we checked the stability of the composites by calculating the total energy for each model. Also we calculated the total energy per atom forasmuch the models have the different number of atoms. In Fig. 3.24 one can see the negative values of the total energy, what means the favorable interaction of CNT's atoms and tobermorite's atoms.

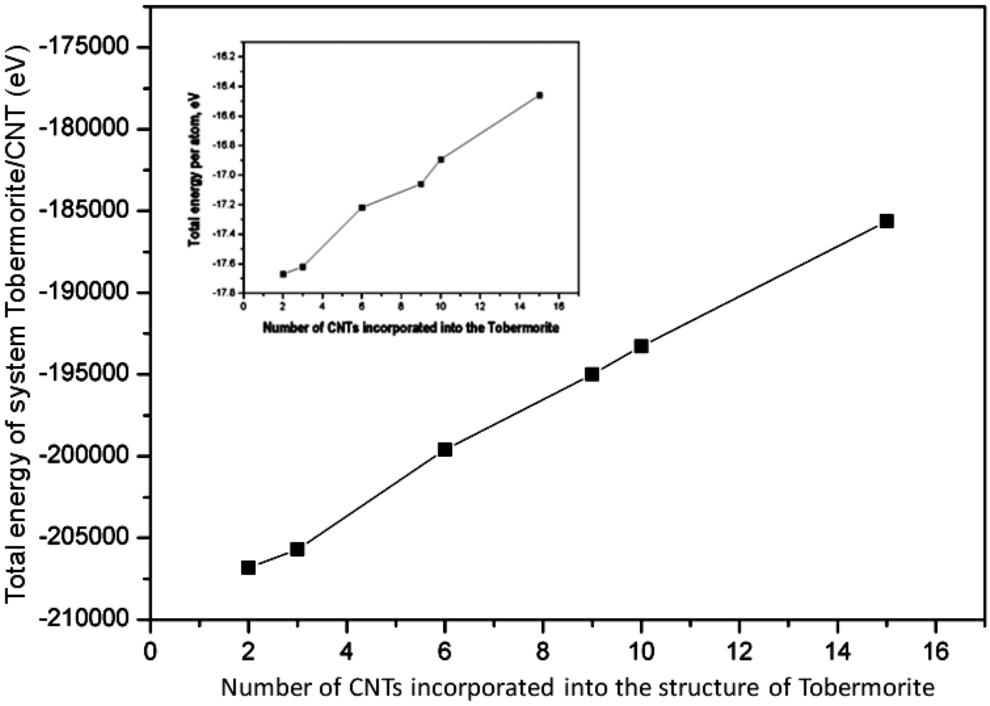

Fig. 3.24. Effect of the number of CNT incorporated into the structure of tobermorite on the total energy.

The concentration of CNTs by weight of cement was calculated at the atomic level using the atomic mass. Table 3.17 summarizes the weight percent concentration of CNTs corresponding to the number of CNT incorporated into tobermorite.

Table 3.17: Weight percent of CNT concentration corresponding to the number of CNT incorporated into the Tobermorite 11Å.

	Number of CNTs incorporated into the Tobermorite 11Å					
	2	***3***	***6***	***9***	***10***	***15***
Weight percent concentration of CNTs (%)	0.62	0.93	1.92	2.97	3.31	5.2

In the following, the mechanical properties were estimated. Fig. 3.25 shows the obtained mechanical properties of the Tobermorite 11Å modified by different concentrations of CNTs. Results show that the CNT's quantity inserted into the Tobermorite 11Å affects the values of bulk, shear and Young's moduli. Bulk, shear and Young's moduli attain the best values of 62.71 GPa, 49.28 GPa and 117.16 GPa respectively during the CNT's modification of 5,2 % by weight of tobermorite.

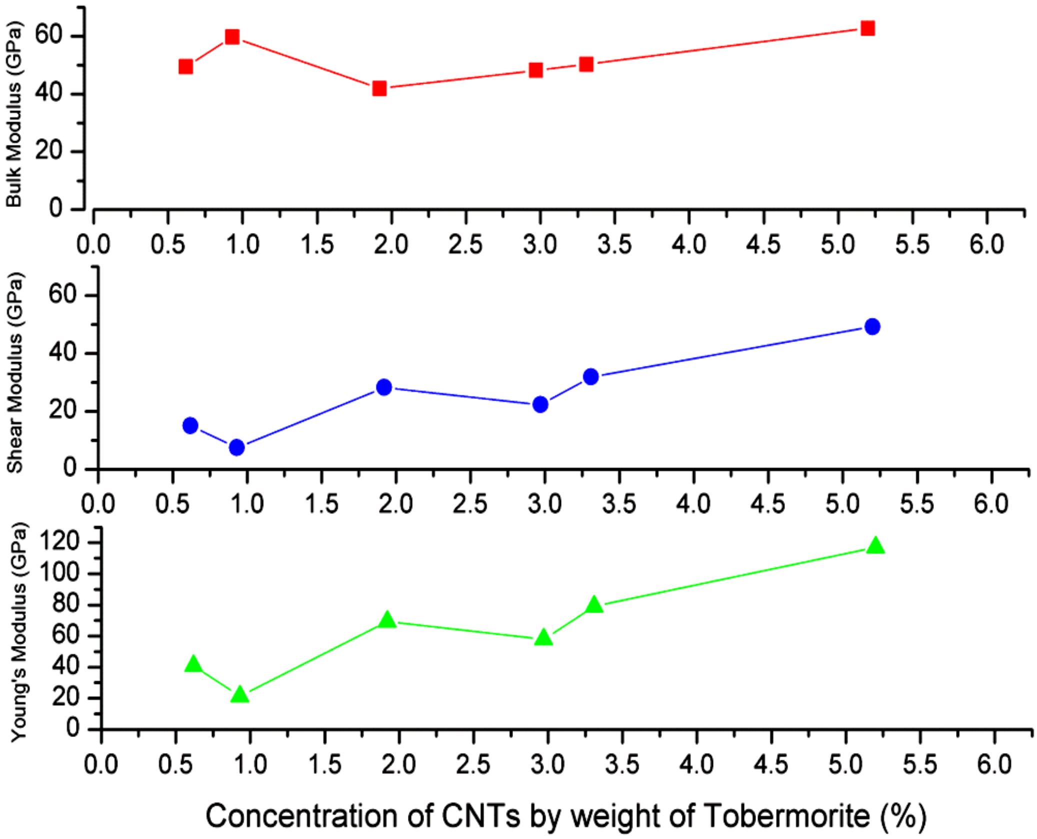

Fig. 3.25. Effect of the CNT's concentration on the mechanical properties of system tobermorite/CNT.

To the best of our knowledge, there is no published work available on molecular dynamics study of density effect of CNTs into the structure of Tobermorite 11Å. On the assumption of this fact, we compared our results with the experimental works. It is important to notice that cement composite is formed by different components. For the foregoing reasons, in the experimental investigations the percentage of CNT by weight of cement was calculated taking into account the summation of all components of cement. In addition, it is critical to underline here that different type of carbon nanotubes influence the final results. Despite these facts we demonstrated the favorable agreement between the experimental values of Young's modulus and those obtained in the present study (Table 3.18).

Table 3.18: Young's Modulus of the system tobermorite/CNT compared to previous experimental data.

Reference	*Method*	*Matrix*	*Type of CNT*	*Young's Modulus (GPa)*
Present work	MD	Tobermorite 11Å	SWCNT (0.6 wt.%)	41
			SWCNT (0.9 wt.%)	21.29
			SWCNT (1.9wt.%)	69.17
			SWCNT (2.9 wt.%)	58
			SWCNT (3.3 wt.%)	79.01
			SWCNT (5.2 wt.%)	92.32
[20]	RVE numerical study	Cement model	SWCNT (0.09 wt.%)	20.34
			SWCNT (0.22 wt.%)	23.72
			SWCNT (0.42 wt.%)	40.73
			SWCNT (0.72 wt.%)	63.64
			SWCNT (1.2 wt.%)	92.28
[18]	Experimental study	Cement paste	MWCNT (0.08 wt.%)	21.9
[35]			MWCNT (0.08 wt.%)	13
[16]		Mortar	MWCNT (0.08 wt.%)	25
			MWCNT (0.1 wt.%)	27.5
			MWCNT (0.3 wt.%)	21.3
			MWCNT (0.5 wt.%)	20.1
[55]		OPC paste	MWCNT (0.038wt.%)	18.28
			MWCNT (0.075wt.%)	20.84

3.4.8. Conclusion

The present part of our study describes the possibility of the simulation of cement modified by different types of CNTs. In the first part, the system Tobermorite 11Å with different types of carbon nanotubes was studied to fix the best type of CNT for modification of cement matrix. The total energy of all models shows the attractive force between atoms of tobermorite's structure and CNT's structure. The calculated work of separation demonstrated that the best adhesion is attained with "Armchair" CNT type with diameter 2.275Å. Modification of the Tobermorite 11Å by the same CNT (2,2) with a diameter of 2.275Å increases the mechanical quantities such as shear modulus, plane stress and Young's modulus at the same time. The "Zigzag" CNT with a diameter of 3.135 Å gives the increasing of bulk modulus.

Besides, our study provides the information about brittle/ductile behaviors of the composite, modified by CNTs and gives clear explanation about the anisotropy of these systems.

Different models representing the concrete modified by CNTs were constructed to study the density effect of carbon nanotubes in the cementitious composites. Optimal concentration of CNT was fixed. The best concentration allowing increase bulk, shear and Young's moduli was 5.2 % of weight of tobermorite.

3.5. Pressure effect on the mechanical properties of the concrete modified with carbon nanotubes. Case of Tobermorite 11Å with Ca/Si ratio of 0.83 and Tobermorite 11Å with Ca/Si ratio of 1.

3.5.1. Input preparation

Based on our previous studies which show the most relevant carbon nanotube's type for every Ca/Si ratio basing on the estimation of the atoms interaction between CNT's structure and tobermorite's structure, we chose two type of single-walled CNT: "Armchair" CNT (2,2) with diameter 2.715 Å and "Zigzag" CNT (3,0) with diameter 2.351 Å. The length of these nanotubes is approximately equal of 17Å. Four systems are studied: Tobermorite 11Å with ratio Ca/Si=1 modified by one CNT type "Armchair"; Tobermorite 11Å with ratio Ca/Si=1 modified by 15 CNT type "Armchair"; Tobermorite 11Å with ratio Ca/Si=0.83 modified by one CNT type "Zigzag" and Tobermorite 11Å with ratio Ca/Si=0.83 modified by 6 CNT type "Zigzag". The same parameters used in the previous parts of study were used to prepare the input file.

3.5.2. Pressure effect

We study here, in details, the mechanical properties of Tobermorite 11Å (Ca/Si=1) modified with CNT (2,2). As mentioned above, CNT can be deformed due to the application of external force perpendicularly to the Z-axis direction. However, we apply -first- the uniaxial pressure in all directions as shown in Fig. 3.26d. The obtained values for the bulk, shear, Young's and stress moduli are presented in Fig. 3.26a-c. When the uniaxial pressure is applied along X-axis one can note that for shear, Young's and stress moduli there are stable values with a fluctuation at 900 MPa. For the bulk modulus variation, there is a peak at 950 MPa. Obtained results for tobermorite/CNT system can be compared with the previous studies [31, 56] of CNT, where one can note that the striking stiffness in the axial direction of CNT and the pressure resistance of the new composite is maintained. Fig. 3.26b shows that for mechanical properties, under unixial pressure applied along Y-axis, there is constant values of bulk, shear, Young's and stress moduli with some fluctuation at 350 MPa, 750 MPa, for each modulus.

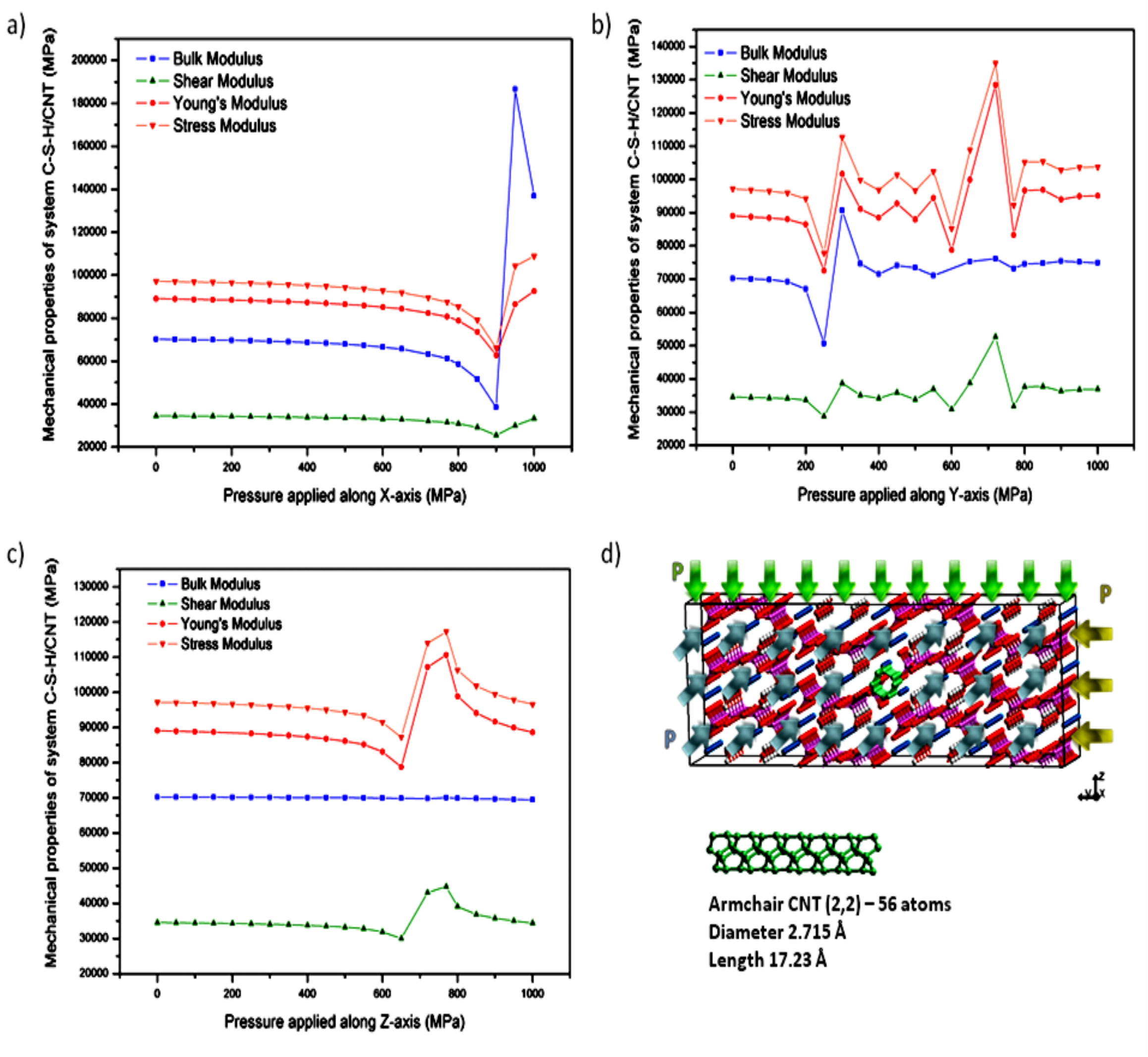

Fig. 3. 26. Effect of the uniaxial pressure applied along X-axis (a), Y-axis (b), Z-axis (c) on the mechanical properties of the system C-S-H/CNT; and schematic view of the tobermorite/CNT under the pressure (d).

Regarding the uniaxial pressure applied along Z-axis show a kind of structural phase transition in the pressure range of 700 MPa and 800 MPa. This could be explained by the elasticity of the circular cross section of CNT during the application a pressure perpendicularly to the axial nanotube's direction [59].

The radial distribution function (RDF) was calculated for the main points of peak. Fig. 3.27a-c shows the RDF of tobermorite/CNT atoms at 0 MPa, 720 MPa and 770 MPa. In the absence of external uniaxial pressure (Fig. 3.27a), numerous peaks for the pair of C-C atoms are observed, which indicates a strong grouping of atoms with each other. Several peaks of different pairs of tobermorite's atoms and tobermorite/CNT's atoms are also discernible, what confirm the crystalline structure of the material. By increasing the pressure up to 720 MPa (Fig. 3.27b), there is disappearance of a small peak, which is viewed at a distance of 2.2 Å at zero pressure. One can assume that this is due to the nanotube deformation under pressure; whereas ni significant change is noticed for concrete structure. However, with increasing pressure to 770 MPa (Fig. 3.27c), the peaks show an effective distance at which the atoms cannot move closer to each other. The obtained results are the first regarding the effect of the pressure on the mechanical properties of the tobermorite/CNT system. We have the possibility to compare the radial distribution function of pair C-C with previous theoretical studies. For our structures there are three main peaks at the distances 1.5 Å, 2.5 Å, and 2.8 Å that agree well with previous published studies (Fig. 3.27d) obtained from classical molecular dynamics method [60,61].

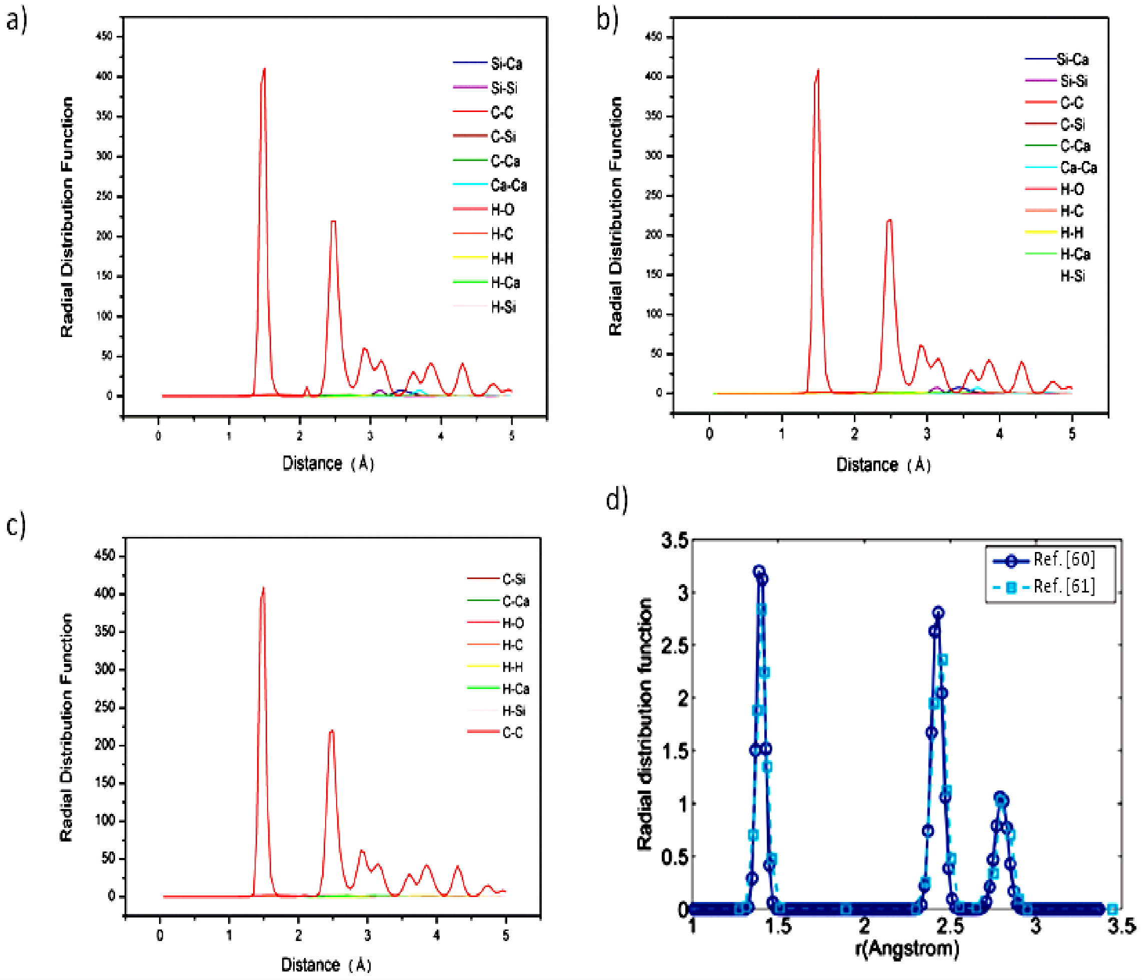

Fig. 3.27: Radial distribution function of the atoms for tobermorite/CNT without applied pressure (a), under uniaxial pressure of 720 MPa (b), under uniaxial pressure of 770 MPa (c); the radial distribution function for the pair C-C from the Ref. [60,61].

To investigate the other models we have been limited by the application of uniaxial pressure along Z-direction. Studying the Tobermorite 11Å (Ca/Si =0.83) modified by the most relevant type of CNT for tobermorite with this ratio, i.e. “Zigzag” CNT with diameter of 2.351 Å we may observe for all moduli (Fig. 3.28a-d) only the fluctuations in the area of obtained values. Consequently, the aspect of the CNT’s type is of great importance. In case of C-S-H modified by “Zigzag” CNT, there is no phase transition, and the structure is not sensitive to the external pressure.

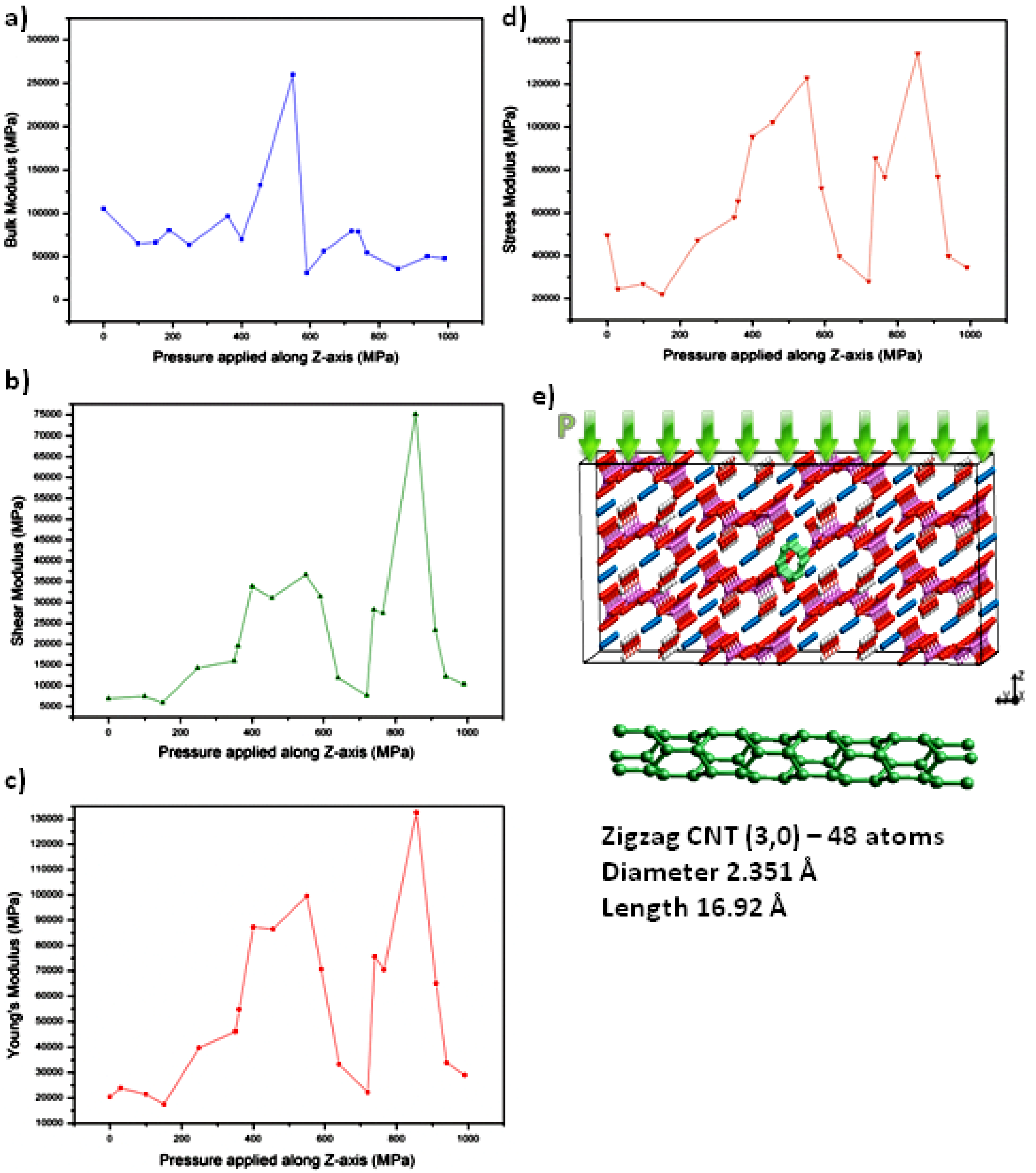

Fig. 3.28. Effect of the uniaxial pressure applied along Z-axis on the Bulk Modulus (a), Shear Modulus (b), Young's Modulus (c), Stress Modulus (d) of the system C-S-H/CNT; and schematic view of the specimen tobermorite/CNT under the pressure (e).

Moreover, the structures modified by a number of CNT were investigated as well. An important point is that in the case of the modification of Tobermorite 11Å structure (Ca/Si =1) by only one "Armchair" CNT, we had a phase transition between the pressure values of 700MPa and 800MPa. However in the case of the modification the Tobermorite 11Å structure (Ca/Si =1) by "Armchair" CNT with a quantity of 5.2% by weight of tobermorite, i.e. the case of 15 nanotubes (Fig. 3.29e), we noticed the fluctuations for all mechanical properties (Fig. 3.29a-d). For

Tobermorite 11Å structure (Ca/Si =0.83) mixed t "Zigzag" CNT with 1.7% by weight of tobermorite, i.e. 6 nanotubes (Fig. 3.30e), the fluctuation tendency for bulk, shear, Young's and stress moduli (Fig. 3.30a-d) is maintained during the application of different values of external pressure such as in the case of one nanotube.

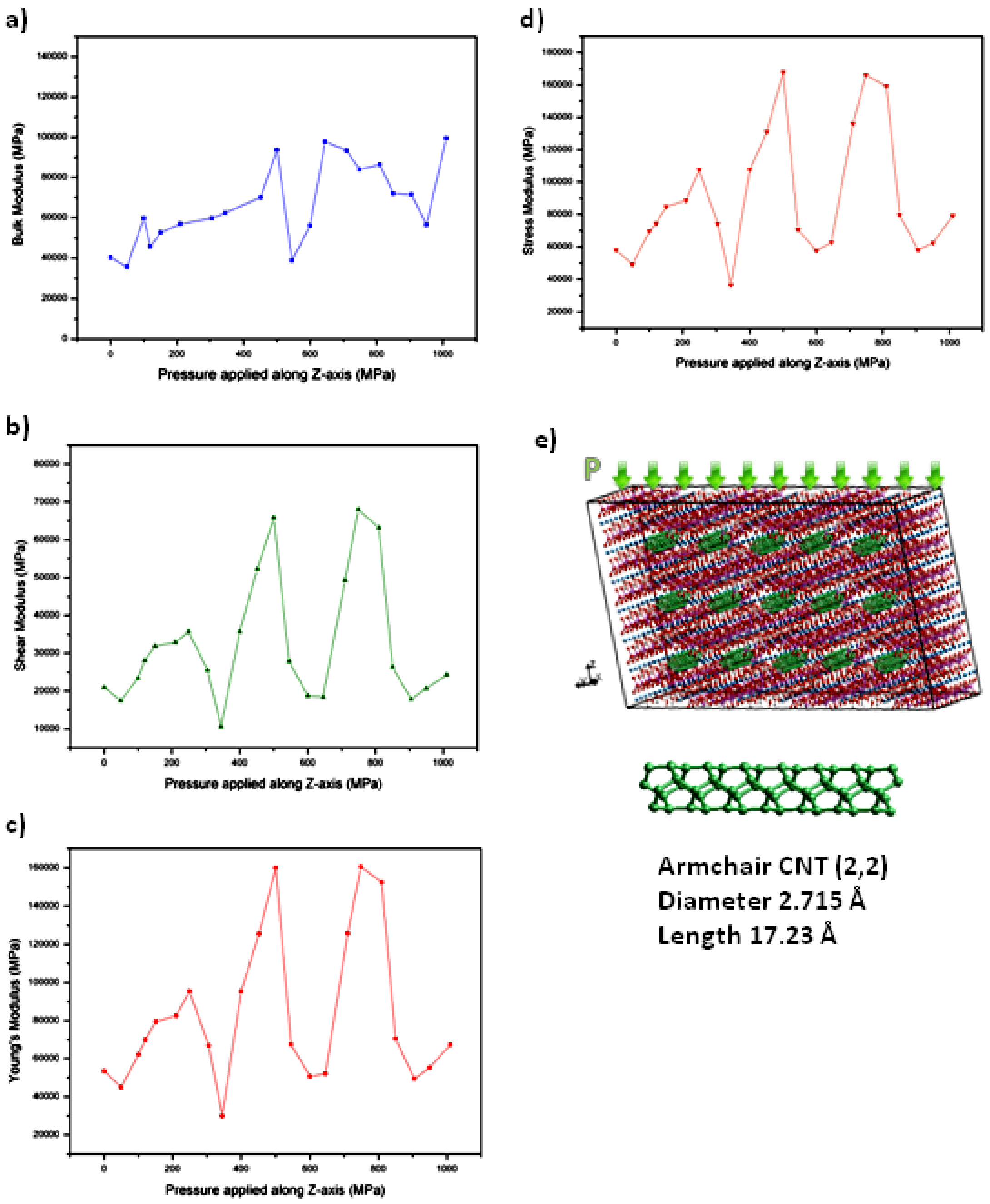

Fig. 3.29. Effect of the uniaxial pressure applied along Z-axis on the Bulk Modulus (a), Shear Modulus (b), Young's Modulus (c), Stress Modulus (d) of the system C-S-H/CNTs; and schematic view of the specimen tobermorite/CNT under the pressure (e).

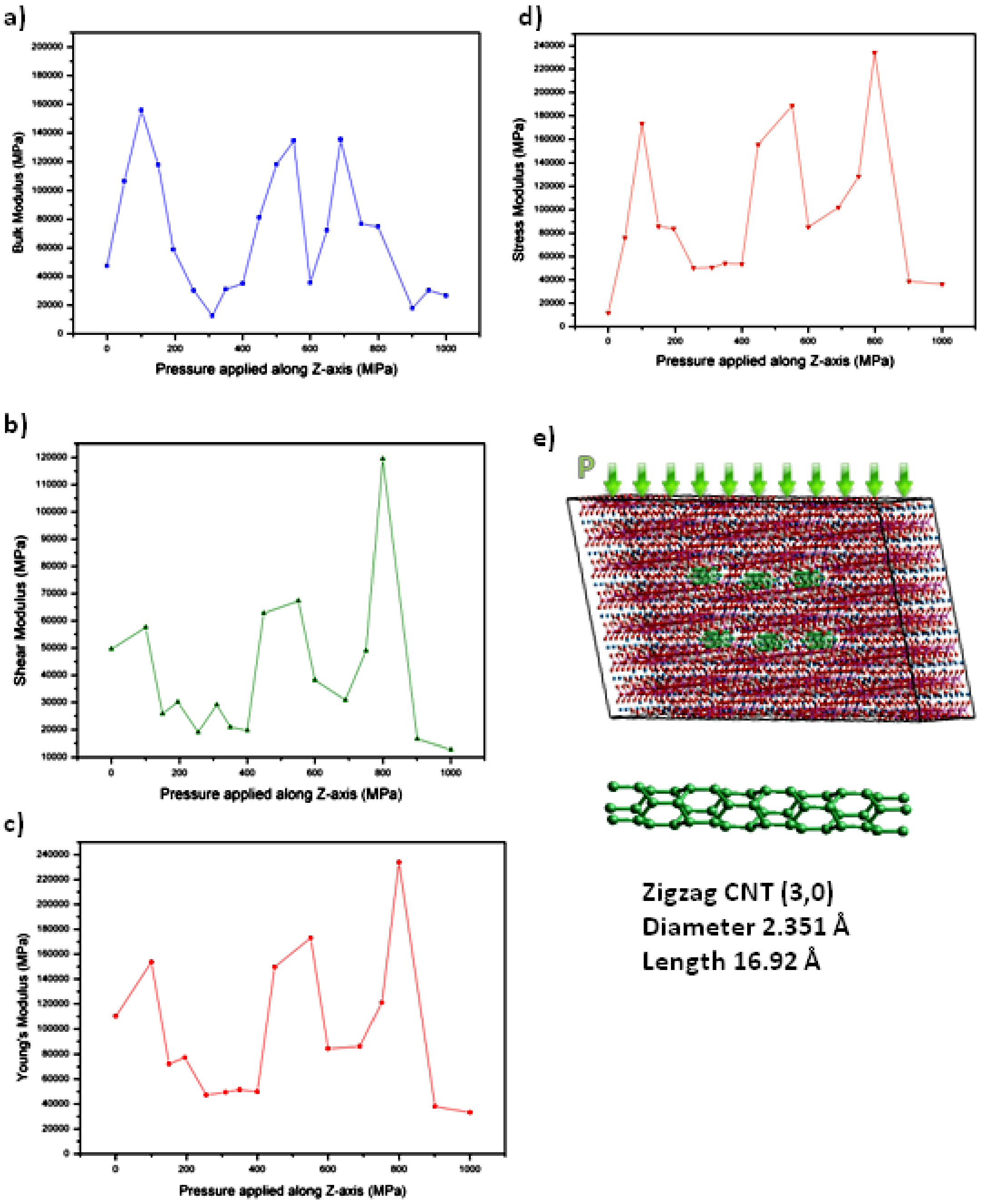

Fig. 3.30. Effect of the uniaxial pressure applied along Z-axis on the Bulk Modulus (a), Shear Modulus (b), Young's Modulus (c), Stress Modulus (d) of the system C-S-H/CNTs; and schematic view of the specimen tobermorite/CNT under the pressure (e).

3.5.3. Conclusion

The present investigation aimed to predict the mechanical properties under uniaxial external pressure for the structures of Tobermorite 11Å modified by carbon nanotubes. We may conclude that CNT incorporated into the structure of the cement composite can keep the behavior of CNT as it is under external pressure. This means that CNT acquires the elastic behavior under an external force applied perpendicularly to the nanotube's axis direction. In addition, the type and number of CNT incorporated into the structure of concrete play the main role.

In conclusion, we notice that Tobermorite 11Å (Ca/Si = 1) modified by one "Armchair" CNT with diameter of 2.717 Å show a phase transition under a pressure in the range of 700 MPa and 800 MPa. However this effect disappears when the number of CNT increases. For Tobermorite 11Å (Ca/Si = 0.83) modified by one "Zigzag" CNT with diameter of 2.351 Å we have stable values of bulk, shear, Young's and stress moduli with some fluctuations in the case of one CNT as well as for the case with a number of CNT.

References

[1] B. Peng, M. Locascio, P. Zapol, S. Li, S. L. Mielke, G. Schatz, H. D. Espinosa, Measurements of near-ultimate strength for multiwalled carbon nanotubes and irradiation-induced crosslinking improvements, Nature nanotech. 3 (10) (2008) 626–631.

[2] D. Qian, M. F. Yu, R. S. Ruoff, G. J. Wagner, W. K. Liu, Mechanics of carbon nanotubes, Appl. Mech. Rev. 55 (6) (2002) 495–533.

[3] K. T. Lau, C. Gu, D. Hui, A critical review on nanotube and nanotube/nanoclay related polymer, Composites Part B, 37 (6) (2006) 425–426.

[4] C. Li, T. W. Chou, Elastic moduli of multi-walled carbon nanotubes and the effect of van der Waals forces, Compos. Sci. Technol. 64 (11) (2003) 1517–1524.

[5] R. F. Gibson, A review of recent research on mechanics of multifunctional composite materials and structures, Compos. Struct. 92 (12) (2010) 2793-2810.

[6] J. P. Salvetat, J. M. Borard, N. H. Thomson, A. J. Kulik, L. Forro, W. Bennoit, L. Zuppiroli, Mechanical properties of carbon nanotubes, Appl. Phys. A, 69 (3) (1999) 255–260.

[7] T. Ji, Y. Feng, M. Qin, W. Feng, Thermal conducting properties of aligned carbon nanotubes and their polymer composites, Composites Part A, 91 (1) (2016) 351–369.

[8] N. Khandoker, S. S. Hawkins, R. Ibrahim, C. P. Huynh, F. Deng, Tensile Strength of Spinnable Multiwall Carbon Nanotubes, Procedia Eng. 10 (2011) 2572–2578.

[9] M. F. Yu, O. Lourie, M. J. Dyer, T. F. Kelly, R. S. Rouff, Strength and breaking mechanism of multiwalled carbon nanotubes under tensile load, Science, 287 (5453) (2000) 637–640.

[10] E. T. Thostenson, Z. Ren, T. W. Chou, Advances in the science and technology of carbon nanotubes and their composites: a review, Compos. Sci. Technol. 61 (13) (2001) 1899–1912.

[11] M. Moniruzzaman, K. I. Winey, Polymer Nanocomposites Containing Carbon Nanotubes, Macromolecules, 39 (16) (2006) 5194–5205.

[12] M. C. Paiva, B. Zhou, K. A. Fernando, Y. Lin, J. M. Kennedy, Y. P. Sun, Mechanical and morphological characterization of polymer–carbon nanocomposites from functionalized carbon nanotubes, Carbon, 42 (14) (2004) 2849–2854.

[13] B. X. Yang, H. S. Jia, K. Pramoda, S. H. Goh, Enhancement of the mechanical properties of polypropylene using polypropylene-grafted multiwalled carbon nanotubes, Compos. Sci. Technol. 68 (12) (2008) 2490–2497.

[14] S. Iijima, Helical microtubules of graphitic carbon, Nature, 354 (1991) 56–58.

[15] M. S. Konsta-Gdoutos, Highly dispersed carbon nanotube reinforced cement based materials, Cem. Concr. Res. 40 (7) (2010) 1052–1059.

[16] G. Y. Li, P. M. Wang, X. Zhao, Mechanical behavior and microstructure of cement composites incorporating surface-treated multi-walled carbon nanotubes, Carbon, 43 (6) (2005) 1239–1245.

[17] J. M. Makar, J. J. Beaudoin, Carbon Nanotubes and their Application in the Construction Industry, in: Proceedings of the 1st International Symposium on Nanotechnology in Construction, Paisley, Scotland , 2003.

[18] J. M. Makar, J. Margeson, J. Luh, Carbon nanotube/cement composites – early resultsand potential applications, in: Proceedings of the 3rd International Conference on Construction Materials: Performance, Innovations and Structural Implications, Vancouver, Canada, 2005.

[19] M. S. Konsta-Gdoutos, Z. S. Metaxa, S. P. Shah, Multi-scale mechanical and fracture characteristics and early-age strain capacity of high performance carbon nanotube/cement nanocomposites, Cement Concrete Comp. 32 (2) (2010), 110–115.

[20] Y. Saez de Ibarra, J. J. Gaitero, E. Erkizia, I. Campillo, Atomic force microscopy and nanoindentation of cement pastes with nanotube dispersions, Psys. stat. sol. 203 (6) (2006) 1076–1081.

[21] A. Cwirzen, K. Habermehl-Chirzen, V. Penttala, Surface decoration of carbon nanotubes and mechanical properties of cement/carbon nanotube composites, Adv. Cem. Res. 20 (2) (2008) 65–73.

[22] Z. S. Metaxa, M. S. Konsta-Gdoutos, S. P. Shah, Nanotechnology of Concrete: The Next Big Thing is Small, in Session at the ACI Fall 2009 Convention, New Orleans, LA, United States, 2009.

[23] S. P. Shah, M. S. Konsta-Gdoutos, Z. S. Metaxa, P. Mondal, Nanoscale Modification of Cementitious Materials, in: Proceedings of the 3rd international symposium on nanotechnology in construction, Prague, Czech Republic, 2009.

[24] S. Musso, J. M. Tulliani, G. Ferro, A. Tagliaferro, Influence of carbon nanotubes structure on the mechanical behavior of cement composites, Compos. Sci. Technol. 69 (11-12) (2009) 1985–1990.

[25] K. P. Chong, E. J. Garboczi, Smart and designer structural material systems, Prog. Struct. Eng. Mat. 4 (4) (2002) 417–430.

[26] P. Faucon, J. M. Delaye, J. Virlet, Molecular Dynamics Simulation of the Structure of Calcium Silicate Hydrates: I. Ca4+xSi6O14+2x(OH)4−2x(H2O)2(0≤x≤1), J. Solid State Chem. 127 (1) (1996) 92–97.

[27] P. Faucon, J. M. Delaye, J. Virlet, J. F. Jacquinot, F. Adenot, Study of the structural properties of the C-S-H(I) by molecular dynamics simulation, Cem. Concr. Res. 27 (10) (1997) 1581–1590.

[28] C. Plassard, E. Lesniewska, I. Pochard, A. Nonat, Nanoscale experimental investigation of particle interactions at the origin of the cohesion of cement, Langmuir, 21 (16) (2005) 7263–7270.

[29] A. G. Kalinichev, R. J. Kirkpatrick, Molecular dynamics modeling of chloride binding to the surfaces of calcium hydroxide, hydrated calcium aluminate, and calcium silicate phases, JACS 14 (8) (2002) 3539–3549.

[30] J. Tersoff, Empirical interatomic potential for carbon, with applications to amorphous carbon, Phys. Rev. Lett. 61 (25) (1988) 2879–2882.

[31] M. M. J. Treacy, T. W. Ebbesen, J. M. Gibson, Exceptionally high Young's modulud observed for individual carbon nanotubes, Nature, 381 (1996) 678–680.

[32] A. Krichnan, E. Dujardin, T. W. Ebbesen, P. N. Yianilos, M. M. J. Treacy, Yound's modulus of single-walled nanotubes, Phys. Rev. B, 58 (1998) 14013–14019.

[33] O. Lourie, H. D. Wagner, Evaluation of Young's modulus of carbon nanotubes by micro-Raman spectroscopy, J. Mater. Res. 13 (9) (1998) 2418–2422.

[34] O. Lourie, D. M. Cox, H. D. Wagner, Buckling and collapse of embedded carbon nanotubes, Phys. Rev. Lett. 81(8) (1998) 1638–1641.

[35] M. F. Yu, B. S. Files, S. Arepalli, R. S. Ruoff, Tensile loading of ropes of single wallcarbon nanotubes and their mechanical properties, Phys. Rev. Lett. 84 (24) (2000) 5552–5554.

[36] J. P. Salvetat, G. A. D. Briggs, J. M. Bonard, R. R. Bacsa, A. J. Kulik, T. Stockli, N. A. Burnham, L. Forró, Elastic and shear moduli of single-walled carbon nanotube ropes, Phys. Rev. Lett. 82(5) (1999) 944–947.

[37] T. W. Tombler, C. W. Zhou, L. Alexeyev, J. Kong, H. J. Dai, L. Liu, C. Jayanthi, M. Tang, S. Y. Wu, Reversible electromechanical characteristics of carbon nanotubes under local-probe manipulation, Nature 405 (2000) 769–772.

[38] C. Li, T. W. Chou, A structural mechanics approach for the analysis of carbon nanotubes. Int. J. Solids Struct. 40(10) (2003) 2487–2499.

[39] J. P. Lu, Elastic properties of carbon nanotubes and nanoropes, Phys. Rev. Lett. 79(7) (1997) 1230–1297.

[40] V.N. Popov, V.E.Van Doren, M. Balkanski, Elastic properties of single-walled carbon nanotubes, Phys. Rev. B 61(4) (2000) 3078–3084.

[41] S. R. Hamid, The Crystal Structure of the 11A Natural Tobermorite Ca2.25[Si3O7.5(OH)1.5].1H2O, Zeitschrift für Kristallographie 154 (1981) 189-198.

[42] C. Plassard, E. Lesniewska, I. Pochard, A. Nonat, Investigation of the surface structure and elastic properties of calcium silicate hydrates at the nanoscale, Ultramicroscopy 100 (2004) 331–338.

[43] A. Zaoui, Insight into elastic behavior of calcium silicate hydrated oxide (C-S-H) under pressure and composition effect, Cem. Concr. Res. 42 (2) (2012) 306–312.

[44] F. Sanchez, L. Zhang, Interaction energies, structure, and dynamics at functionalized graphitic structure–liquid phase interfaces in an aqueous calcium sulfate solution by molecular dynamics simulation, Carbon 48 (4) (2010) 1210–1223.

[45] Z. Y. Ong, E. Pop, Molecular dynamics simulation of thermal boundary conductance between carbon nanotubes and SiO2, Phys. Rev. B 81 (2010) 155408.

[46] F. Sanchez, L. Zhlang, Molecular dynamics modeling of the interface between surface functionalized praphitic structures and calcium-silicate-hydrate: Interaction energies, structure, and dynamics, J. Colloid Interface Sci. 323 (2008) 349–358.

[47] M. Eftekhari, S. Mohammadi, Molecular dynamics simulation of the non linear behaviour of the CNT-reinforces calcium silicate hydrate (C-S-H) composite, Composites Part A, 82 (2016) 78–87.

[48] R. Shahsavari, M. J. Buehler, R. J.-M. Pellenq, F. J. Ulm, First-principles study of elastic constants and interlayer interactions of complex hydrated oxides: case study of tobermorite and jennite, Am. Ceram. Soc. 92 (2009) 2323–2330.

[49] J.E. Oh, S.M. Clark, H.R. Wenk, P.J.M. Monteiro, Experimental determination of bulk modulus of 14 Å tobermorite using high oressure synchrotron X-ray diffraction, Cem. Concr. Res. 42 (2012) 397–403.

[50] L. Jin, X. Du, G. Ma, Macroscopic effective moduli and tensile strength of saturated concrete, Cem. Concr. Res. 42 (2012) 1590–1600.

[51] M. Musiał, J. Grosel, Determining the Young's modulus of concrete by measuring the eigenfrequencies of concrete and reinforced concrete beams, Constr. Buld. Mater. 121 (2016) 44–52

[52] O. Bahr, P. Schaumann, B. Bollen, J. Bracke, Young's modulus and Poisson's ratio of concrete at high temperatures: Experimental investigations, Mater. Design. 42 (2013) 421–429.

[53] P.A. Danoglidis, M.S. Konsta-Gdoutos, E.E. Gdoutos, S.P.Shah, Strength, energy absorption and self-sensing properties of multifunctional carbon nanotube reinforced mortars, Constr. Build. Mater. 120 (2016) 265–274.

[54] B. Zou, S.J. Chen, A.H. Korayem, F. Collins, C.M. Wang, W.H. Duan, Effect of ultrasonication energy on egineering properties of carbon nanotube reinforced cement pastes, Carbon 85 (2015) 212–220.

[55] S. Wansom, N. J. Kidner, L. Y. Woo, T. O. Mason, AC-impedance response of multi-walled carbon nanotube/cement composites, Cem. Concr. Compos. 28 (2006) 509–519.

[56] B.S. Sindu, S. Sasmal, S.Gopinath, Numerical simulation of CNT incorporated cement, World. Acad. Sci. Eng. Technol. 6 (2012) 8–26.

[57] K. Gopalakrishnan, B. Birgisson, P. Taylor, N.O. Attoh-Okine, Nanotechnology in Civil Infrastructure, Berlin, Germany: Springer, 2011.

[58] A. Krishnan, E. Dujardin, T. W. Ebbesen, P. N. Yianilos, M. M. J. Treacy, Young's modulus of single-walled nanotubes, Phys. Rev. B 58 (1998) 14013–14019.

[59] S. Iijima, C. Brabec, A. Maiti, J. Bernholc, Structural flexibility of carbon nanotubes, J. Chem. Phys. 104 (1996) 2089–2092.

[60] H. Zhao, K. Min, N. R. Aluru, Size and chirality dependent elastic properties of graphene nanoribbons under uniaxial tension, Nano Lett. 9 (8) (2009) 3012–3015.

[61] A. Fasolino, J. H. Los, M. I. Katsnelson, Intrinsic ripples in graphene, Nat.Mat. 6 (11) (2007) 858–861.

GENERAL CONCLUSIONS

GENERAL CONCLUSIONS

In this thesis, the possibility of the concrete's modification by carbon nanotubes (CNTs) has been studied. We have performed five sub-studies with the objective to realize the complex investigation and to give extensive analysis of new composite material based on cement binder and containing CNTs. The Molecular Dynamics (MD) method was chosen to accomplish our investigation. A Model of Tobermorite 11Å was taken to represent the calcium silicate hydrate (C-S-H) gel, the principal hydration product in hardened cement paste.

The first part of our study was devoted to the investigation of the different types of Single Walled Carbon Nanotubes (SWCNTs). Obtained mechanical properties for the "Zigzag" and "Armchair" types of SWCNTs with different diameters were found in favorable agreement with previous available works.

Having examined the different types of CNTs we passed to the investigation of the influence of CNTs incorporated in the concrete. To do this, we have created a hole into the structure of tobermorite. It is important to note, that the bridging tetrahedral silica may be missing in the Drierketten type of silicate chains observed in tobermorite like C-S-H. This model allows us to find the less stable silicon atoms in silicon chains and to remove them with interstitial calcium, in order to keep the neutral charge in all system.

Then in the second part we investigated the incorporation of different types of SWCNTs into the matrix of Tobermorite 11Å with Ca/Si ratio of 0.83. The necessary distance between CNT and tobermorite was fixed at ~2Å. Under this distance the creation of the new formation nearby the surface of CNTs was observed. The best type of CNTs the allowing increase of all mechanical parameters such as Bulk, Shear, Young's and Plane Stress moduli was also fixed. It is "Zigzag" type CNT (3,0) with a diameter of 2.351 Å. This type of CNT has the best adhesion with tobermorite's structure. Furthermore, it was noticed, that the CNTs with the bigger diameters such 3.319 Å and 4.073 Å can change the behavior of new composite from brittle towards ductile. In addition, the values of the anisotropy were evaluated for the cement composite with carbon nanotubes. The obtained components of elasticity tensors affirmed the effect of the attribution of the elastic behavior depending up the direction of the CNT's insertion. It was also identified that, the modification of concrete by CNTs can change of the elastic wave velocities that have a great role of interpretation of the seismic data. The low value of both waves was found in the case of concrete's modification by "Zigzag" type CNT (4,0) with a diameter of 3.135 Å.

The inserting of CNTs also changes the piezoelectric constants. It can be noted here that the type and diameter of carbon nanotube (CNT) play an important role.

The part of our study investigated the density effect of “Zigzag” type CNT (3,0) with a diameter of 2.351 Å on the Tobermorite 11Å properties. We found that optimal concentration of SWCNTs equals to 1.7 % per weight of tobermorite gives an increase of shear and Young’s moduli; and 2.6 % per weight of tobermorite with an increase of bulk modulus. In addition, the Poisson’s ratio has also been calculated. It shows the best elastic behavior of composites modified by CNTs lies in concentration range from 0.5% to 2.6 % per weight of tobermorite.

Fourth part of our study provides insight into the influence of different CNT’s types into Tobermorite 11Å with Ca/Si ratio equals to 1. Our calculations suggested that there is the possibility to increase the Shear, Young’s and Plane Stress moduli at the same time when we mofified the tobermorite’s structure with “Armchair” type CNT (2,2) with a diameter equal of 2.275 Å. Furthermore, this type of CNT gives the best adhesion between the structure of tobermorite and CNT’s structure, which increase greatly the longitudinal and transversal waves velocities. Regarding the Pugh’s ratio we stated that besides of CNT (2,2), the CNT (5,0) can also reduce the weakness of the composite. At another point Poisson’s ratio value increases tobermorite modified with CNT (3,0), CNT (4,0) and CNT (3,3). The calculated components of elasticity tensors show that only one specimen with CNT (4,0) has the greatest value of elastic constant, than the one without CNT in the direction of nanotube’s insertion. The calculated Zener factor suggests that all structures exhibits anisotropic elasticity. The best concentration allowing the increase of bulk, shear and Young’s moduli was 5.2 % of weight of tobermorite.

Fifth part of our study provided information about the behavior of concrete modified by CNT under uniaxial pressure. In all cases, except the one of modification with CNT (2,2) of Tobermorite 11Å with Ca/Si ratio equal 1, we have the stabe values with some flactuation of mechanical properties during the loading pressure from 0 to 1000 MPa. The phase transition appears when pressure is applied in the range from 700 MPa to 800 MPa for the case of modification with CNT (2,2).

List of Figures

List of Tables

Abstract

Concrete plays a very important role in all areas related to civil engineering because of its availability, durability and speed to accomplish many construction projects. In addition, civil engineering is a dynamic field that is constantly evolving. Therefore, the production of new generations of concrete with improved physical, structural and technical properties is very important, but it is not possible without the use of various types of additives. Carbon nanotubes are promising materials that possess specific properties allowing their uses for a wide variety of composite materials, including concrete.

Some experimental studies have revealed that carbon nanotubes can improve the mechanical properties of concrete with a small amount of additives, providing a less defective structure of the cement matrix. However, the results are still insufficient and need to be elucidated on the processes occurring at the nano-scale in the concrete structure modified by carbon nanotubes. Thus, this thesis has as main objective the study of the improvement of the mechanical properties of the concrete modified by the carbon nanotubes, using Molecular dynamics method.

In order to model the atomic structure of the Calcium Silicate Hydrates (C-S-H) gel, Tobermorite 11Å was selected with two different Ca/Si ratios corresponding to 0.83 and 1. Various types of nanotubes incorporated into the Tobermorite 11Å structure were tested to study mechanical properties of the resulting new composite. In addition, the effect of the concentration of carbon nanotubes in the cement was also detailed. Finally, we studied the effect of uniaxial pressure on the concrete structure including carbon nanotubes. The work concludes that it is possible to improve the mechanical characteristics of concrete by inserting nano-materials in general, and carbon nanotubes in particular.

Résumé

Le béton joue un rôle très important dans tous les domaines liés au génie civil en raison de sa disponibilité, sa durabilité et sa rapidité pour accomplir de nombreux projets de construction. En outre, le génie civil est un domaine dynamique qui évolue en permanence. Par conséquent, la production de nouvelles générations de béton avec des propriétés physiques, structurales et techniques améliorées est très importante, mais elle n'est pas possible sans utiliser divers types d'additifs. Les nanotubes de carbone sont des matériaux prometteurs qui possèdent des propriétés spécifiques permettant leurs utilisations pour une grande variété de matériaux composites, y compris le béton.

Certaines études expérimentales ont révélé que les nanotubes de carbone peuvent améliorer les propriétés mécaniques du béton avec une petite quantité d'additifs, en fournissant une structure moins défectueuse de la matrice de ciment. Cependant, les résultats sont encore insuffisants et nécessitent d'être élucidés sur les processus se produisant à l'échelle nanométrique dans la structure en béton modifiée par les nanotubes de carbone. Ainsi, cette thèse, a pour objectif principal l'étude de l'amélioration des propriétés mécaniques du béton modifié par les nanotubes de carbone, à l'aide de la méthode de dynamique Moléculaire.

Afin de modéliser la structure atomique du gel de la Silicate de Calcium Hydratée (C-S-H), nous avons choisi la Tobermorite 11Å avec deux rapports différents de Ca/Si correspondants à 0,83 et 1. Divers types de nanotubes incorporés dans Tobermorite sont testés pour étudier les propriétés mécaniques du nouveau composite résultant. En outre, l'effet de la concentration de nanotubes de carbone dans le ciment est également détaillé. Enfin, nous étudions l'effet de la pression uniaxial sur la structure du béton incluant des nanotubes de carbone. Nos travaux montrent qu'il possible d'améliorer les caractéristiques mécaniques du béton en insérant des nanomatériaux en général, et des nanotubes de carbone en particulier.